2013-10-30

Fine-scale Distributions of Plankton and Larval Fishes: Implications for Predator-prey Interactions near Coastal Oceanographic Features

Adam Tyler Greer
University of Miami, adam.t.greer@gmail.com

UNIVERSITY OF MIAMI

FINE-SCALE DISTRIBUTIONS OF PLANKTON AND LARVAL FISHES: IMPLICATIONS FOR PREDATOR-PREY INTERACTIONS NEAR COASTAL OCEANOGRAPHIC FEATURES

By

Adam Tyler Greer

A DISSERTATION

Submitted to the Faculty
of the University of Miami
in partial fulfillment of the requirements for
the degree of Doctor of Philosophy

Coral Gables, Florida

December 2013

UNIVERSITY OF MIAMI

A dissertation submitted in partial fulfillment of
the requirements for the degree of
Doctor of Philosophy

FINE-SCALE DISTRIBUTIONS OF PLANKTON AND LARVAL FISHES: IMPLICATIONS FOR PREDATOR-PREY INTERACTIONS NEAR COASTAL OCEANOGRAPHIC FEATURES

Adam Tyler Greer

Approved:

_____ Robert K. Cowen, Ph.D. Professor of Marine Biology & Fisheries	_____ Su Sponaugle, Ph.D. Professor of Marine Biology & Fisheries
_____ Peter B. Ortner, Ph.D. Professor of Marine Biology & Fisheries	_____ Mei-Ling Shyu, Ph.D. Professor of Electrical & Computer Engineering
_____ Jonathan A. Hare, Ph.D. Chief of Oceanography Branch NOAA NEFSC Narragansett, Rhode Island	_____ M. Brian Blake, Ph.D. Dean of the Graduate School

GREER, ADAM TYLER (Ph.D., Marine Biology and Fisheries)

Fine-scale Distributions of Plankton and Larval Fishes: Implications for Predator-Prey Interactions near Coastal Oceanographic Features (December 2013)

Abstract of a dissertation at the University of Miami.

Dissertation supervised by Professor Robert K. Cowen.
No. of pages in text. (170)

Describing the distributions of organisms on scales relevant to individuals (1-100 m) is critical to understanding predator-prey interactions within the plankton. This has driven the development of plankton imaging technology with synoptic physical parameters (temperature, salinity, depth), which facilitates high-resolution taxonomic and spatial descriptions. We utilized a novel *In Situ* Ichthyoplankton Imaging System (ISIIS) that addressed some shortcomings of other imaging systems by allowing for the simultaneous sampling of both abundant (e.g., copepods, appendicularians, marine snow) and rare (e.g., fish larvae, medusae, ctenophores) members of the plankton community. The main objectives of this study were 1) to describe the physical and biological characteristics of the fine-scale environments near ubiquitous coastal features (fronts, thin layers, and internal waves), and 2) how these descriptions related to trophic interactions potentially affecting the early life stages of fishes.

ISIIS was deployed in three separate environments with characteristic hydrographic regimes favorable to the formation of thin layers, internal waves, and fronts. In northern Monterey Bay, thermal stratification led to the development of thin layers of diatom aggregates dominated by *Pseudo-nitzschia* spp. A variety of gelatinous taxa tended to aggregate within or below thin layers, while copepods seemed to avoid the

thin layers and were often found near the surface. The vertical separation of predators and prey showed support for predation avoidance by copepods, with thin layers creating a strong gradient in light levels facilitating contact predation by gelatinous zooplankton at depth. The physical environment near Stellwagen Bank was dominated by a tidally driven oscillation between high stratification and internal wave activity. Copepods were found near the surface, sometimes aggregating in a thin layer several meters shallower than the chlorophyll-*a* maximum. Larval fishes were found to strongly correlate with the copepods, suggesting they feed on concentrations of prey much higher than average. After the passage of internal waves, larval fish correlation with prey was reduced, while predators, which were abundant at depth, had higher correlation with larval fishes. Internal waves reduced patchiness for a variety of taxa, potentially creating less favorable planktonic habitat for larval fishes. At the shelf-slope front near Georges Bank, we investigated the impact of horizontal gradients on the distribution of plankton. Almost all plankton taxa were found in high abundance on the shelf side of the front. A particle solidity metric showed distinct habitat partitioning of different plankton taxa around the front, with copepods and appendicularians forming a near surface layer just above the convergence of isopycnals defining the front. These grazers were spatially separate from diatom aggregates, which were abundant in zones of high chlorophyll-*a* fluorescence. The distributions of gelatinous zooplankton and fish tended to follow isopycnals that converged at the front. Taken together, this body of work shows common 5-10 meter scale vertical extent of many planktonic taxa despite the dramatic differences in hydrographic properties.

ACKNOWLEDGEMENTS

I am extremely thankful for the advice, patience, and guidance of many people who have helped to make this dissertation possible. First, I am grateful for the opportunity that my advisor, Bob Cowen, gave me by accepting me into his lab. He balanced the important skills of allowing me intellectual freedom while steering me towards crucial topics in biological oceanography. His guidance and knack for asking the tough questions has definitely made me a better scientist and communicator. My other committee members have all been valuable in distinct ways. Su Sponaugle and Peter Ortner both provided extensive knowledge of larval fish, zooplankton ecology, and sampling, and helped push me for clarity in my writing. My ability to access information and be in contact with the right people was greatly enhanced by Jon Hare, and he was also helpful during the writing process. Mei-Ling Shyu introduced me to the world of data science and gave me many ideas for analysis and organization of large datasets. I have no doubt that collaborations between ocean scientists and people like Dr. Shyu will become more common in the future as datasets expand and our ability to understand them relies more and more on sophisticated data management and mining techniques. There are also many other scientists who have helped shape my thinking throughout my graduate school career including Jean-Olivier Irisson, Lars Stemmann, David Die, Steve Smith, John Walter, Joe Serafy, Margaret McManus, John Ryan, and Brock Woodson.

When I first arrived at RSMAS, Cedric Guigand took me under his wing and taught me to think like an engineer, fully understanding the nuts and bolts of imaging systems. Even though we had a few small mishaps in the field, Cedric would always come up with a solution that allowed us to keep collecting data. In the lab, Cedric and I

had many conversations about ISIIS data and interpretation, which have definitely improved this body of work. I have great admiration for him for both his technical and scientific expertise.

Significant portions of this dissertation would not have come to fruition without the efforts of others. Dorothy Tang was invaluable in helping analyze the plankton images. Additional help came from undergraduate volunteers Ben Grassian and Jenna Binstein. The captain and crew of the NOAA ship Delaware II and Jim Christmann of the R/V Shana Rae were responsible for successful field sampling. Jerry Prezioso, Dave Richardson, and Scott Sperber helped with field data collection and net sample processing. Margaret McManus, Jeff Sevadjian, and Amanda Timmerman analyzed the moored profiler data and reviewed versions of Chapter 2. Assistance with some of the identifications of gelatinous zooplankton was provided by Claudia Mills, Phil Pugh, Mike Ford, Gustav-Adolf Paffenhöfer, and Don Deibel.

My labmates and friends at RSMAS have made my time in graduate school incredibly enjoyable. Officemates Martha Hauff, Jessica Luo, and Jonathan Kool provided interesting conversation and (sometimes) passionate debate. I also enjoyed spending time in the field with other lab members including Sean Bignami, Katie Shulzitski, Esther Goldstein, Joel Llopiz, Evan D'Allesandro, Kristen Delano-Walter, and Tauna Rankin. Other people I must thank for making graduate school a fun experience are Geoffrey Shideler, Falko Judt, Will Komaromi, Marcela Ulate-Medrano, Dave Weinstein, Ross Cunning, Nathan Vaughan, Mark Fitchett, Andy Kough, Ben Shaw, Andrew Margolin, and many others whom I will miss greatly.

Funding for my graduate education and field work came from a variety of sources including the National Science Foundation, the National Oceanographic and Atmospheric Administration, and the National Resource Damage Assessment. Additional support came from the RSMAS Alumni Fellowship, a Living Marine Resources Cooperative Science Center Fellowship, and the Captain Harry T. Vernon Scholarship.

Lastly, but most importantly, I would like to thank my family. My parents, John and Gay, provided me with books, VHS tapes, and a 26 gallon aquarium that fueled my curiosity for the ocean as a child. I will always be indebted to them, my sister Lesley, and my brother Scott, for their love, support, and encouragement for me to follow my dream of studying ocean life. Finally, I would like to thank my wife and best friend Jenny who has been so patient and helpful throughout my graduate school career. I feel incredibly lucky to have such a wonderful person in my life.

TABLE OF CONTENTS

LIST OF TABLES

LIST OF FIGURES

CHAPTER 1: GENERAL INTRODUCTION AND SCOPE OF DISSERTATION

As outsiders, the ocean appears to be a uniform habitat lacking the wide array of ecological niches seen in the terrestrial world. The apparent uniformity of this fluid and seemingly well-mixed environment drove early ocean scientists, led by Victor Hensen, to mistakenly assume zooplankton found in net tows were uniformly distributed throughout the water; therefore, a few small volume samples could be used to characterize vast swaths of ocean (Hensen 1895; Wiebe and Benfield 2003). This assumption was challenged by Haekel (1890) who found evidence of plankton variability in both time and space and claimed Hensen's assumptions resulted in misleading conclusions. Despite this, the assumption of uniform or random plankton distributions was largely accepted until the 1950s, when the deployment of plankton pumps detected consistent strong variation between small scale samples (Barnes and Marshall 1951; Anraku 1956; Taft 1960), driving the investigation into the causes and consequences of plankton patchiness that continues to this day (Wiebe and Benfield 2003).

Plankton patchiness, through its effect on environmental conditions experienced by individual animals, is biologically relevant (directly or indirectly) for the life histories of almost all marine organisms from the smallest microbe to large cetaceans; however, research has strongly emphasized the impact of plankton patchiness on the population variability of commercially important fish populations. Hjort (1914) is credited with recognizing that processes in the larval phase have a large impact on adult population variability. Since average concentrations of prey for larval fish have been found to be insufficient for maintaining metabolic processes, larval fish must find patches of high

densities of prey (Lasker 1975; Davis et al. 1991). Vlymen (1977) used a search model to determine that anchovy larvae require a minimum of 30% above average food concentration to survive, thus random or uniform distributions would lead to mass starvation and recruitment failure. Detecting patches of food is thought to allow fishes to grow quickly through their most vulnerable stages, thus increasing their probability of survival into the juvenile stage (Miller et al. 1988).

In addition to fast growth through feeding, larval fishes must avoid a suite of potential predators (Bailey and Houde 1989; Houde 1987; Rothschild 1986), including larger fishes, ctenophores, polychaetes, chaetognaths, and medusae (Houde 2002). Llopiz and Cowen (2008) showed that most larval fishes were satiated, which indicates that predation is an important factor in determining larval survival. This is in contrast to earlier hypotheses that claim larval starvation to be a major source of mortality, i.e., Cushing's match/mismatch hypothesis (1975). It must be taken into consideration, however, that the Llopiz and Cowen (2008) study occurred in subtropical waters, where there is an absence of seasonal upwelling leading to plankton blooms. The vast difference between the subtropical environment and the temperate environment where Cushing developed his hypothesis suggests that different processes operate during the larval stage of fishes depending on prevailing oceanographic conditions in the region of interest. These hypotheses emphasize the potential differences in the mechanisms influencing patchiness across different ecosystems, but in all systems, the predator abundances and distributions are not well described due to sampling biases.

Larval fish habitat, defined as the spatio-temporal position of a larva that is characterized by the physical, biological, and chemical properties of that space (Werner

2002; Hernandez et al. 2009), changes most rapidly with depth (a possible exception is strong horizontal fronts) due to vertical stratification causing sharp environmental gradients. Depth patterns of fishes in relation to family and ontogenetic stage have been of interest in numerous studies (Cowen and Castro 1994; Leis 1991; Hernandez et al. 2009) because correlations of taxa with physical characteristics can suggest what may be driving their distribution i.e., transport to favorable recruitment areas, increased food availability, or predator avoidance. However, little is known about what fine-scale physical features and/or zooplankton densities are driving these patterns because sampling resolution has been inadequate (Cowen 2006).

Physical features influencing patchiness

A variety of physical features have been implicated in causing environmental heterogeneity that contributes to the formation of plankton patches, including fronts, thin layers, and pycnoclines, and this structure can be altered on relatively short time scales (hours to days) by the passage of eddies and internal waves. These physical features interact with biological processes of predation, reproduction, growth, and fine-scale behavior to further modify the distributions of organisms in time and space, resulting in what biological oceanographers interpret as plankton patchiness (Steele 1978). Thin layers, fronts, and internal waves are all features that likely play an important role in the structure of larval fish habitat but are poorly understood with regards to their impact on predator-prey interactions.

Thin layers are defined as horizontal aggregations of phytoplankton or zooplankton a few centimeters to meters thick, ranging up to kilometers in the horizontal

direction, and persisting for hours to days (Dekshenieks et al. 2001; Rines et al. 2002). Thin layers have become a topic of recent interest for biological oceanographers because of the potential trophic impacts of concentrated biological activity, and they also may provide a mechanism to subdivide the pelagic environment (Kiørboe 2008; Alldredge et al. 2002), much like vertical fronts. These extreme concentrations of organisms are thought to have a trophic impact, which likely increases with active accumulation of phytoplankton grazers within the layer (Cowles et al. 1998). These relatively dense layers of plankton can occur in a variety of marine systems including estuaries (Donaghay et al. 1992), coastal shelves (Cowles and Desiderio 1993), open ocean (Bjornsen and Nielsen 1991), and fjords (Holliday et al. 1998; Alldredge et al. 2002; Dekshenieks et al. 2001). With the advent of acoustic technology, thin layers can be more easily located within the water column, but little is known about the spatial positioning of different zooplankton taxa (McManus et al. 2005; Holliday et al. 1998). McManus et al. (2005) found that zooplankton thin layers were present in the daylight hours but dissipated in the evening; cycling in synchrony with diel vertical migration. Benoit-Bird et al. (2010) showed that thin zooplankton layers were only associated with thin phytoplankton layers when 18-20% of the full water column chlorophyll fluorescence was contained within the phytoplankton layer. This suggests that thin layers can have major trophic impacts, especially if they have very high biomass density relative to the surrounding water column.

There are a few physical conditions that seem to be necessary for thin layer formation. Thin layers tend to be associated with vertical temperature gradients and localized lack of turbulence (Cowles et al. 1998) but have also been detected in relatively

turbulent environments with large vertical density gradients (Wang and Goodman 2009). These layers can stretch for hundreds or thousands of meters and have been observed to persist for days even when physical properties of the water column change (Rines et al. 2002). A general rule for thin layer formation and persistence is that convergent forces must outweigh divergent ones (Stacey et al. 2007). Vertical location of thin layers typically is within or at the base of a pycnocline (McManus et al. 2005), but the presence of a pycnocline is not necessary for thin layer formation (Dekshenieks et al. 2001).

Biological processes such as active swimming and spatial variation in grazing rates are also involved in the persistence of thin layers (Cowles et al. 1998). While physical processes have more often been implicated for thin layer formation (Ryan et al. 2008), in reality, the influence of biological and physical factors likely exists on a continuum, with biological processes influencing the shape of the layers (Benoit-Bird et al. 2009). Stratified environments provide the conditions necessary for the formation of plankton thin layers or patches, which can form via a few different mechanisms: passive mechanisms, active aggregation, or spatially variable growth rates over time (Folt and Burns 1999). Passive mechanisms of aggregation would be most dominant if buoyancy is similar among taxa, as seen in thin layers of marine snow (MacIntyre et al. 1995). Copepods, one of the most dominant primary heterotrophs, have been shown to be able to change swimming speeds and stay within food patches at small scales, which likely allows them quickly respond to increased food concentrations (Tiselius 1992). High phytoplankton concentrations indicate which areas of the water column are most productive, yet they have been shown to be negatively correlated with zooplankton grazing rate (Folt et al. 1993), and, depending on the predominant species, can even have

negative impacts on zooplankton growth due the production of toxic aldehydes (Miralto et al. 1999; Tosti et al. 2003). Despite these potential deleterious effects, field studies have mixed observations of zooplankton in and around phytoplankton layers (Holliday et al. 2003; McManus et al. 2003) but sometimes distinctly separated vertically (Alldredge et al. 2002).

Internal waves, by propagating along pycnoclines, have the capacity to mix or break up plankton patches that tend to occur along density discontinuities. In coastal systems, internal waves form typically through the interaction of tidal currents with some form of abrupt topography (e.g. Stellwagen Bank- Halpern 1971; Lai et al. 2010, South China Sea- Klymak et al. 2006, New Jersey Shelf - Shroyer et al. 2011). Internal waves have been implicated as mechanisms of cross shelf transport (Shanks 1983; Shanks 1995; Lamb 1997), sediment resuspension (Butman et al. 2006), and nutrient input into the upper ocean layer (Brickman and Loder 1993). Haury et al. (1979, 1983) provided the first high resolution plankton abundance measurements in relation to internal waves, documenting zooplankton abundance and temperature out of phase with chlorophyll-*a* fluorescence. Thermocline depth after internal wave passage was deeper, while in front of the packet, the thermocline shoaled near the surface. The interaction of these features with the distributions of larval fishes in relation to predators (gelatinous zooplankton) and prey is unknown.

Sharp gradients in the physical environment can also occur in the horizontal direction. These zones where two different bodies of water meet are known as fronts, and they have been associated with a variety of ocean topographies such as seamounts, canyons, and shelf-breaks (see Genin 2004 for review). The interaction of currents with

these topographies often results in upwelling, enhancing the nutrient content of the frontal zone and leading to aggregation of zooplankton and fish. This kind of trophic cascade, known as bottom-up control, has been suggested by Mackas et al. (1997) who observed dense aggregations of euphausiids and Pacific hake near upwelling zones at the shelf-break off of Vancouver Island. For larval fishes, fronts can serve as a convergent mechanism by which they can obtain higher concentrations of food (Miller 2002). Fronts also can concentrate other zooplankton, such as hydromedusae. These osmoconformers (ion concentration inside equals the surrounding water) actively reduce their rate of swimming when salinity changes rapidly, causing them to aggregate at salinity fronts (Graham et al. 2001). Although fronts are known as regions of increased biological activity, they may include a tradeoff for larval fishes between increased food availability and increased predation. How fronts may influence the distributions of a variety of planktonic taxa is unknown mainly because, like the other physical features discussed, fine-scale spatio-temporal patterns have not been resolved, and many of the fragile gelatinous species are severely under sampled using traditional net-based sampling systems (Remsen et al. 2004).

Progression of sampling technology

Sampling of larval fishes, predators, and prey has evolved towards higher resolution systems, allowing for more process-oriented research into the early life stages of fishes. The importance of resolving finer scale vertical distributions is exemplified by the modification of sampling technology, as plankton nets evolved from the single opening Tucker trawls (Tucker 1951) to systems sampling multiple discrete depths (e.g.,

Davies and Barham 1969; Frost and McCrone 1974). Based on these Tucker trawl modifications, Wiebe et al. (1976) developed the Multiple Opening and Closing Net Environmental Sampling System (MOCNESS), enabling sequential net sampling at different depths to describe vertical changes in the plankton densities. Several modifications of the MOCNESS included the addition of fine-scale physical data sampling instruments (Burd and Thomson 1993) and the addition of double frames (Wiebe et al. 1985). Guigand et al. (2005) introduced further modification to MOCNESS by using two sub-systems, a 4 m^2 coarse mesh net and a 1 m^2 fine mesh net, to simultaneously sample fish larvae and their planktonic prey, revealing new information on the trophodynamics of the early life stages of fishes (Llopiz and Cowen 2008).

The general weakness of net based systems integrating spatially over a minimum of 10's of meters in depth led to the development of alternative techniques to elucidate even finer scale structure in the plankton. Acoustic methods have been used extensively to describe plankton concentration variability, and abundance estimates from these methods often do not agree with concentrations acquired from MOCNESS tows, indicating the presence of small scale patchiness (Holliday et al. 1989; Wiebe et al. 1996). Taxonomic identification is a limitation with acoustic methods as the sample volumes of many dominant zooplankton taxa do not correlate well with acoustic backscatter data (Wiebe et al. 1996), and it has been noted that different taxa can display unique backscatter signals, with smaller zooplankton often mimicking the signal of the surrounding water (Stanton et al. 1994).

The desire to sample on small scales with good taxonomic resolution has driven the recent development of camera-based systems, which, when combined with image

analysis software, can allow for automated taxonomic identification, thereby reducing the number of labor hours needed to complete biodiversity studies (Weeks and Gaston 1997). The video plankton recorder (VPR) (Davis et al. 1992) has been used to quantify zooplankton *in situ* and can accurately quantify small gelatinous organisms that are under-sampled by plankton nets (Benfield et al. 1996). The ability of the VPR and other camera based systems to preserve fragile organisms by imaging *in situ* has made it ideal for use in studies of colonial organisms (Dennett et al. 2002) and orientation of zooplankton (Benfield et al. 2000). Other imaging systems include the Shadowed Image Particle Profiling and Evaluation Recorder (SIPPER) (Samson et al. 2001), Optical Plankton Counter (OPC) (Herman 1988, 1992), and HOLOMAR underwater holographic camera system (Watson et al. 2003). These systems utilize different imaging techniques, but all are approaches to examine small scale planktonic distributions in the marine environment, with their own strengths and weaknesses associated with sampling a small volume of water. All target the most abundant members of the plankton community such as copepods, appendicularians, and several phytoplankton species.

A main division in these optical systems is between those which take images (e.g., VPR, SIPPER), allowing for taxonomic resolution, and those which count particles based on optical properties (OPC). The OPC is designed to count the number of particles present in the water column between 250 μm and 2 cm in size, but it has low taxonomic identification ability (Herman 1992). For this reason, it has been used in conjunction with net samples in a variety of studies (Woodd-Walker et al. 2000; Labat et al. 2002; Baumgartner 2003). However, Remsen et al. (2004) found that the OPC, when compared to SIPPER (collects images), underestimated particle density due to aggregation of many

mesozooplankton. They found that 29% of mesozooplankton were within 4 mm of their nearest neighbor, causing the OPC to count these groups of organisms as one particle, which was a significant source of error even in the oligotrophic waters of the Gulf of Mexico (Remsen et al. 2004). The OPC also severely under-sampled gelatinous organisms due to its requirement of opacity to enumerate particles. The researchers concluded that the best biomass estimates came from *in situ* imaging systems (such as SIPPER) that were not affected by particles being aggregated, detected gelatinous organisms, and provided some taxonomic identification ability.

Several imaging systems are specifically designed to sample larger volumes of water, allowing them to examine questions about the small scale distributions of larger, rarer mesozooplankton such as fish larvae, shrimps, polychaetes, and gelatinous organisms. These systems include the Zooplankton Visualization and Imaging System (ZOOVIS) (Benfield et al. 2003) and the Underwater Video Profiler (UVP) (Gorsky et al. 2000), but neither of them sample as much water per second as the *In Situ* Ichthyoplankton Imaging System (ISIIS), which uses silhouette photography (Ortner et al. 1979) with a small point source to image plankton across a large (40 cm) depth of field (Cowen and Guigand 2008). The combination of this shadowgraph imaging technique and a high-resolution (68 μm pixel size) line scan camera allows ISIIS to quantify organisms within a size range of 500 μm to 13 cm, sampling approximately 70 L s^{-1}. The only larger volume imaging system is the Large Area Plankton Imaging System (LAPIS) (Madin et al. 2006), but this system is designed to sample organisms at least several millimeters in size, as demonstrated by its 600 μm pixel resolution (much too large to resolve copepods, appendicularians, and small fish larvae). In addition, ISIIS is

towed at a speed of 5 kts, which is over twice as fast as a typical LAPIS or ZOOVIS tow speed of 1-2 kts (Madin et al. 2006; Trevorrow et al. 2005), minimizing the statistical bias introduced by vehicle avoidance (a common problem when sampling larger fish larvae and euphausiids). The UVP is towed vertically like a CTD (conductivity, temperature, and depth measurer) at a speed of 1 m s^{-1} (Gorsky et al. 2000), making it also inadequate to sample faster moving plankton. In many ways, ISIIS bridges the gap between the large volume and small volume camera systems by combining large volume capabilities and fast tow speed with a high-resolution camera.

The goal of this dissertation is to utilize a novel, high-resolution imaging system (ISIIS) to investigate ubiquitous fine-scale physical features and their impact on the distributions of larval fishes, their prey (copepods and appendicularians), and potential predators including ctenophores, siphonophores, medusae, polychaetes, and chaetognaths. Fine-scale spatial relationships of these organisms with oceanographic boundaries and other taxa can provide indirect evidence of drivers of plankton distributions causing plankton patchiness. The second chapter of this work describes the fine-scale abundances of a variety of gelatinous zooplankton in Monterey Bay and their spatial relationships to copepods, appendicularians, and diatom-dominated thin layers. Application of automated particle counting provided unique information on particle size distributions and a foundation for some of the image processing techniques used in subsequent chapters. The third chapter focuses on tidally generated internal waves near Stellwagen Bank and their impact on the distributions of larval fishes, prey (copepods), zooplankton predators, and patch characteristics, utilizing different ISIIS sampling patterns to resolve horizontal and vertical patterns. The interaction of these waves with a

near surface copepod thin layer is also described. While chapters 2 and 3 are primarily focused on vertical gradients and their modification, the fourth chapter describes fine-scale abundances of fish larvae, zooplankton, and particles in relation to a shelf slope front containing strong horizontal gradients in salinity and density. This chapter also utilizes a solidity metric to quantify the composition of each enumerated particle. In total, this body of work describes fine-scale abundances of planktonic organisms in relation to oceanographic boundaries in both the horizontal and vertical directions, lending insight into processes influencing the distributions of many taxa. In addition, fine-scale pattern descriptions can improve the calculations of trophic transfer and encounter rates (Sutor and Dagg 2008), providing biological oceanographers with a more mechanistic understanding of the development of plankton patchiness and how it may affect the survival of larval fishes.

CHAPTER 2: RELATIONSHIPS BETWEEN PHYTOPLANKTON THIN LAYERS AND THE FINE-SCALE VERTICAL DISTRIBUTIONS OF TWO TROPHIC LEVELS OF ZOOPLANKTON

Thin layers of phytoplankton are well-documented, common features in coastal areas around the world, but little is known about the relationships of these layers to higher trophic levels. We deployed the *In Situ* Ichthyoplankton Imaging System (ISIIS) to simultaneously quantify three trophic levels of plankton, including phytoplankton, primary consumers (copepods and appendicularians), and secondary consumers (gelatinous zooplankton). Over a two week sampling period, phytoplankton thin layers, primarily composed of *Pseudo-nitzschia* spp., were common on two of the five sampling days. Imagery showed copepods aggregating in zones of lower chlorophyll-*a* fluorescence, while appendicularians were more common at greater depths and higher chlorophyll-*a* levels. All gelatinous zooplankton generally increased in abundance with depth. *Bolinopsis* spp. ctenophores underwent a "bloom," and they were the only species observed to aggregate within phytoplankton thin layers. The vertical separation between copepods, phytoplankton, and gelatinous zooplankton suggests that copepods may use the surface waters as a predation refuge, only performing short migrations into favorable feeding zones where gelatinous predators are much more abundant. Thin layers containing dense diatom aggregates obstruct light reaching deeper waters (>10 m), which may allow gelatinous zooplankton to avoid visual predation as well as improve the effectiveness of contact predation with copepod prey.

Background

Thin layers are dense aggregations of phytoplankton or zooplankton spanning a few centimeters to meters in depth and sometimes several kilometers horizontally (Dekshenieks et al. 2001; McManus et al. 2003). Concentrations of organisms within thin layers can be orders of magnitude greater than above or below the layer (Donaghay et al. 1992), and persist on time scales of hours to days depending upon physical, chemical, and biological conditions (Sullivan et al. 2010). Thin layers are of interest ecologically because they may serve as zones of enhanced biological interactions in the vertical dimension (Alldredge et al. 2002), much like fronts do in the horizontal, with the trophic impact of a thin layer increasing in relation to its temporal persistence (Cowles et al. 1998). As thin layers can occur in a variety of marine systems including estuaries (Donaghay et al. 1992), coastal shelves (Cowles and Desiderio 1993), and fjords (Holliday et al. 1998; Alldredge et al. 2002; Dekshenieks et al. 2001), they may be important contributors to community structure in shallow water environments.

Trophic interactions in relation to phytoplankton thin layers are influenced by the degree of spatial overlap between thin layers, grazers, and zooplankton predators. While it may seem that grazers would seek an aggregated food source within thin layers, several studies have produced counter-intuitive results where grazers were found to spend a majority of time just outside of a thin layer (Bochdansky and Bollens 2004; Benoit-Bird et al. 2010; Talapatra et al. 2013). One possible explanation for these observations is that zooplankton predators (including gelatinous zooplankton) may influence the distribution of grazers through predation or modification of grazer behavior. Linking the distribution of phytoplankton, zooplankton, and gelatinous zooplankton aggregations is challenging

due to sampling limitations. For example, the relative positioning of different zooplankton taxa in relation to phytoplankton thin layers is poorly described (Holliday et al. 1998, 2003, 2010) because it is difficult or impossible to distinguish acoustic returns from organisms of similar acoustic impedance (typically similarly sized). Further, common gelatinous zooplankton are extremely difficult to sample with traditional net sampling systems [e.g., MOCNESS (Wiebe 1976)], which destroy fragile gelatinous bodies. Gelatinous zooplankton are also thought to have low acoustic detectability, except for large (> 10 cm) specimens (Monger et al. 1998; Brierley et al. 2005), thus their association with thin layers and grazers was not known until this contribution.

Although gelatinous zooplankton are known to aggregate within temperature discontinuities (Arai 1976; Graham et al. 2001), field studies relating gelatinous zooplankton distributions to the well-understood physical processes of thin layer formation are limited. The frontal zone at the edge of the upwelling shadow has been implicated as a retention mechanism for the large (30 cm bell diameter) scyphomedusa *Chrysaora fuscescens*, with highest concentrations located near the thermocline (Graham 1994). Hydromedusae have been found to be abundant in Monterey Bay (Raskoff 2002) and consistently aggregate in salinity discontinuities, regardless of whether or not prey is present, indicating that they may use physical cues to aggregate there (Frost et al. 2010).

In Monterey Bay, CA, USA, thin layers of phytoplankton typically form during upwelling favorable (northwesterly) winds when the northern (sheltered) region of the bay tends to be thermally stratified (Graham and Largier 1997; McManus et al. 2008). The upwelling season spans between the months of March-October (Pennington and Chavez 2000). During upwelling events, cold, nutrient-rich filaments cross the mouth of

the Bay (Rosenfeld et al. 1994), and a cyclonic gyre, known as the "upwelling shadow," forms in the northeastern part of the bay. When present, the upwelling shadow increases the surface water residence time in the Bay (Breaker and Broenkow 1994; Graham and Largier 1997). Water in the upwelling shadow is sheltered from the winds, which results in decreased mixing, and diurnal heating results in high thermal stratification (Graham 1993). These characteristics provide optimal conditions for thin layer formation. Density discontinuities formed via thermal stratification may serve as a mechanism to slow the sinking rate of particles, creating thin phytoplankton layers of non-motile organisms such as diatoms (MacIntyre et al. 1995; Alldredge et al. 2002). When the upwelling winds subside or reverse direction, *i.e.*, "relaxation events," surface waters in the upwelling shadow zone are advected from the Bay to the northwest within 2-3 days if the event persists (Woodson et al. 2009). Under these conditions, California Current waters, characterized by relatively warm temperatures, low salinity, and low nutrient concentrations (Rosenfeld et al. 1994; Ramp et al. 2005; Ryan et al. 2008, 2009) are advected towards shore to replace exiting waters, disrupting the stratified conditions favorable to thin layer formation.

To elucidate trophic effects of phytoplankton thin layers and directly sample the gelatinous community, we deployed a towed *In Situ* Ichthyoplankton Imaging System (ISIIS) (Cowen and Guigand 2008) to synoptically sample zooplankton abundance and related environmental parameters (including chlorophyll-*a* fluorescence) in northern Monterey Bay. The goals of this study were: 1) to describe the environmental conditions and their relationship to thin layers, 2) to relate fine-scale changes in abundance of different zooplankton taxa to environmental conditions, and 3) to compare and contrast

the fine-scale vertical distributions of three distinct planktonic trophic levels (phytoplankton, primary consumers, and gelatinous zooplankton), their relationship to physical discontinuities, and the implications for predator-prey interactions.

Materials and Methods

Study site and sampling period

Monterey Bay is an open embayment located on the central coast of California, USA. The study area was in the northeastern part of the bay where the upwelling shadow tends to form during active upwelling (Fig. 1). All sampling was conducted over 5 days between June 28 and July 7, 2010 in conjunction with a large physical oceanographic study investigating lateral mixing on the inner shelf (Woodson et al. in revision).

Moored vertical profiler and wind data

To continuously monitor hydrographic and chlorophyll-*a* fluorescence variability in northern Monterey Bay waters, an autonomous vertical profiler (Brooke Ocean Technology SeaHorse) was deployed on the 20 m isobaths, in the center of the ISIIS sampling array at 36.9325˚N 121.9244˚W. The SeaHorse provided profiles every 30 minutes from near-surface to near-bottom with a Sea Bird 19 CTD, a Sea Bird 43 Oxygen sensor, and a Wet Labs WetStar fluorometer with a sampling frequency of 4 Hz. For the period between July 5 and July 7, 2010, the SeaHorse collected data on 54% of its profiles. Some data loss occurred near the end of deployment due to issues with the gripper mechanism, creating gaps in the time series.

Regional scale wind forcing (and thus upwelling/relaxation conditions) was obtained using hourly averaged wind velocities from the National Data Buoy Center's buoy number 46042 located at 36.789˚N 122.404˚W, about 51 km WSW from the profiling sites. The direction and magnitude of these winds indicate whether or not active upwelling was occurring.

Imaging system sampling

The *In Situ* Ichthyoplankton Imaging System (ISIIS) contains a Piranha II line scan camera from Dalsa with 68 μm pixel resolution, imaging plankton in the size range of 680 μm to 13 cm. ISIIS uses a shadowgraph imaging technique, in which a collimated light source is projected across a sampled parcel of water, and the silhouettes created by the plankton blocking the light source are then captured by the camera (Cowen and Guigand 2008). The ISIIS line scan camera shoots a continuous image at 36,000 scan lines per second, but parses the image into frames that correspond to a 13 cm x 13 cm area of view with a depth of field of *ca.* 35 cm, giving an individual image volume of 6.4 L. At the usual tow speed (2.5 ms^{-1}), 1 m^3 of water is sampled every 7.7 s. In addition to the camera system, ISIIS was equipped with motor actuated fins for depth control, a Doppler velocity log (600 micro, Navquest), and environmental sensors including a CTD (SBE49, Seabird Electronics) and fluorometer (ECO FL (RT), Wetlabs – chlorophyll-*a* fluorescence). All sensors sampled the water < 1 m above the imaging area at a rate of 2 Hz, and a correction was applied to address this offset.

The system was deployed in a "tow-yo" fashion behind an 18 m research vessel, the R/V Shana Rae, running at a constant speed of 2.5 ms^{-1} through the water, with

approximately 4-5 water column undulations per transect from the near surface to a maximum depth of ~18 m to stay at least 5 m from the bottom. A total of ten transects (3 km each) centered over the 20 m isobath were performed on each day of sampling (Fig. 1), with the exception of July 5, when only five transects were completed due to temporary technical issues. All sampling was conducted during the day except for samples on June 30, which were collected at night. Due to the optical technique utilized by ISIIS, ambient light has no effect on image quality (Cowen and Guigand 2008).

Thin layer identification

In the ISIIS profiles, thin layers of fluorescence were defined as in Sullivan et al., (2010), but the maximum layer thickness criteria was adjusted from <3 m to <5 m (*sensu* Sevadjian et al., submitted). The method in Sullivan et al. (2010) describes the intensity and thickness of the chlorophyll maximum in each fluorescence profile. ISIIS chlorophyll-*a* profiles were first smoothed using a low pass filter, and the first derivative was calculated to determine background fluorescence, layer thickness, and intensity. The depth of the fluorometer was calculated using the pressure sensor mounted on the upper pod of ISIIS and corrected for the minor physical offset and vehicle pitch.

Phytoplankton sampling

Water samples were taken to assess the phytoplankton community on the days of ISIIS sampling using a 5-L Aquatic Research Instruments discrete point water sampling bottle attached < 0.2 m from the intake tubes on a high-resolution profiler on a separate small vessel. The bottle was triggered using real time depth and chlorophyll-*a*

fluorescence activity, with samples taken near surface (~3 m), within the chlorophyll maximum, and below the chlorophyll maximum (>15 m). The bottle samples were stored on ice and gently mixed before analysis in the lab within 5 hours of returning from the field. Phytoplankton were counted and identified to genus using a PhycoTech 0.066 mL phytoplankton counting cell at 40X magnification and a Zeiss A1 Axoioscope. Triplicates were performed for each sample and averaged.

Image data analysis

ISIIS images were viewed using the VisionNow software (Boulder Imaging, Inc.), and a standard 'flat-fielding' transformation was applied to remove background noise from each image. For quantification of gelatinous zooplankton, three vertical profiles from each of ten daily transects were examined (30 profiles on each sampling day, 15 profiles on July 5). The profiles were approximately evenly spaced across the study area (~1 km separation) and corresponded to different sections of the transect (offshore, middle, and inshore). We refer to these units as 'profiles' even though they spanned a horizontal range of ~300 m and an average depth of 15 m (~5 meters above bottom). Gelatinous zooplankton were identified to genus or species level. Identifications of the ctenophores and siphonophores were verified by experts in the field.

Measurements of length and angle of swimming orientation were made for a subset of ctenophore specimens (n = 225 for *Pleurobrachia* spp., n = 274 for *Bolinopsis* spp., n = 200 for *Bolinopsis* spp. size frequencies). The angle of orientation of the mouth (an indicator of general swimming direction) was measured using ImageJ v1.44p (Rasband 1997-2012) by bisecting the imaged specimen from aboral to oral end. The

software recorded the orientation angle and length of each specimen. Differences in size distributions of *Bolinopsis* spp. ctenophores among days were assessed using one-sided Komolgorov-Smirnov tests. For sampling the highly abundant copepods and appendicularians (< 5 mm in size), 1/6th of a frame was subsampled on one profile from each transect (10 profiles per day), and 1 out of every 20 frames was examined, generating ~2 samples per m of depth on each profile. This subsampling procedure was sufficient because there were typically several copepods and appendicularians in each image.

Because diatom aggregates (also known as 'flocculations' or 'flocs', Alldredge et al., 2002) were overwhelmingly the most common specimen in the images, we could use automated particle analysis available in ImageJ (Rasband, 1997-2012, 'Particle Analyzer') to calculate particle size and shape features from one profile through a thin layer on July 5. First, images were thresholded (converted to black and white pixels), and particles greater than 250 pixels in size were counted and sized, which effectively removed all of the copepods and appendicularians. ImageJ's 'Particle Analyzer' measured the major and minor axis of an ellipse fit to each particle, and the information from the maximum sized particle per frame was extracted. Since most of the diatom flocs were oblong in shape, the minor axis was used as a proxy for diameter. The ratio of the major to minor axis was used as a shape descriptor (lower values mean the particle is round – higher values more oblong). Values in pixels were converted to mm based on a known 13 cm field of view. Thin layer particles from June 28 were not measured because flocs were so dense that individual particles could not be distinguished for analysis.

Data processing and GLMMs

Physical and biological data were merged to yield to precise environmental values (temperature, salinity, depth, and chlorophyll-*a* fluorescence) for each jelly found in the images. To obtain average vertical distributions, all 30 profiles from each day were used, and the volume sampled in each 1 m depth bin was calculated based on the amount of time ISIIS spent in that depth bin. Counts of copepods and appendicularians were converted to concentrations by calculating the volume of water sampled in $1/6^{th}$ of an ISIIS image and multiplying. Data analysis and visualization was performed in R (v2.15.2) (R Core Team 2012) using the packages "plyr" (Wickham 2011) and "ggplot2" (Wickham 2009).

Physical and biological data were processed to quantify average environmental values and the total count of each jelly taxon for each m^3 of water sampled with ISIIS. This was accomplished by binning jelly data by the time it took to sample 1 m^3 of water (7.7 s) to yield ind. m^{-3} for each jelly taxon; only the five most abundant taxa (*Pleurobrachia* spp., *Bolinopsis* spp. (small and large size classes), *Eutonina indicans*, *Muggiaea* spp., and *Sphaeronectes* spp.) were binned. Then, using the average timestamp within each jelly bin, each jelly count per m^3 was matched to the nearest timestamps of chlorophyll-*a* fluorescence, temperature, salinity, and depth. Depths and the thin layer analysis (discussed previously) were used to create thin layer categorical variables: each m^3 was characterized as being "Above a thin layer", "Within a thin layer", "Below a thin layer", or "Thin layer absent from profile."

Generalized Linear Mixed Models (GLMMs) with log link function were implemented to determine the influence of sampling date, depth, fine-scale chlorophyll-*a*

fluorescence, and thin layer categorical variables (no thin layer, above, below, and within thin layer) on the number of gelatinous organisms per m^3. Although many ecological processes are expected to be nonlinear, preliminary plots showed some linear trends with respect to several explanatory variables. Also, the use of a linear model allowed for more intuitive interpretation of coefficients (similar interpretation as standard least squares modeling). Due to the collinearity of depth and temperature, temperature was dropped from the model, and salinity was removed because there was little change along each profile. Models were fitted in R (v2.15.2) (R Core Team 2012) with the package 'lme4' (Bates et al. 2012) using the Laplace approximation, and the significance of model coefficients was assessed using Wald Z tests. Interaction terms were not used because they can obscure the effects of the individual predictor variables (Gotelli and Ellison 2004), and preliminary analyses produced no indication of strong interactions.

GLMM is an approach to generalized linear modeling that allows for a correlation structure to be incorporated into a model by differentiating between fixed and random effects. For this study, the spacing of organism counts was on the scale of meters; therefore, there was the potential for adjacent observations to be correlated (violation of independence) within a sampling profile (Zuur et al. 2009). This correlation structure was accounted for by including the profile number as a random effect in the model. The model output produces coefficients that are proportional to the effect of a 1 unit increase of the variable on the expected concentrations of the organisms. Therefore, a positive coefficient indicates that the response variable (organism concentration) will increase in proportion to the value of that coefficient. GLMMs allow for modeling non-normal distributions (e.g., Poisson, binomial, etc.), and the use of random effects which

essentially enables the user to parse out clusters of data that may contain autocorrelation (Bolker et al. 2009). Correlation of residuals that was present when performing ordinary generalized linear modeling was eliminated through the use of a random profile effect.

Indices of patchiness and spatial overlap

While the random effects within the GLMM accounted for autocorrelation within a profile, a more intuitive measure of patchiness over the entire sampling area was obtained using the scale independent Lloyd's index of patchiness (Lloyd 1967).

$$\text{Patchiness} = 1 + [(\sigma^2\text{-m}) / m^2] \quad \text{(eq. 1)}$$

σ^2 is the sample variance and m is the sample mean. A random distribution was assumed to follow the properties of the Poisson distribution, having equivalent means and variances, and would therefore have a patchiness index of 1. Indices > 1 indicated aggregation of organisms. Lloyd's patchiness was applied for each day of sampling across all 1 m^3 sample bins.

To investigate the degree of spatial overlap of copepods and appendicularians with gelatinous predators, a spatial overlap index (O) was used (Williamson and Stoeckel, 1990):

$$O = \frac{\sum_{z=1}^{m}(N_z * n_z)m}{\sum_{z=1}^{m}(N_z) * \sum_{z=1}^{m}(n_z)} \quad \text{(eq. 2)}$$

z represents the depth strata, *m* is the number of depth strata sampled. N_z and n_z correspond to the concentration of copepods or appendicularians and the concentration of gelatinous zooplankton, respectively. If the overlap index > 1, this indicates spatial overlap of taxa. An index < 1 indicates spatial separation. The index was calculated for each profile measured for copepods and appendicularians. To give an adequate number of

samples per strata (>10), data were pooled into 3 m depth strata, and all samples taken below 15 m were discarded because depth was variable among profiles.

Results

Water column properties and thin layers

The study period (July 28 to July 7, 2010) began after ~14 days of generally consistent upwelling favorable winds (Fig. 2.2A). However, a small relaxation event on June 28 and brief relaxation events shortly after likely led to a breakdown in thermal stratification in the study area by June 30 (Fig. 2.2B). Although upwelling (northwesterly) winds became consistent after June 30, persistent, strong stratification did not occur again until July 5. The winds on July 5 weakened and changed direction, but stratification did not decrease until the final day of sampling (July 7) when the winds had been calm for 2-3 days. July 7 was marked by lower overall chlorophyll fluorescence activity (mean chlorophyll-*a* maximum 1.004 volts), and reduced thermal stratification. Salinity was fairly constant throughout the study (Δ 0.06), but the autonomous profiler showed a distinct small drop in salinity just prior to the July 2 sampling date (Δ 0.03), potentially indicating the influx of California Current water (J.P. Ryan, MBARI, pers. comm.). However, temperature/salinity diagrams from a concurrent study (Woodson et al. in revision) demonstrated that offshore influx of water was minimal.

Thin layers were present on all days of sampling with the exception of June 30, which was the only sampling performed at night. Thin layers were most common on June 28 and July 5 (thin layers observed on 47% and 87% of profiles with thin layers, respectively), which were also the days with higher chlorophyll-*a* maxima and strong

thermocline and oxycline (Table 2.1, Fig. 2.2B). *Pseudo-nitzschia* spp. was the dominant phytoplankter on all sampling days with some temporal variation in concentration (see Timmerman, 2012).

Automated particle counting revealed changes in the fine-scale structure of diatom flocs above, within, and below a thin layer. Above the layer, particles were few in number but increased in concentration and size with depth (Fig. 2.3A). The higher major to minor axis ratio indicates the particles above the layer were oblong in shape and likely sinking (Fig 2.3B). Within the high chlorophyll-*a* thin layer, flocs were numerous, large in size, and relatively round (Fig. 2.3). Below the layer, flocs were few in number but highly variable in size and shape.

Copepod and appendicularian abundances and vertical distributions

Copepods and appendicularians displayed strong temporal variability in both their overall abundances and vertical distributions. Mean copepod concentration was highest on days when thin layers were present, but the vertical distributions indicate that they did not aggregate within zones of high chlorophyll-*a* fluorescence (Table 2.1, Fig. 2.4). Mean appendicularian concentration was highest on the last day of sampling (July 7). Lloyd's index of patchiness was consistently >1 for both groups on all days, indicating that there was aggregation (Table 2.1).

The GLMMs revealed differences between the vertical distributions of appendicularians and copepods. When a thin layer was present in a profile, appendicularians were more abundant in all zones of the water column, while copepod concentrations were not influenced by the presence of thin layers (Table 2.2). The two

groups had opposing responses to chlorophyll-*a* fluorescence; copepods, although not influenced by thickness of the chlorophyll-*a* maximum, generally tended to aggregate outside of zones of high cholorophyll-*a*, and appendicularians were slightly more common when chlorophyll-*a* was higher (Table 2.2). The model results are supported by 1 m bin averaged concentrations (Fig. 2.4), where copepods displayed a bimodal distribution with peak concentrations outside the zones of high chlorophyll-*a* fluorescence, whereas appendicularians showed a weak increase in abundance with depth and near zones of higher chlorophyll-*a*. The spatial overlap index showed that appendicularians consistently had more fine-scale spatial overlap with gelatinous zooplankton than did copepods, with an exception being the one night sampling period when the overlap indices were approximately equal (June 30, Fig. 2.5).

Gelatinous zooplankton abundance and vertical distribution

A total of 35,208 gelatinous animals were identified in the ISIIS profiles. Five species groups were most common, including *Pleurobrachia* spp. and *Bolinopsis* spp. ctenophores, *Eutonina indicans*, and the siphonophores *Muggiaea* spp., and *Sphaeronectes* spp. (Fig. 2.6). There were also several other species encountered in the images, including rare taxa such as *Sarsia tubulosa*, hydromedusae from the family Pandeidae, anthomedusae from the family Moerisiidae, and the scyphomedusa *Chrysaora fuscescens*. *Bolinopsis* spp. was divided into two size classes because initially many small ctenophores without tentacles were extracted from the images, but it was later determined that almost all (>99%) of these ctenophores were juvenile *Bolinopsis* spp.

Overall abundances and the vertical distributions of the five most common gelatinous taxa (Fig. 2.6) changed dramatically throughout the study period. On June 28 abundances were low, but there were distinct vertical patterns with *Pleurobrachia* spp. most abundant near the surface, all taxa relatively common near the chlorophyll-*a* fluorescence maximum, and *Eutonina indicans* was more common at depth (Fig. 2.7). By July 2, *Eutonina indicans* and small *Bolinopsis* spp. were the most abundant, with *Eutonina indicans* highly patchy and aggregated at depth (Table 2.3, Fig. 2.7). July 5 was marked by a significant increase in *Bolinopsis* spp. ctenophores (0.54 instantaneous exponential growth rate between July 2 and July 5 – assuming no advection), as well as peak abundances for the other two ctenophore groups (Fig. 2.7). The two siphonophore species (*Muggiaea* spp. and *Sphaeronectes* spp.) also reached relatively high abundances on July 5 and remained common on July 7 (Fig. 2.7). The concentration of all six common jelly taxa combined tended to increase in relation to depth on all days of sampling (except for June 28), regardless of the prevalence of thin layers (Table 2.4, Fig. 2.7).

Generalized Linear Mixed Models (GLMMs) with a random profile effect accounting for small scale autocorrelation revealed different influences of biological and physical parameters among gelatinous taxa. Model coefficients showed taxa were more likely to be present and in higher concentrations (counts) at greater depths, and they were highly aggregated in their distributions (Tables 2.3 and 2.4). *Eutonina indicans* was most abundant at greater depths and had the most aggregated distribution, with extremely high concentrations on July 2 (maximum concentration of 251 ind. m^{-3}). Concentrations of *Bolinopsis* spp. were positively influenced by higher chlorophyll-*a* (Table 2.4), while the

concentrations of other taxa were either slightly elevated (*Pleurobrachia* spp.) or unaffected. Only *Bolinopsis* spp. was more abundant within thin layers, but several taxa were in higher concentrations below thin layers (Table 2.4).

Measurements of *in situ* orientation and daily size structure were made as indicators of behavioral characteristics and growth, respectively, of ctenophores within the bay. The *in situ* orientation of the *Bolinopsis* spp. ctenophores indicated that they were typically cruising the water column vertically, with oral end (and lobes) pointed down, perpendicular to the thin layers and/or chlorophyll maximum (Fig. 2.8A), while *Pleurobrachia* spp. had less consistent orientation (Fig. 2.8B), though with a predominately vertical (oral end up) orientation. Length/frequency histograms of a subsample *Bolinopsis* spp. ctenophores for each day show a significant increase in size on subsequent sampling days (one-sided Komolgorov-Smirnov tests, Fig. 2.9). A linear growth rate extracted from the modal size (rounded to nearest 0.2 mm) was 0.45 mm d^{-1}, assuming ctenophores are being sampled from the same population.

Discussion

Fine-scale distribution data obtained by ISIIS showed strong vertical heterogeneity in three separate trophic levels including phytoplankton, primary consumers, and gelatinous zooplankton, with >2 orders of magnitude difference between surface and 15 m depth concentrations of the jellies. Water column stratification likely caused passive accumulation of non-motile diatoms *Pseudo-nitzschia* spp., the most abundant phytoplankter in the study area. Thin layers were most common on days when the water column was thermally stratified (June 28 and July 5), and GLMMs fit to

organism counts per m^3 showed differing patterns between zooplankton taxa in relation to thin layers, chlorophyll-*a* fluorescence, and depth.

Diatom dominated thin layers and primary consumers

The temporal persistence was the primary difference between the thin layers on June 28 and July 5, and the lack of motility of the dominant phytoplankter had a large influence on the assumed mechanism of formation. The layer on June 28 could have been present for up to 10 d due to consistent, strong upwelling winds before the study began. Because of these winds, the upwelling shadow had likely retained water within the bay for up to 14 d, with *Pseudo-nitzschia* spp. located at the base of the pycnocline. These non-motile diatoms have been previously shown to accumulate at density interfaces (MacIntyre et al. 1995; Cheriton et al. 2009), and high thermal stratification likely kept *Pseudo-nitzschia* spp. in a thin layer near the pycnocline on June 28, but the diatoms were possibly actively growing above the layer where oxygen was relatively high (ΔO_2 2.1 mL L^{-1}). The thin layer on July 5 was also driven by thermal stratification but was newly formed and had higher abundances of smaller phytoplankton (Timmerman 2012). Size/shape descriptors obtained from thin layer particles on July 5 is consistent with the concept of diatoms flocculating and settling at a thermocline because within the thin layer, particles were larger, rounder, and more abundant. In other cases, thin layers are composed of motile species of phytoplankton, such as the dinoflagellate *Akashiwo sanguinea* (Rines et al. 2009). In these later cases, behavioral cues, rather than sinking and settlement in diatoms, may play a more important role.

Although there was a non-uniform distribution of fluorescent activity on all days, the primary diatom consumers, copepods, were not found in high concentrations within thin layers. A GLMM showed a negative influence of chlorophyll-*a* on copepod concentrations. Copepods were typically most abundant near the surface, where chlorophyll-*a* fluorescence was low, and also sometimes aggregated below thin layers (July 5). Copepod aggregations outside of chlorophyll-*a* maxima have been documented previously using water samples and acoustic methods (Herman 1983; Nielsen et al. 1990; Jaffe et al. 1998; Alldredge et al. 2002; McManus et al., 2005; Holliday et al. 2003, 2010). The thin layers on July 28 were deeper, more intense in their chlorophyll-*a* fluorescence, and thicker than the layers on July 5 (Table 1), which may have affected the vertical distributions of copepods. *Pseudo-nitzschia* spp. in our study was producing the toxin domoic acid, which has been demonstrated to inhibit grazing in krill (Bargu et al. 2006; Timmerman et al. in press), and it may have a similar effect on other grazers, such as copepods, thereby increasing the persistence of a bloom. Although domoic acid has been shown experimentally to have no effect on feeding and growth in copepods (Lincoln et al. 2001), copepods could still preferentially occupy waters that contain fewer toxins. There were indications of bimodal vertical distributions in copepods on all sampling days, with the exception of June 30, which was the only night sampling period and had a deeper and diffuse chlorophyll-*a* profile (no thin layers). Even on the night of June 30, the copepods were not observed to aggregate inside the zone of high chlorophyll-*a* fluorescence. Diatoms within thin layers tended to form dense flocs; it is possible that on the edges of thin layers, copepods may find diatoms in a more ‘palatable’ form, or they utilize short excursions into the layers to feed (Bochdansky and Bollens 2004).

Vertical distributions of zooplankton predators and prey

Although depth was not a significant predictor variable in the GLMM, copepod peak abundances tended to occur within the shallowest 5 m of the water column, where chlorophyll-*a* levels and gelatinous predator abundances were low. For every profile, the lowest measured values of chlorophyll-*a* fluorescence were found near the surface, which tended to be dominated by copepods. In contrast, *Bolinopsis* spp. ctenophores were particularly abundant within and below thin layers (and at greater depths in general). The spatial overlap index between copepods and gelatinous zooplankton was < 1 indicating spatial separation, which is consistent with the concept of predation avoidance. Thus, it is possible that the copepods in Monterey Bay use the surface as a predation refuge and make short bouts into the deeper predator infested waters to feed. Such a strategy would allow the copepods to minimize their predation risk while still being able to feed, and is consistent with the 'predation avoidance' hypothesis of vertical migration (Zaret and Suffern 1976) supported by several copepod behavior studies (e.g., Neill 1990; Dawidowicz et al. 1990). Field evidence has also shown that copepods vertically migrate depending on their body condition, only risking vertical migration into predator heavy zones if their oil sac is depleted (Hays et al. 2001). In addition, copepods grow faster and reproduce more in water with higher temperatures (Bonnet et al. 2009), so occupying the surface waters could have multiple positive effects on the population.

Appendicularians had a positive relationship with depth and chlorophyll-*a* fluorescence, potentially due to less predation pressure (as compared to copepods). Of the species in this study, appendicularians are only known to be preyed upon by *Eutonina indicans* (Wrobel and Mills 1998), so when compared to copepods, the predation risk of

occupying thin layers is likely substantially less. Food availability, therefore, may be the primary influence on their distributions. Appendicularians are capable of feeding on a wide range of phytoplankton sizes, including pico and nanoplankton, which are abundant in nutrient-poor offshore waters of Monterey Bay (Ryan et al. 2009). The positive association of appendicularians within and around thin layers may indicate that properties associated with thin layer formation (i.e., water column stability and concentrated sources of phytoplankton) are favorable to appendicularian population growth.

Gelatinous zooplankton (predators of copepods and appendicularians) were more abundant at greater depths on all sampling days, regardless of the stratification regime present, and this pattern may exist due to a combination of three factors: negative effects of copepods on gelatinous zooplankton reproduction, contact predator advantages, and avoidance of visual predators. Copepods demonstrated less spatial overlap with jellies compared to appendicularians. Although the ctenophores in this study tend to consume copepods (Reeve et al. 1978; Greene 1986), they have a complex relationship with these prey. Studies using enclosures of ctenophores have shown that high concentrations of copepods can severely reduce the survival of larval ctenophores (Stanlaw et al. 1981). Therefore, above certain prey concentrations, ctenophores may become less effective predators due to inhibited reproductive success. Another potential benefit to jellies occupying deeper waters is that ambient light levels influence the competitive advantage of contact versus visual predation. An experiment by Sørnes and Aksnes (2004) demonstrated that *Bolinopsis* spp. feeding reaches an asymptote at high prey concentrations, and when light levels are lower, tactile predation becomes more advantageous than visual predation. While irradiance was not measured in this study, a

previous study in the same area found that several wavelengths of light experience ~100 fold reductions below a thin layer of *Pseudo-nitzschia* spp. in Monterey Bay (Sullivan et al. 2010). Attenuation of light was almost certain to increase in the region of the pycnocline during our study, with diatom flocs larger and more abundant within thin layers. The thin layer of *Pseudo-nitzschia* spp., therefore, could set up microhabitats in which visual predation on copepods dominates above the thin layer (perhaps by planktivorous fishes), while tactile predation is more advantageous below. Jellies also have many visual predators (Oviatt and Kremer 1977; Link and Ford 2006) that can likely be avoided by occupying zones of lower light levels. Therefore, surface waters may be zones of the water column where jellies are less fecund, inferior predators (outcompeted by visual predators), and exposed to higher visual predation by their own suite of predators.

Gelatinous zooplankton and diatom thin layers

The idea of jellies aggregating at density discontinuities is not new (Arai 1976; Mills 1984; Graham et al. 2001; Jacobsen and Norrbin 2009), but the results of this study demonstrate that only one species (*Bolinopsis* spp.) tends to aggregate within thin layers and vertical density discontinuities. This may indicate that the vertical swimming of *Bolinopsis* spp. results in increased probability of thin layer encounter, as species with a horizontal or random swimming pattern would not be expected to encounter vertical density discontinuities as frequently as a vertical swimmer. Indeed, the *Bolinopsis* spp. ctenophores in this study as well as others (Reeve et al. 1978; Toyokawa et al. 2003) suggest precise vertical orientation in this species is common. In contrast, *Pleurobrachia*

spp. displayed a more variable swimming pattern, perhaps related its behavior of swimming straight or in an arc to spread its tentacles for feeding (Reeve et al. 1978). When feeding, *Pleurobrachia* spp. drifts passively (Purcell 1991), so it could be subjected to microturbulence causing variable orientation.

Of all the jellies examined, only *Bolinopsis* spp. was found in significantly higher abundance within thin layers. This raises the question why a zooplankton predator would occupy a thin layer of phytoplankton, especially when its prey items are abundant above and below the layer. ISIIS images displayed precise vertical orientation behavior of *Bolinopsis* spp., which is known to cruise the water column vertically in pursuit of prey (Reeve et al. 1978). Moving through a density interface (pycnocline) would cause the vertical cruising speed of the *Bolinopsis* spp. to be reduced (by physical mechanisms), thereby causing an accumulation of ctenophores where passively sinking *Pseudo-nitzschia* spp. tended to aggregate. In addition, while traces of diatoms have been found in the guts of *Bolinopsis* spp., they cannot maintain their size on these prey items alone, suggesting that diatom consumption may be a method to ward off starvation (Reeve 1980). Indeed, carbon and nitrogen stable isotope analysis demonstrates *Bolinopsis* spp. occupies a relatively low trophic position in the food web (Toyokawa et al. 2003). Alternatively, the ctenophores may actively seek temperature discontinuities and slow their swimming speed within them. Based on mesocosm experiments, it is likely that these ctenophores are actively responding to the density discontinuities (Frost et al. 2010), but further controlled studies on *Bolinopsis* spp. would be needed to distinguish between these passive and active aggregation mechanisms.

Jelly blooms

The jelly "bloom", defined as a rapid increase in population abundance (Graham et al. 2001), of *Bolinopsis* spp. ctenophores between June 30 and July 5 may have been due to retention of ctenophores within the bay coupled with extremely fast growth rates. In captivity, *Bolinopsis* spp. has been shown to be capable of growing over 10 mm per day, and initiates reproduction when it becomes fully lobate at a size of ~10 mm (Greve 1970). According to temperature/salinity diagrams, the bay waters were retained during our study (i.e., not replaced by offshore California current water; Woodson et al. in revision), so a bloom could have formed within the bay. Tidal ellipses occurred below the thermocline (Woodson et al. in revision) that may have acted as a retention mechanism, keeping ctenophores within the bay. Thin layers are also known as zones of reduced flow (McManus et al. 2005), so *Bolinopsis* spp. occupying these zones within the thermocline could have increased retention, improving chances of a bloom. When food and flow conditions are favorable, remarkable growth rates, combined with simultaneous hermaphroditism (capable of self-fertilization) and high fecundities (Baker and Reeve 1974; Reeve et al. 1978; Costello et al. 2006) likely allow this species to form blooms. The reduction in *Bolinopsis* spp. abundance on July 7 may have been due to cannibalism, which is known to occur in a closely related species (*Mnemiopsis leidyi*) (Javidpour et al. 2009); however, trends in abundance with depth on July 7 indicate that ctenophores were possibly aggregating within 5 m of the bottom, which we were unable to sample. The increase in length of *Bolinopsis* spp. over time, low Lloyd's patchiness, and the circulation patterns suggest the phenomenon observed on July 5 was a "true bloom" and

not just a congregation of gelatinous animals due to physical convergence (Graham et al. 2001).

On the other hand, the high abundance of *Eutonina indicans* on July 2 was likely an "apparent bloom" because dense aggregations were present on only ~3 profiles in waters deeper than the 20 m isobath, causing Lloyd's patchiness to be extremely high (14.452, Table 3). In addition, laboratory obtained size at age of *Eutonina indicans* suggests the organisms we sampled were likely >50 days old (Rees 1978), and therefore were likely advected into the area well before the study commenced.

Importance of behavior in thin layer trophic interactions

Zooplankton studies using high resolution instruments sometimes appear to show avoidance of thin layers of diatoms. In a recent study by Talapatra et al. (2013), two vertical profiles with an imaging system showed thin layers of *Chaetoceros socialis* and high particle counts within the vicinity of the pycnocline. In the first ascent, the zooplankton were located outside several, but not all, of the particle concentration peaks. In the second ascent, the zooplankton appeared to avoid the layers with elevated particle concentration (Talapatra et al. 2013). Other field studies demonstrate that trophic interactions can occur within thin layers on sub-hour time scales, and the grazers spend more time within thin layers when a higher fraction of water column phytoplankton is contained within the layers (Holliday et al. 2010; Benoit-Bird et al. 2010). The temporal resolution of sampling in our study may not have been adequate to capture these brief events often enough to yield a statistically significant overlap.

The primary fluorescent organisms in this study were *Pseudo-nitzschia* spp., which lack swimming ability, so if passive accumulation was occurring across all taxa, then all observed plankton would strongly overlap with the chlorophyll-*a* fluorescence activity. This was not the case. In fact, similarly sized copepods and appendicularians had very different vertical distributions, indicating that behavior is an important driver of vertical distributions of zooplankton in this system. The density discontinuities present near the chlorophyll maximum combined with consistent vertical swimming of *Bolinopsis* spp. may have led to accumulation and spatial overlap with higher chlorophyll-*a* levels and thin layers. Surface waters containing low abundances of gelatinous predators may serve as a predation refuge for copepods, which tend to aggregate at the surface despite low amounts of chlorophyll-*a* fluorescence activity in this zone. Further studies on copepod condition in different portions of the water column would elucidate some of the drivers of the strong spatial offset we observed between copepods and chlorophyll-*a* fluorescence. Copepods must strike a balance between predation avoidance and feeding, and the increases in jelly abundance with depth show that there are trade-offs to venturing into zones of higher phytoplankton concentrations.

In situ imaging technology provided a unique glimpse at an often overlooked component of marine food webs, gelatinous zooplankton, and to place them into the context of thin layers, which are common features in coastal environments. Acoustic surveys have detected thin layers but, unlike optical systems, are biased towards plankton with either an exoskeleton or gas bladder. The results of this study demonstrated that zooplankton of similar size, whose distributions are thought to be driven by physical forcing, can have strong differences in their vertical distributions. Optical systems

provide an ideal platform to better understand behavioral tendencies of zooplankton through both high resolution sampling and *in situ* orientation information. These characteristics should be considered (in conjunction with the physical environment) for studies on the causes of vertical heterogeneity in coastal ecosystems.

Tables

Table 2.1. Statistics of chlorophyll-*a* aggregation on various sampling days for profiles examined for gelatinous zooplankton (n=15 for July 5, n=30 for all other days), primary consumer (copepods and appendicularians) abundances, and aggregation statistics.

Date	June 28	June 30	July 2	July 5	July 7
Mean chlorophyll max (volts) (SE)	2.163 (0.086)	1.306 (0.031)	1.504 (0.027)	1.610 (0.022)	1.004 (0.023)
Mean depth of chlorophyll max (m) (SE)	8.620 (0.291)	12.249 (0.354)	6.189 (0.310)	7.031 (0.162)	9.626 (0.381)
Profiles with thin layers	14	0	7	13	6
Percent of profiles with thin layers	47%	0%	23%	87%	20%
Mean copepod concentration (ind. m^{-3}) (SE)	5301 (97.54)	5067 (81.66)	4282 (71.78)	8453 (264.37)	4644 (90.55)
Maximum copepod concentration (ind. m^{-3})	20421	23612	29994	37014	22336
Copepods Lloyd's patchiness	1.23	1.26	1.38	1.53	1.42
Mean appendicularian concentration (ind. m^{-3}) (SE)	5870 (79.81)	2176 (38.45)	5474 (104.01)	4835 (126.16)	10610 (102.47)
Maximum appendicularian conc. (ind. m^{-3})	17868	10848	22974	19145	25527
Appendicularian Lloyd's patchiness	1.08	1.17	1.56	1.29	1.08

Table 2.2.: Fixed effects for Poisson GLMMs for copepods and appendicularians. Profile number was treated as a random effect to account for spatial autocorrelation between nearby samples. Model coefficients and significance levels are shown. An additional parameter of nearest total gelatinous zooplankton count was added to assess the impact of gelatinous abundance in the immediate area of the sample. Significance was assessed using Wald z tests. P value significance codes are as follows: $P > 0.05$ = ns, $0.01 < P < 0.05$ = *, $0.001 < P < 0.01$ = **, and $P < 0.001$ = ***.

Model formula:

Count ~ Profile number + date + depth + fluorometry + thin layer category

	Copepods		Appendicularians	
Model parameters	Coeff.	P	Coeff.	P
Date 6/30	-0.0303	ns	-0.7718	**
Date 7/2	-0.4422	*	-0.4557	*
Date 7/5	0.2197	ns	-0.3453	ns
Date 7/7	-0.3388	ns	0.6776	**
Depth	-0.0020	ns	0.0073	***
Fluorometry	-0.5006	***	0.1858	***
Above layer	0.2708	ns	0.3737	*
Below layer	-0.2777	ns	0.4160	*
Within layer	0.0519	ns	0.3708	*

Table 2.3. Summary statistics for gelatinous zooplankton abundances

Species	Date	Mean conc. (inds m^{-3})	St Error	Max conc. (inds m^{-3})	Lloyd's patchiness	Proportion of m^3 sampled with >1 jelly per m^3
Pleurobrachia spp.	June 28	0.8175	.1002	9	2.7515	.4079
	June 30	2.0591	.2762	20	2.5039	.6517
	July 2	1.3516	.1991	16	2.9293	.4726
	July 5	4.3396	.4989	37	2.3829	.7090
	July 7	3.6206	.7682	44	3.9983	.5832
Small Bolinopsis spp.	June 28	0.7299	.1050	13	3.8088	.3274
	June 30	3.1833	.4730	54	3.5806	.7088
	July 2	5.3894	.9034	68	3.7191	.6144
	July 5	6.0784	1.1129	72	3.6205	.5896
	July 7	1.1194	.2392	28	5.7178	.2955
Large Bolinopsis spp.	June 28	0.5188	.06850	8	3.3044	.2880
	June 30	0.3014	.09649	10	7.5519	.1690
	July 2	1.4234	.3218	35	5.5256	.3932
	July 5	28.1157	2.4464	144	2.0584	.8022
	July 7	8.8258	1.4861	75	3.3481	.6634
Eutonina indicans	June 28	0.5206	.07849	10	3.2553	.3077
	June 30	0.3747	.05064	5	2.0379	.2668
	July 2	4.6711	1.4786	251	14.4520	.6522
	July 5	1.7201	0.2696	14	2.3148	.5858
	July 7	1.0391	0.2672	18	4.6522	.3601
Muggiaea spp.	June 28	0.1270	.03056	3	3.3450	.1020
	June 30	0.1568	.02687	2	2.1685	.1303
	July 2	0.3081	.05988	5	3.5151	.1966
	July 5	0.8209	.2435	15	5.3587	.3396
	July 7	0.6732	.06055	7	2.0605	.3933
Sphaeronectes spp.	June 28	0.1825	.05863	7	10.6655	.1002
	June 30	0.5601	.05812	9	2.3047	.3483
	July 2	0.7713	.1240	11	3.5151	.2665
	July 5	0.7351	.2733	33	5.3587	.2575
	July 7	1.3659	.1373	17	2.0605	.4462

Table 2.4. Fixed effects from GLMMs for the 6 most common gelatinous taxa. Models use organism counts per m^3 as a response variable to sampling date, depth, chlorophyll-*a* fluorescence (chl-a), and thin layer categorical variables. Sampling date coefficients are fit relative to the first date of sampling (June 28), and thin layer variables are fit relative to the "no thin layer present" category. The profile number was used as a random effect to account for the correlation structure within a profile.

	Pleurobrachia spp.		Bolinopsis spp. (small)		Bolinopsis spp. (large)		Eutonina indicans		Muggiaea spp.		Sphaeronectes spp.	
Model Param.	Coeff.	P	Coeff.	P	Coeff.	P	Coeff.	P	Coeff.	P	Coeff.	P
June 30	1.0040	***	1.6893	***	-0.3890	ns	-0.1937	ns	0.4787	ns	1.7076	***
July 2	0.5112	*	1.9158	***	1.0617	***	1.6779	***	0.9152	**	1.8341	***
July 5	1.8751	***	2.5120	***	4.5574	***	1.2858	***	1.9323	***	1.8660	***
July 7	1.3433	***	0.0226	ns	3.6138	***	0.4729	ns	2.2906	***	2.9988	***
Depth	0.0816	***	0.0256	***	0.0902	***	0.1165	***	0.0855	***	0.1926	***
Chl-a	0.2125	***	0.8031	***	0.8783	***	-0.0062	ns	0.3243	**	0.1995	ns
Above layer	-0.0031	ns	-0.6358	*	0.2510	ns	-0.1618	ns	0.0306	ns	-0.9434	**
Below layer	0.2975	ns	0.1850	ns	0.8286	***	0.6243	*	0.5855	*	0.2359	ns
Within layer	0.3037	ns	0.4358	*	0.7570	**	0.1522	ns	0.3661	ns	0.2080	ns

Figures

Figure 2.1. Sampling track from each day of ISIIS sampling. Ten transects, each *ca.* 3 km long and 500 m apart are shown in gray. The black dot on the inset figure shows the location of the SeaHorse profiler in the middle of the 5th transect.

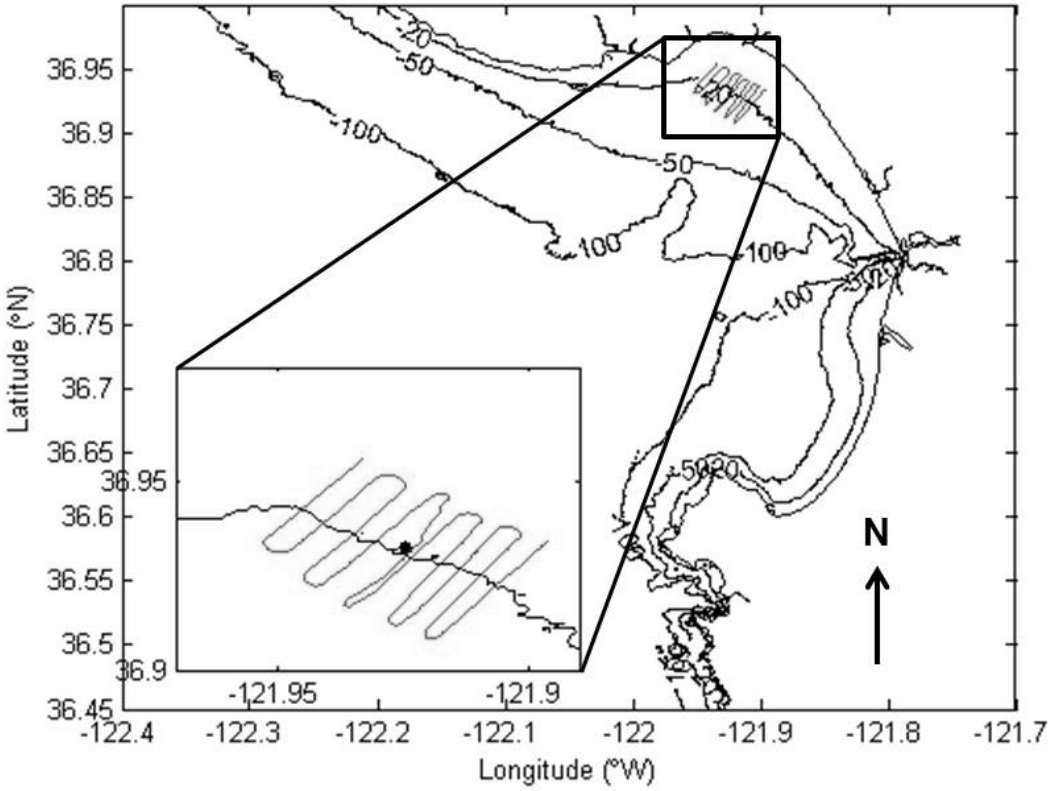

Figure 2.2. A) Prevailing wind speed and direction between June 11, 2010 and July 8, 2010 from nearby NDBC station 46042. Winds with a significant northerly component (negative y value) are 'upwelling' winds. Black stars denote the times when sampling with ISIIS. Black horizontal line shows the time range when the SeaHorse profiler was in use. B) SeaHorse profiler data showing water column properties throughout the study period. Thin fluorescent layers (most common on June 28 and July 5) are correlated with high thermal stratification. Gaps in SeaHorse data were due to technical difficulties with the instrument.

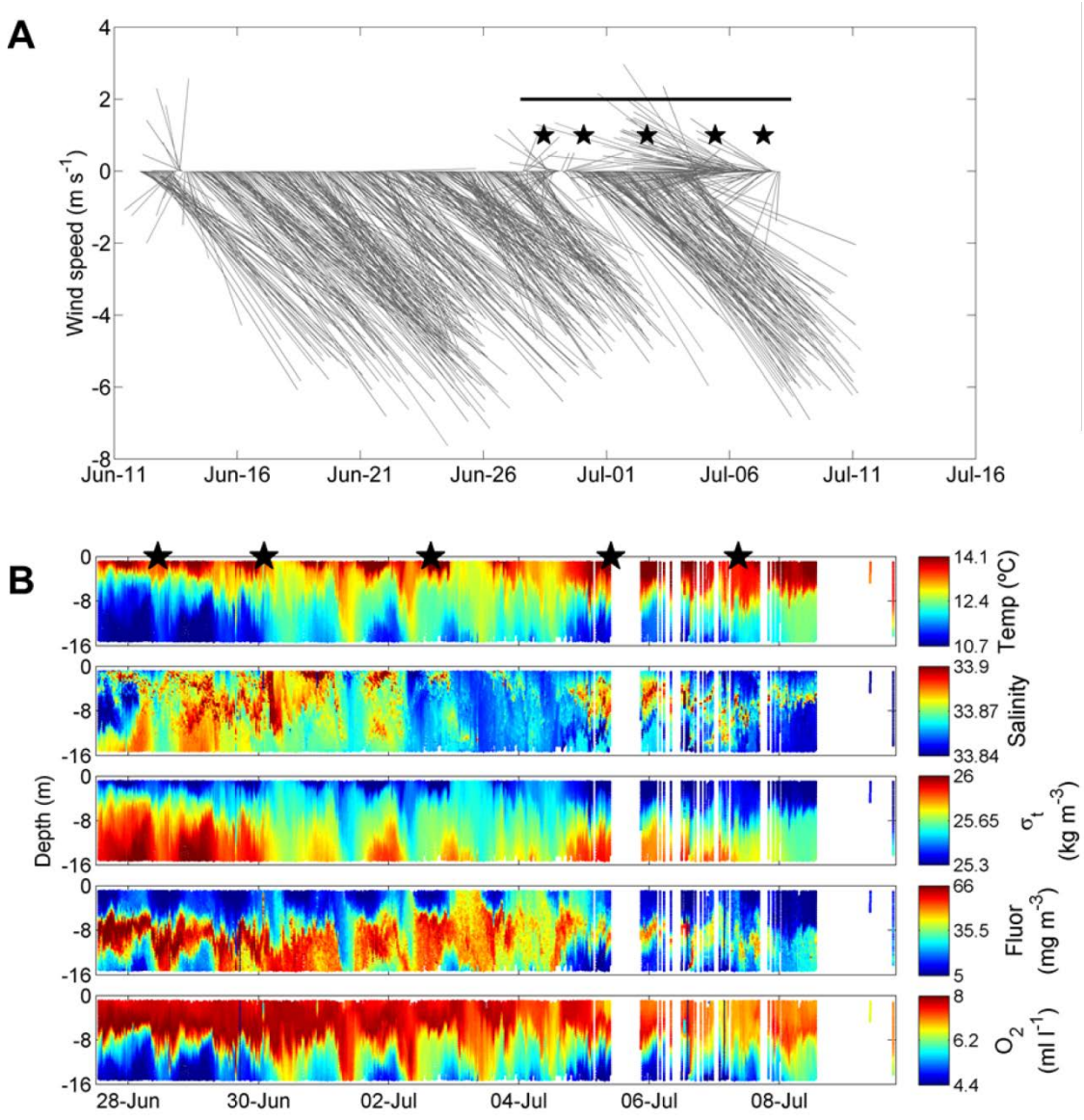

Figure 2.3. A) Average minor (horizontal) axis of particles in each ISIIS frame gives an estimate of diatom floc size. Size of each point is proportional to the number of flocs in each ISIIS image. Color corresponds to chlorophyll-*a* fluorescence (volts) B) Ratio of major (vertical) to minor (horizontal) axis. Higher ratios mean the particles are oblong and likely sinking at a fast rate. Lower ratios indicate a more round particle that is likely sinking slowly.

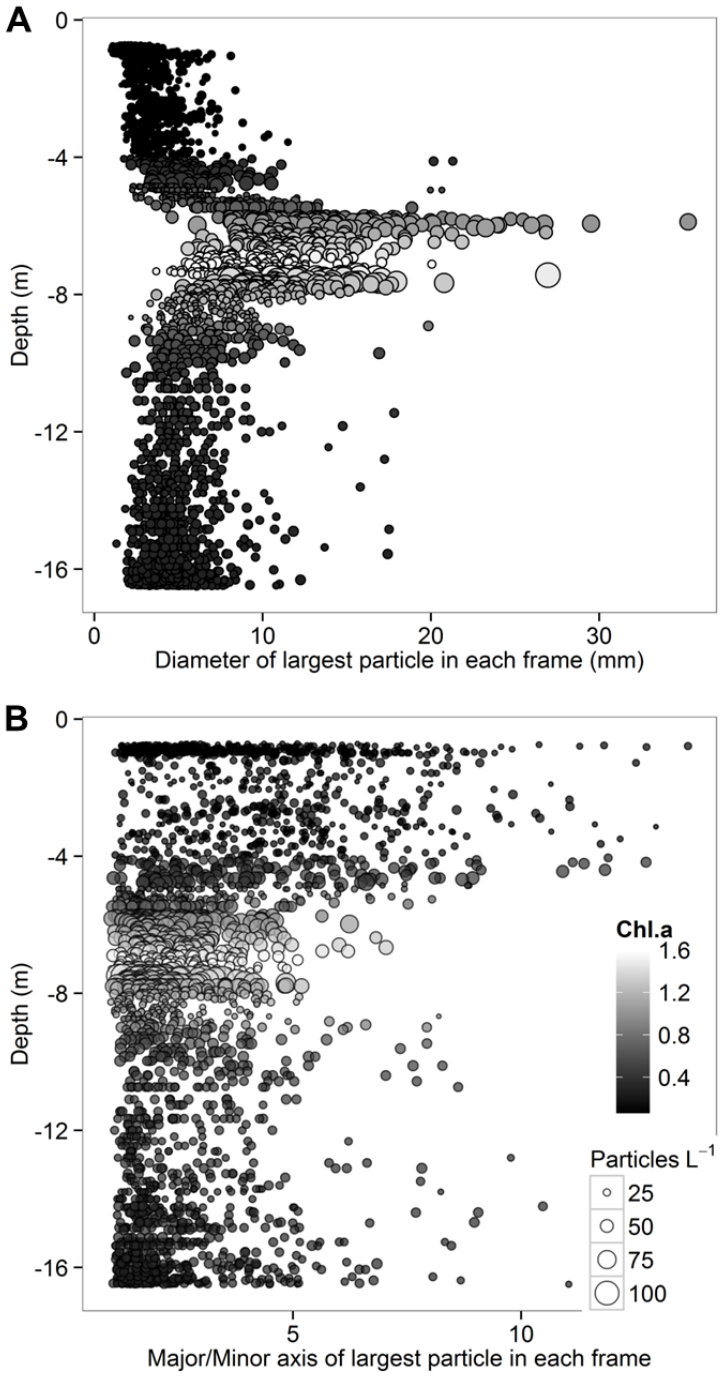

Figure 2.4. Average concentration of chlorophyll-*a* fluorescence (volts) and zooplankton (ind. m^{-3} * 10^4) in 1 m depth bins on each of the 5 ISIIS sampling days.

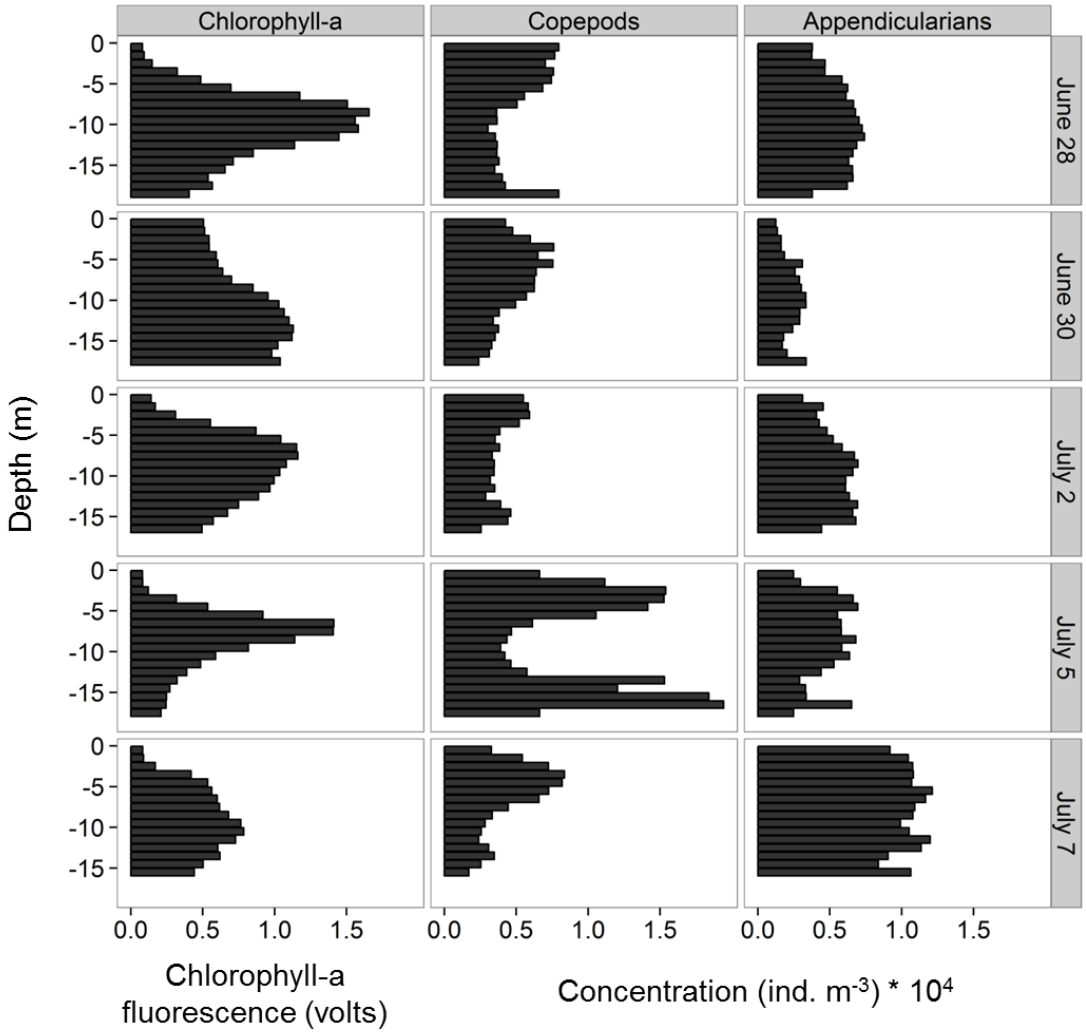

Figure 2.5. Spatial overlap index between primary consumers (copepods and appendicularians) and total gelatinous zooplankton abundance in 1 m^3 surrounding the sample. Indices > 1 indicate spatial overlap, and indices < 1 indicate spatial separation. Error bars represent 1.96 times the standard error of the index.

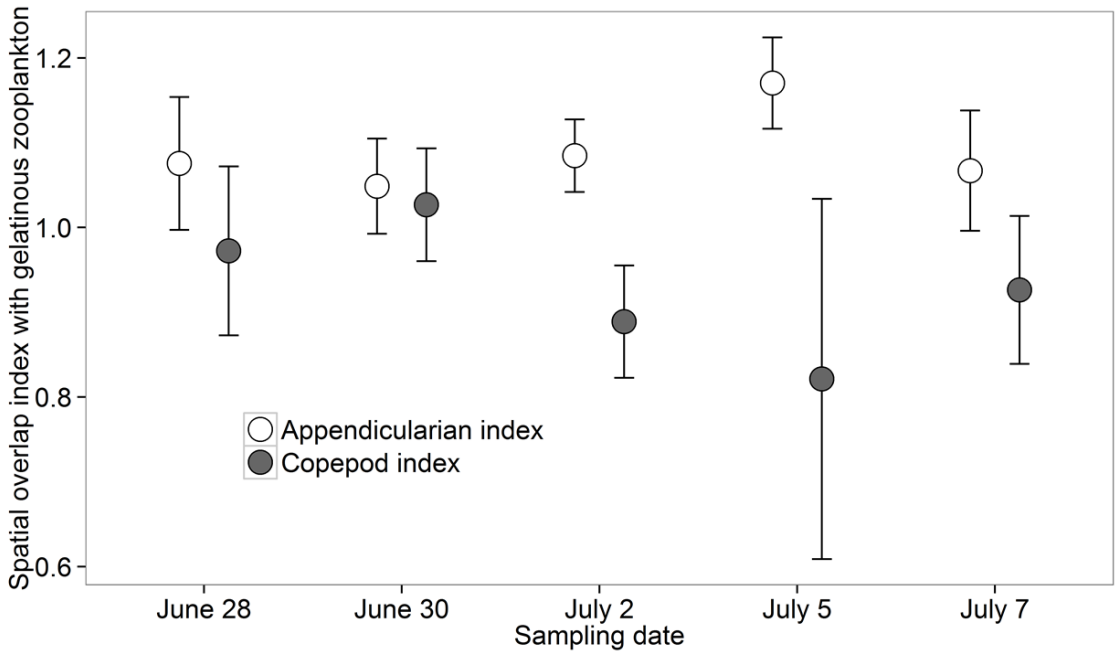

Figure 2.6. Six most abundant gelatinous groups throughout the study area and diatom aggregates as detected by ISIIS A) *Pleurobrachia* spp. B) Small *Bolinopsis* spp. C) Large *Bolinopsis* spp. D) *Eutonina indicans* E) *Muggiaea* spp. F) *Sphaeronectes* spp. – notice the cormidia bearing developing sexual medusoids. G) *Pseudo-nitzschia* spp. diatom flocs within a thin layer from July 5. Scale bars are 5 mm for A-F, 20 mm for G.

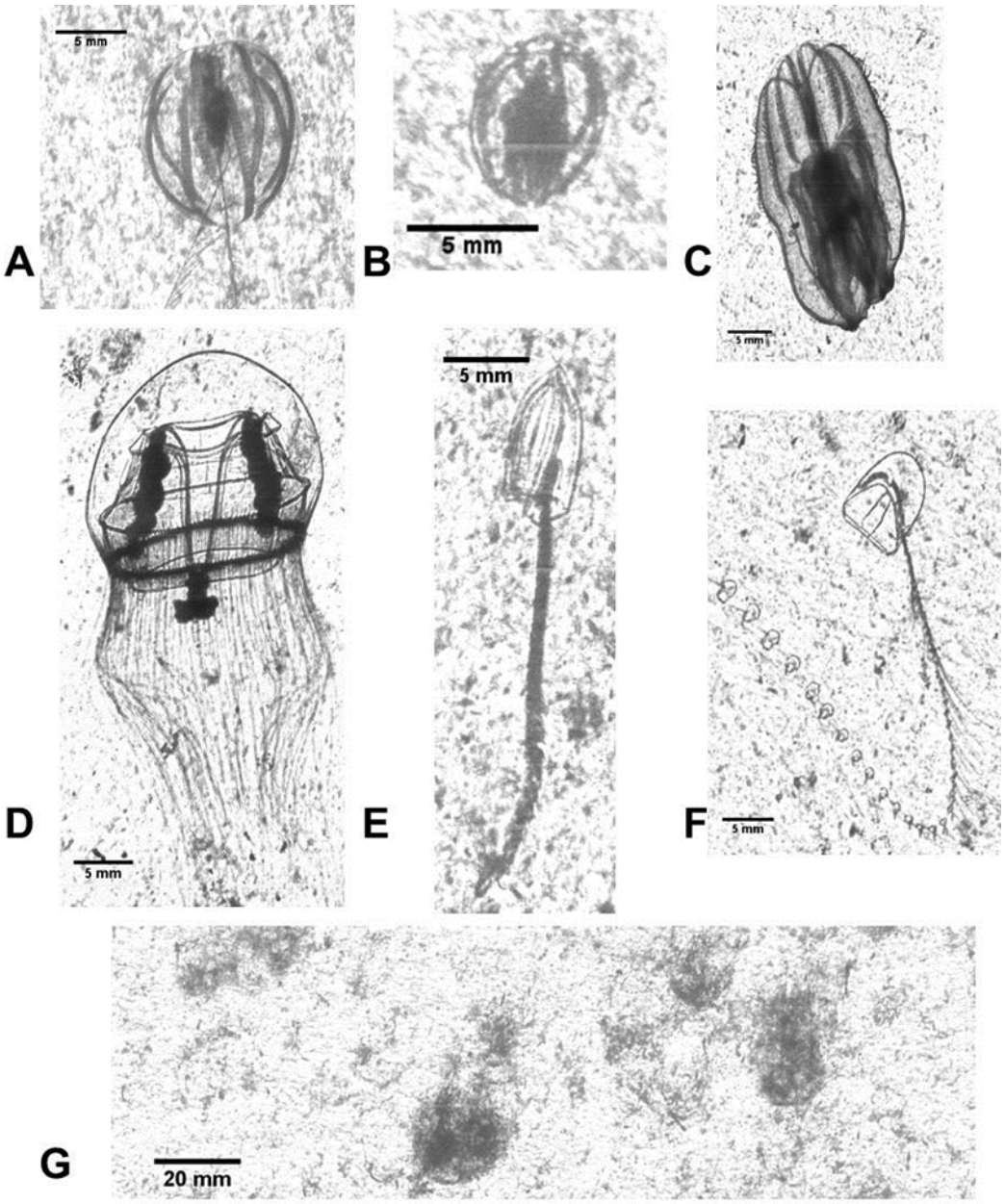

Figure 2.7. A) Water column average concentration of different gelatinous zooplankton by day of sampling. Each profile through the water column was considered a sample (n = 30 per sampling day, n = 15 on July 5), and error bars represent 1.96 * standard error. B) Vertical distribution (ind. m^{-3}) of gelatinous zooplankton in 1 m vertical depth bins. Bars are stacked (non-overlapping).

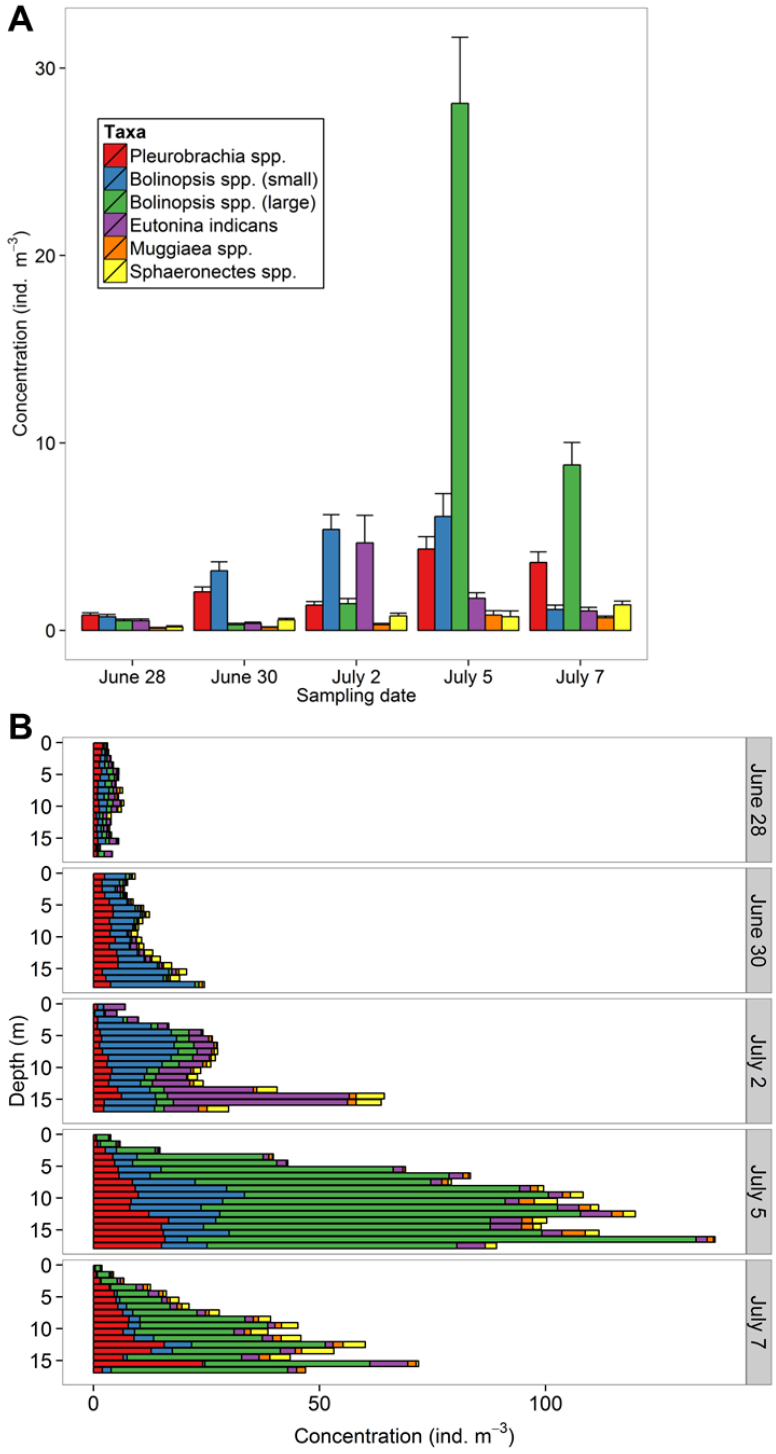

Figure 2.8. Polar histograms showing angle of *in situ* orientation (and swimming) of the oral end for subsets of A) *Bolinopsis* spp. (n = 274) and B) *Pleurobrachia* spp. (n = 225) ctenophores. 180 degrees is towards the surface, 0 degrees is towards the benthos. Much more consistent vertical orientation is displayed in *Bolinopsis* spp.

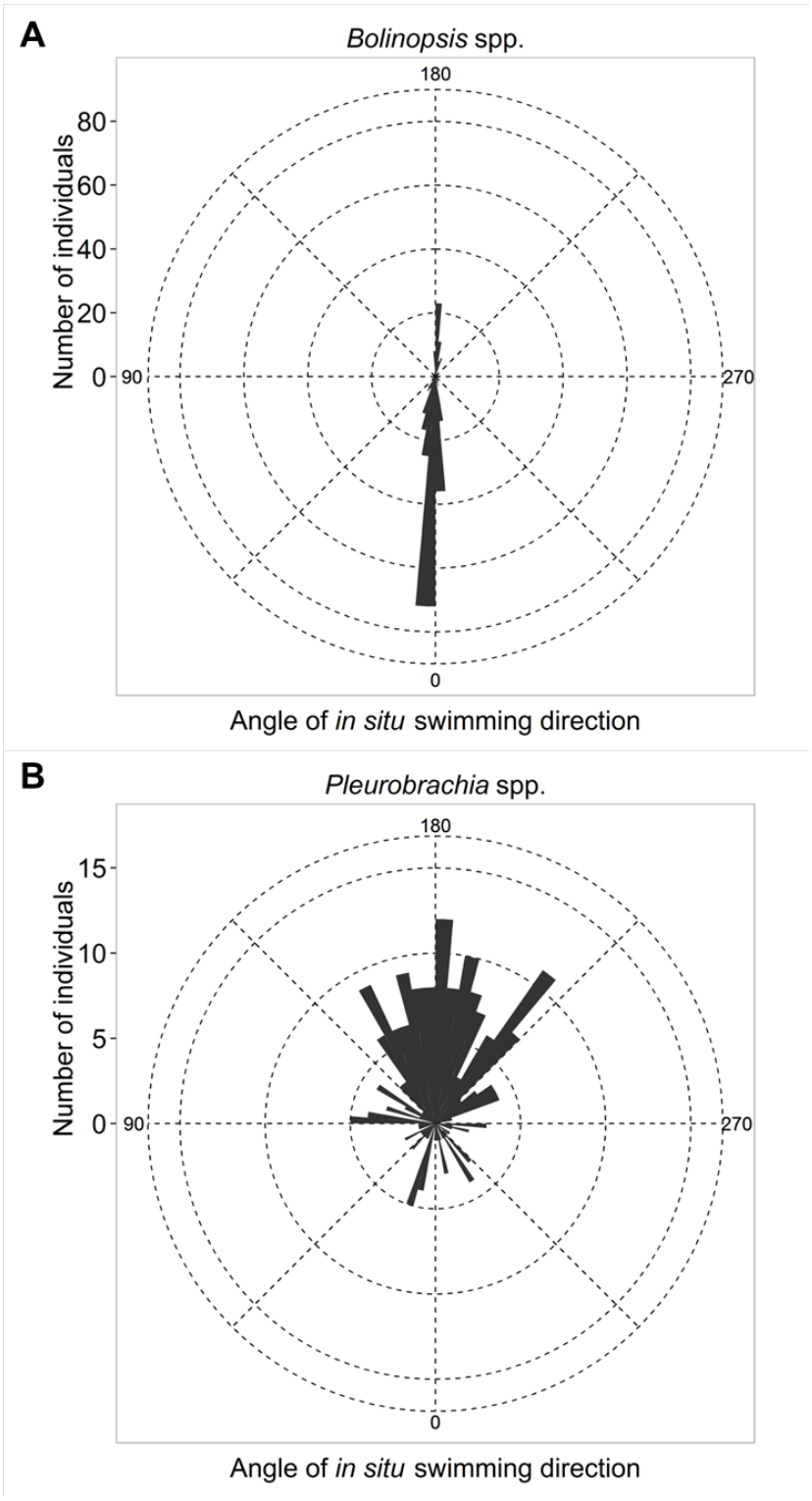

Figure 2.9. Length/frequency histograms of *Bolinopsis* spp. (small and large size classes pooled) from 4 days of sampling. One-sided Komolgorov-Smirnov tests revealed significant right shifts in size distributions between sampling days.

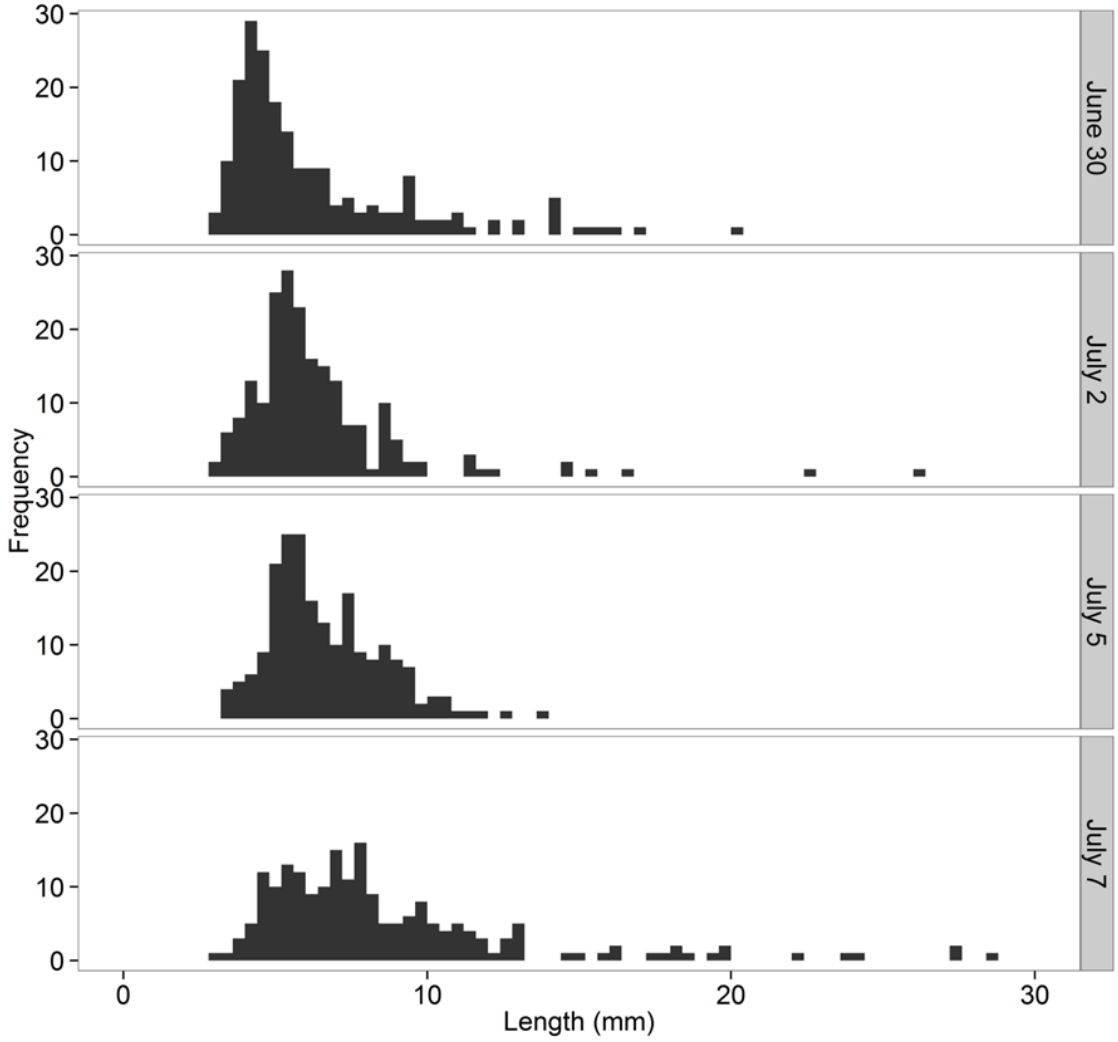

CHAPTER 3: THE ROLE OF STRATIFICATION AND INTERNAL WAVES IN LARVAL FISH INTERACTIONS WITH POTENTIAL PREDATORS AND PREY

Tidally driven internal wave packets in coastal environments have the potential to influence patchiness of larval fishes, their prey, and their planktonic predators. We used the *In Situ* Ichthyoplankton Imaging System (ISIIS) to synoptically sample larval fishes, copepods, and planktonic predators (ctenophores, hydromedusae, chaetognaths, and polychaetes) across these predictable, tidally driven features in the summer near Stellwagen Bank, Massachusetts, USA. Full water column profiles and fixed depth transects (~10 m depth) were used to quantify vertical and horizontal components of the fish and invertebrate distributions during stratified and internal wave conditions. Larval fishes, consisting mostly of *Urophycis* spp., *Merluccius bilinearis*, and Labridae, were concentrated near the surface and displayed ontogenetic vertical migration. Average larval patch sizes were smaller during the internal wave phase of sampling. Copepods formed a near surface thin layer, several meters above the chlorophyll-a maximum, during the stratified conditions that was absent when internal waves were propagating. In contrast, ctenophores and other predators were much more abundant at depth, but concentrations near 10 m increased immediately after internal waves mixed the water column. During the internal wave phase of sampling, the fine-scale abundance of larval fishes was more correlated with the abundance of gelatinous predators and less correlated with copepods. Vertical mixing caused by internal waves can disperse patches of zooplankton and force surface dwelling larval fishes into deeper water where the probability of predator contact is increased, generally creating conditions potentially less favorable for larval fish growth and survival on short time scales.

Background

Patchiness of habitat, conspecifics, predators, nutrients, and prey characterize the plankton over a wide range of spatial and temporal scales (Haury 1978). More than simply a statistical annoyance (Steele 1976), variation in the planktonic environment is biologically important for both modeling and empirical studies (Vlymen 1977; Davis et al. 1991; Pitchford and Brindley 2001; Lough and Broughton 2007). Biological interactions are thought to drive small scale patchiness, while physical forces may dominate on larger scales (Mackas et al. 1985; Pinel-Alloul 1995; McClatchie et al. 2007). Describing plankton patchiness at fine scales and resolving underlying mechanisms requires high-resolution field sampling. Recent developments in plankton imaging technology allow for measurements at the scale of individuals (cm to m), potentially revealing information on trophic interactions and aggregation in the context of fine-scale environmental variables.

Growth, survival, and recruitment of the early life stages of fishes is thought to be highly influenced by patchiness of their predators, prey, and even conspecifics (Houde and Lovdal 1985; McGurk 1986; Davis et al. 1992). Because eggs are released from individuals, larvae begin life in highly patchy distributions that gradually disperse (decreasing patchiness) with age and size. Through differential survival and active swimming near prey resources or schooling behavior, patchiness increases again as larvae develop, creating a U-shaped curve of patchiness with age (Hewitt 1981; Matsuura and Hewitt 1995). The sizes of larval patches and spatial relationships among individual larval fishes, predators, and prey are unknown, but such empirical data are important for parameterizing biophysical models of fish population dynamics.

Water column stratification provides one condition necessary for the formation of prey and/or predator aggregations (Lasker 1975; Norrbin et al. 1996). How this may translate to larval fish growth is unclear, as metrics of larval conditions indicate that the relationship between larval growth and mixed vs. stratified conditions appears to be taxon dependent (Buckley and Lough, 1987; Dower et al. 1998). Faster growth is expected to lead to higher survivorship and thus increased recruitment (Houde 1987; Miller 1988; Hare and Cowen 1997), but predation also plays a strong role and is often under-studied due to the variety of larval fish predators (Bailey and Houde 1989; Cowan and Houde 1993), including many that are not well sampled using net-based systems (e.g., ctenophores, hydromedusae, siphonophores). An understanding of the spatial distribution of larval fishes, and their predators and prey is therefore important for quantifying predation pressure (inferred from spatial overlap) as well as describing the feeding environment on a spatial scale experienced by individual larvae. Observations on this spatial scale can potentially explain how larvae successfully feed when average concentrations of food are low (Llopiz and Cowen 2008).

One key physical mechanism that may influence plankton patchiness is internal waves, which are common physical features that develop in areas of strong stratification with (usually) some degree of abrupt topography. Internal waves propagate along the thermocline, displacing passive plankton by 10s to 100s of meters in depth (Haury et al. 1979; Liu and Hsu 2001) and can cause substantial vertical mixing (Wallace and Wilkinson 1988), leading to increased biological productivity (Holloway and Denman 1989; Sangrá et al. 2001). Internal waves have been implicated as mechanisms of phytoplankton patchiness, aggregating phytoplankton below internal wave crests and

above troughs (Kushnir et al. 1997; Lennert-Cody and Franks 2002), and similar effects have been shown for zooplankton (Haury 1979, 1983). Wind-driven currents are often alongshore, so the propagation of internal waves may be an important mechanism for cross-shelf transport and the settlement of organisms associated with a benthic habitat (e.g., decapod crustaceans and many species of fish). Thin layers and zooplankton patches, which may form during stratified regimes, could be displaced or dispersed by internal wave activity (Cheriton et al. 2009).

Stellwagen Bank, approximately 40 km east of Massachusetts Bay (USA), is an area where internal waves are a common, predictable feature. The summer months between July and September are characterized by strong thermal stratification and the presence of internal wave packets that propagate across Stellwagen Basin during the barotropic tide. First described by Halpern (1971), these internal wave packets typically consist of 8-10 waves with a 6-8 min period and a 200-400 m wavelength, which propagate west along the thermocline at ~0.5 m s^{-1} (Haury et al. 1978). The internal waves can also contain "trapped cores" when they reach zones where the wave amplitude is higher than the bottom depth (typically < 30 m deep), resulting in transportation of particles towards the Massachusetts coast (Scotti and Pineda 2004). Thus, internal waves are a potential transport mechanism for larvae of benthic organisms returning to shore to settle (Shanks 1983). The internal hydraulic jump is now recognized as the primary mechanism behind the formation of these internal waves, resulting in a deepened thermocline behind the internal wave packet and a surface shoaling thermocline preceding it (Lai et al. 2010). The ~30 m vertical displacement of the thermocline within the internal wave packet can cause near bottom currents to reach speeds >0.2 m s^{-1}

leading to resuspension and transport of sediments eastward along the bottom in the opposite direction of the cross shelf tidal current (Butman et al. 2006).

The predictability and solid understanding of the mechanisms of internal wave formation at Stellwagen Bank (Lai et al. 2010) make it an ideal location to investigate some fundamental questions about plankton patchiness as it relates to fish early life history. What is the effect of internal wave propagation on the concentration of larval fishes and potential prey items (copepods)? Which zooplankton predators aggregate in the vicinity of larval fishes, and how does this change with internal wave propagation? These and other questions regarding the fine-scale distributions of different zooplankton provide insight into trophic relationships in the context of stratification and internal wave activity.

Materials and Methods

Study site

Stellwagen Bank is located ~25 mi (41 km, 22 n mi) off the coast of Massachusetts, USA and is known to be a productive fishing ground, home to a diverse assemblage of fishes and marine mammals; many of which are adapted to searching for aggregated prey resources (De Robertis 2002). The bank slopes steeply on its western side into Stellwagen Basin, and it is gently sloped on the eastern side towards oceanic waters.

Plankton imaging

Previous research on fine-scale plankton distributions has utilized nets or pumps, which severely underestimate many important gelatinous predators in the plankton (Bailey and Houde 1989; Remsen et al. 2004). In addition, calculations of patchiness using concentrations derived from net tows (unequal sample volumes) have been shown to be mathematically flawed (Bez 2000). Imaging technology allows for improved patchiness measurements by using a fixed sample volume size, as well as adopting more robust distance measurements of patchiness that have been used in plant ecology for decades (Pielou 1977; Greig-Smith 1979). To successfully image larval fishes, mesozooplankton, and their prey, large sample volumes and rapid tow speeds are required.

The *In Situ* Ichthyoplankton Imaging System (ISIIS) utilizes a Piranha II line scan camera (Dalsa) with 68 μm pixel resolution, imaging plankton in the size range of ~500 μm to 13 cm. ISIIS uses a shadowgraph imaging technique, in which a collimated light source is projected across a sampled parcel of water, and the silhouettes created by the plankton blocking the light source are then captured by the camera (Cowen and Guigand 2008). The ISIIS line scan camera shoots a continuous image, but parses the image into frames that correspond to a 13 cm x 13 cm area of view with a depth of field of ca. 40 cm, giving an individual image volume of 6.4 L per frame. At the usual tow speed (2.5 m s^{-1}), 1 m^3 of water is sampled every 7.7 s. In addition to the camera system, ISIIS is equipped with motor-actuated fins for depth control, a Doppler velocity log (600 micro, Navquest), and environmental sensors including a CTD (SBE49, Seabird Electronics) and fluorometer (ECO FL (RT), Wetlabs – chlorophyll-a fluorescence). All sensors sampled

the water < 1 m above the imaging area at a rate of 2 Hz. A correction was applied to address this offset on the vertical profiles. The housing of the CTD on ISIIS was not flushing immediately, so temperature data was delayed by 15 s and not used for identification of internal waves.

ISIIS was towed behind the NOAA ship *Delaware II* using two different methods of sampling designed to examine vertical and horizontal components of plankton patchiness. A total of four transects were performed: two full water column "tow-yo's" and two fixed depth transects at ~10 m depth (Fig. 3.1). Approximately 2 hrs before ebb tide, ISIIS was deployed in "tow-yo" fashion, sampling from the surface to 30-50 m deep (~10 m from the bottom) during a ~12 km transect westward towards Stellwagen Bank. After the transect was completed, ISIIS was brought to the surface for the ship to turn, and another transect of approximately equal length (12 km) was performed with ISIIS staying as close to the thermocline as possible (10 m) in the opposite direction of the tow-yo transect. The position of the thermocline was obtained from real-time data from ISIIS during the full water column transect. These same two transects were repeated 2.5 hrs after the start of the flood tide, which was when we expected to see internal wave activity due to the flood tide interaction with Stellwagen Bank (Haury et al. 1979). Each ~13 km transect took approximately 80 min to complete.

Internal wave characterization

Following Haury (1983), the internal wave packet was located visually by identifying high frequency oscillations in the chlorophyll-*a* fluorescence signal from ISIIS. The location of the internal wave packet was confirmed by a strong shift in

temperature in this portion of the transect. The fluorescence signal was smoothed using a low pass filter and fast-Fourier transform was implemented to assess the wave energy occurring at each wavelength. The dominant wavelength was assumed to correspond to the peak spectral density.

Image data analysis

ISIIS images were viewed and analyzed using VisionNow (Boulder Imaging, Inc.) and ImageJ (v1.46r, Rasband 1997-2010). A standard 'flat-fielding' transformation was applied to each image before viewing to remove image artifacts from the line scan camera. For quantification of larval fishes, each vertical profile (downcast) was manually examined, and larval fishes were cropped, measured, and identified to family or genus level. We refer to these the sampling units as 'profiles' even though they spanned a horizontal range of ~750 m and an average depth of 50 m (~10 m above the bottom). Other zooplankton extracted from the profiles included chaetognaths, polychaetes, ctenophores, and hydromedusae. Fixed depth transects were quantified in their entirety, but chaetognaths were not extracted because most of them were too small (<1 cm) to be considered relevant larval fish predators for the larger larval fishes found in this zone of the water column. Measurements of standard length and *in situ* swimming angle of larval fishes were obtained using ImageJ (Rasband 1997-2010). Significance of depth changes with size (ontogenetic vertical migration) was assessed using Kruskal-Wallis tests.

Because the overwhelming majority of small particles in the images were copepods, automated particle counting was implemented using a custom ImageJ macro to count particles in the size range of 25-650 pixels for all transects (upcasts and

downcasts). The correct size range was determined using trial and error on a variety of images capturing different sized copepods. The program first applied a threshold to the images (converted to black and white), which removed the light gray diatom chains present in many of the images, then utilized ImageJ's 'Particle Analyzer' to count the particles in each frame. In rare cases, the ISIIS images had reduced quality due to image turbulence. To flag images where organism counts were potentially erroneous, the macro calculated image histogram statistics, including the pixel mean and standard deviation. Images with a mean pixel value lower than 200 and a standard deviation above 40.5 were noisy and produced inflated counts, and these images were discarded from automated analysis (0.75%, 1285 images total). The accuracy of the counts was assessed by examining particles enumerated by the program and manually determining whether or not they were copepods. 12,973 objects enumerated by the counter were manually examined in five 10 m depth bins to give a depth-specific accuracy for the copepod counter. Each particle was classified as either copepod (true positive), marine snow, shrimp, jelly parts, appendicularian, or double copepod (copepods overlaying each other and counted as 1 particle), and accuracy for each depth bin was calculated by dividing the number of true positives by the total number of particles examined in each depth bin. This depth-specific accuracy was multiplied by the results obtained by the particle counter to correct for errors in estimates of copepod abundances in different portions of the water column. The rate at which the counter missed copepods (false negatives) was not quantified because there were some copepods that were simply below the size limit of the automated counter, and expanding the size range led to a sharp increase in the rate of false positives. Interpolations of the copepod abundances and fluorometry across the full water column

profiles was performed using the R packages "akima" (Akima et al. 2013) and "gstat" (Pebesma 2004).

Timestamps in Julian day (decimal day) were used to merge physical data (temperature, depth, etc.) with the image data. Due to the differences in sampling rate between the imaging and physical data sensors (17 hz vs. 2 hz), individual predator zooplankton and fish larvae were merged to the nearest physical environmental data. This was accomplished via an algorithm that extracted the nearest timestamp from the physical data, which was then used to combine the datasets through an "outer join." Copepods, because of their high abundances, were averaged for every physical data time stamp (0.5 s or ~8 frames) to yield an average count and standard error, which was then converted into a concentration using the known volume of one ISIIS image. These datasets were then combined to give the copepod concentration around each larval fish. Vertical distributions of larval fishes and predator zooplankton were calculated by taking the number of individuals found in each depth bin divided by the volume sampled by ISIIS in that depth bin; thus, no standard error was produced for these rare organisms. Data analysis was performed in R (v2.15.2, R Core Team 2012) with substantial use of the packages "plyr" (Wickham 2011) and "ggplot2" (Wickham 2009) for data analysis and visualization, respectively.

Bongo net sampling

A 61 cm bongo net was fitted with 335 μm mesh to aid in larval fish identification within the images. Two oblique tows were performed immediately after each ISIIS full water column and fixed depth transects (four bongo samples total) spaced approximately

5 km apart. A CTD was mounted on the tow wire, and tows were made between surface and within 5 m of the bottom with a flow meter attached to the center of the net (General Oceanics) to quantify volume of water sampled. Zooplankton samples were immediately preserved in 95% ethanol. Larval fishes were sorted and identified at the Plankton Sorting and Identification Center in Szczecin, Poland.

Distance to next encounter and patchiness statistics

A distance to next encounter (DNE) (Currie et al. 1998) statistic was calculated for fish larvae on the fixed depth transects:

$$DNE = V(T_{i+1} - T_i) \quad \text{(eq. 1)}$$

where V is the average speed of the ship (2.5 m s^{-1}), T_{i+1} is the timestamp in seconds of the next organism encounter, and T_i is the timestamp of the organism of interest. One hundred iterations of a random distribution of 'events' along the transect were used to compare the larval fish DNE histogram to what would be expected from randomness (±1 standard deviation). Other patch statistics were calculated following the methods of Currie et al. (1998) including average linear patch size and number of patches per transect with varying definition of the maximum distance to next neighbor to be considered 'within a patch' (Dmax). This empirical approach is necessary because there is no absolute *a priori* method to determine which organisms are 'within' or 'outside' of a particular patch. Number of patches (np) was calculated as the frequency of DNEs >Dmax in a transect + 1, and average linear patch size was computed as the sum of the 'within patch' distances (DNEs < Dmax) divided by the number of patches:

$$\text{Average linear patch size} = \Sigma(\text{DNEs} < \text{Dmax})/\text{np} \quad \text{(eq. 2)}$$

Lloyd's index of patchiness (Lloyd 1967) was used to asses an overall description of patchiness for 1 m^3 (19.25 m horizontal distance) bin sizes. Fish larvae were divided into five size classes to examine changes in patchiness with size/age (<3 mm, 3-4 mm, 4-6 mm, 6-8 mm and >8 mm).

$$\text{Patchiness} = 1 + [(\sigma^2\text{-m}) / m^2] \quad \text{(eq. 3)}$$

where sample variance and mean are represented by σ^2 and m, respectively. A random distribution has a patchiness index of 1 because of equivalent mean and variance in samples, and 'patchy' distributions have higher variance and thus a patchiness index larger than 1. Horizontal bin sizes of 1 m^3 were also used to assess the fine-scale correlations between fish larvae, prey, and predator taxa. Significance of Spearman correlation coefficients was assessed using the approximation of the student's t-distribution in the R package "Hmisc" (Harrell et al. 2012). Correlations of normally distributed variables (temperature and depth) were assessed using Pearson correlation coefficients.

Results

Physical environment and internal waves

During ebb tide, the water column was highly stratified (Pearson temperature/depth correlation -0.661 for fixed depth transect) with a chlorophyll-*a* maximum near 10 m, qualitatively determined to be dominated by rod shaped diatoms. During flood tide, internal wave activity increased the variability of the depth of the chlorophyll-*a* maximum, and the temperature/depth correlation was much lower (-0.158), indicative of an oscillating thermocline. Excluding observations shallower than 5 m

(maintaining the depth of the ISIIS vehicle was challenging at times), the temperature range was higher during the internal wave phase (maximum of 19.2, minimum of 8.5) (Fig. 3.2A). Oxygen levels were elevated and temperature declined sharply immediately in front of the internal wave packet (travels westward). Levels of chlorophyll-*a* fluorescence were significantly higher during the stratified phase of sampling ($p < .00001$, Kruskal-Wallis test), but in the internal waves sampling phase, fluorescence contained distinct enhanced regions associated with the internal wave packet, consistent with previous observations at Stellwagen Bank (Haury 1978, 1979).

The internal wave packet during the flood tide was identified using the chlorophyll-*a* fluorescence signal from ISIIS. High frequency and amplitude oscillations occurred 4.1 km into the fixed depth transect oriented toward shore. Waves also propagate towards shore, and a fast-Fourier transform indicated that the wavelength of the energy in the oscillations was ~160 m using the average speed of the vehicle through the water of 2.5 m s^{-1} (Fig. 3.2B).

Larval fish distribution and patchiness

A total of 1,803 fish larvae were identified in the images. The most abundant families were Phycidae (27.8%), Merlucciidae (25.2%), and Labridae (11.2%) (Fig. 3.3). Approximately 14% of the fish found were not identifiable to the family level due to orientation into the camera and/or lack of detectible features for a positive identification. An additional 11% were preflexion larvae that were not identifiable to family, but based on the bongo samples, likely belonged to either Phycidae or Merlucciidae. The bongo

nets captured 245 larvae, with a mean concentration of 0.5042 ind. m^{-3}. Phycidae (31.1%) and Merlucciidae (29.8%) made up a majority of the catch.

The abundance of larval fishes in the ISIIS images was strongly related to depth. Despite relatively even sampling throughout the water column during ISIIS profiles, 89.1% of fish larvae found were in the shallowest 10 m of the water column, and 96.2% were found <20 m deep. Peak average concentrations of 5 - 8 ind. m^{-3} occurred within the shallowest 5 m for both the stratified and internal wave phases of sampling (Fig. 3.4). Vertical distributions broken down by standard length size classes (all taxa pooled) revealed ontogenetic vertical migration (Fig. 3.5). The smaller size classes exhibited increased depth variability (<3 mm) or bimodal distributions (3-4 mm and 4-6 mm) during internal wave propagation.

Two different metrics of patchiness revealed that larvae were aggregated in their distributions. Distance to next encounter (DNE) calculated for the fixed depth transects revealed that larvae were more aggregated than would be expected if fish were distributed randomly along the transect (Fig. 3.6A, B). More larvae were greater than 100 m from the next larva during the internal wave phase (26 vs. 10 larvae), creating many more patches at this level of Dmax and translating to a smaller average patch size (Fig. 3.6C). Lloyd's index of patchiness varied in relations to larval fish size, stratification conditions, and whether the metric was calculated for the vertical or horizontal direction. Patchiness was always highest for the smallest size class of preflexion larvae (<3 mm) and generally decreased with increasing size of the larvae. Larvae displayed higher patchiness during the ISIIS full water column profiles than for the fixed depth transect, indicating a stronger component of patchiness occurred in the vertical direction. Only

during the stratified ISIIS profiles did fish larvae show a U-shaped patchiness with size relationship, showing larger individuals aggregating together (Fig. 3.7).

Copepod and predator zooplankton abundance

An automated copepod counter estimated copepod abundance, and manual checking revealed that the counter was very accurate near the surface (97.5% accuracy from 0-10 m), with accuracy declining with depth (minimum accuracy was 80.3% at 40-50 m depth, Table 3.1). The reason for this change in accuracy was the increased abundance of marine snow at depth (fecal pellets, dead diatoms, parts of euphausiid exoskeletons) that the counter was unable to distinguish from copepods. Near the thermocline (10-20 m), the errors in the counter were mostly due to some small shrimps in the same size range as larger copepods (4.1% of objects counted in this depth stratum were shrimps). Multiple copepods overlapping and being counted as one represented only a small issue near the surface where copepods were extremely abundant (8 instances out of 2445 total particles, 0.3%) and likely did not contribute to a significant underestimate of copepod abundances even at the surface where copepod concentrations were high (Table 3.1).

Copepods were generally most abundant a few meters above the chlorophyll-*a* maximum, strongly overlapping the vertical distribution of fish larvae (Fig. 3.8). During the stratified phase of sampling, a copepod thin layer was present at ~5 m depth in the sampling area farthest from Stellwagen Bank, reaching a peak concentration of approximately 300,000 ind. m^{-3} (over 40 times higher concentration than the transect average) and spanning 2-3 km in the dimension of the transect (Fig. 3.8B). Average

concentration of copepods for fixed depth transects was ~7100 ind. m^{-3} for the stratified phase and ~2500 ind. m^{-3} when internal waves were present (Table 3.2).

A total of 22,444 zooplankton predators, including lobate ctenophores, the cydippid ctenophore *Euplokamis* spp., the holoplanktonic polychaete *Tomopteris* spp., chaetognaths, hydromedusae, and siphonophores, were identified in the ISIIS images. Zooplankton predators displayed strong taxon dependent vertical distributions (Fig. 3.9). In the shallowest 10 m of the water column, an area dominated by larval fishes and copepods, gelatinous zooplankton were relatively rare; however, the taxa most abundant in this zone were lobate ctenophores and hydromedusae. Chaetognaths and Euphausiids (not quantified) were most common from 10-20 m, and the community gradually transitioned into one dominated by very high abundances of *Euplokamis* spp. and lobate ctenophores at depth. *Tomopteris* spp., although relatively rare compared to the gelatinous zooplankton, had a wide depth range but was most common from 20-50 m depth. On the full water column profile transects, twice as many predator zooplankton were found in the internal waves phase (12,991) compared to the stratified phase (6,696), predominantly well below the thermocline. Patches of predator zooplankton were consistently larger during the stratified phase (Fig. 3.10A), and the reduced abundances of these organisms strongly corresponded with the position of the internal wave packet (Fig. 3.10B).

Correlations between different zooplankton taxa

For the stratified phase of sampling, positive correlations between taxa were more common than during the internal waves phase. Fish larvae, however, showed a higher

correlation with lobate ctenophores (including *Beroe* spp.) and a lower, though still significant, correlation with copepods during the internal wave phase compared to stratified conditions (Fig. 3.11). The only significant negative correlations were between copepods and lobate ctenophores (and unknown ctenophores) during the internal wave phase.

The internal wave packet had specific effects on the concentration and sizes of fish larvae, predators, and prey. Chlorophyll-*a* fluorescence was higher and more variable within the internal wave packet, and copepod concentrations were lower (Fig. 3.12A). Areas through which the internal wave packet had already passed had higher copepod abundances, and chlorophyll-*a* fluorescence was lowest. Larval fishes in this area were also abundant, but small in size (~5 mm average standard length). In areas that the internal wave packet had not yet reached, copepod abundances were not significantly different from within the wave packet, but chlorophyll-*a* fluorescence was lower. Larval fishes in this zone were less abundant but larger in size (~8 mm average standard length, Fig. 3.12B).

Discussion

Analyses of the fine-scale vertical and horizontal distributions of organisms using ISIIS imagery showed strong differences in overall abundances, patchiness, and correlations among taxa under stratified and internal wave propagation near Stellwagen Bank. Fish larvae and copepods were most abundant in the shallowest 10 m of the water column, while predator zooplankton were abundant in deeper waters but displayed taxon-specific depth preferences. The propagation of internal waves via internal hydraulic jump

altered the thermocline depth both in front of (shallower) and behind (deeper) the internal wave packet. This had strong effects on the feeding and predator environment of the abundant larval fishes in the sampling area contributing to increased spatial overlap with potential predators, decreased abundance and spatial overlap with copepod prey, and smaller larval patch sizes.

Larval fishes must strike a balance between finding food (copepods or nauplii), avoiding predators (larger fishes and a suite of zooplankton predators), and being transported to habitats favorable for settlement and their juvenile life stage. The heterogeneity observed here is indirect evidence that their environment can quickly shift from favorable (abundant prey resources) to poor (abundant predators). Internal waves have been suggested as a mechanism of transport and vertical mixing (Shanks 1983, 1995; Pineda et al. 1999), but sampling technology has been inadequate to examine fine-scale distributions of fishes and their predators simultaneously in relation to these features. The shift from a stratified environment to one that is vertically mixed due to internal waves can have strong effects on the predator-prey interactions in the plankton.

Larval fish patterns

Larval fish distributions varied with size in both the vertical and horizontal directions. Not surprisingly, given the strong depth patterns of abundance, larval fish patchiness was higher on the vertical profiles (vertical component) than the fixed depth transects (horizontal component) for a majority of the size classes. The exceptions were the smallest individuals (<3 mm) who may form generally small patches due to adult batch spawning and limited larval swimming ability (Pepin 2002). The largest size class

(>8 mm) was close to randomly distributed, which may be a product of their rarity in the images. We used a fixed block size for calculating patchiness, but the larval size range quantified was much smaller than those captured by Masuura and Hewitt (1995), who detected a U-shaped pattern in patchiness with increasing larval size. The only sampling transect that produced an indication of a U-shaped patchiness curve with size was the fixed depth stratified phase, while all other sampling of both stratified and internal wave phases showed an exponential decrease in patchiness with size.

Larval fish sizes also changed dramatically in relation to the internal wave packet. The largest larvae in the fixed depth transect were found on the leading side of the packet, mostly consisting of the family Ophidiidae, but in low concentrations. Larger larvae, although rare, were generally more abundant in deeper waters, and the thermocline in front of the internal wave packet was shallow. Near Stellwagen Bank, smaller larvae, which were more abundant near the surface, were found in higher concentrations. This is consistent with the findings of Lai et al. (2010), who modeled downwelling near the slope of Stellwagen Bank and upwelling in the basin portion of our study area during internal wave propagation. These circulation patterns could explain the larval size shifts along the fixed depth transect, where small larvae were downwelled near the bank, and large larvae were upwelled near the basin.

The Distance to Next Encounter (DNE) metric was originally used to measure patch characteristics of particles obtained using the Optical Plankton Counter (Currie et al. 1998). This study, representing the first application of this technique to larval fishes, revealed larger patch sizes occurred during the stratified phase of sampling. The higher

frequency of large gaps between larvae in the internal wave phase of sampling meant there were more larval patches, thus driving the calculation of average patch size down.

Relationship of copepods to adjacent trophic levels and internal waves

Copepods were aggregated above the thermocline and chlorophyll-*a* maximum in both phases of sampling, but were generally found in higher concentrations during the stratified phase. The ISIIS images revealed that diatom chains dominated zones of high chlorophyll-*a* fluorescence, and many species of copepods have been shown to avoid zones of high diatom concentration, potentially due to deleterious effects of a diatom-based diet (Miralto et al. 1999; Leising et al. 2005; Pierson et al. 2005). During the stratified phase, copepods were approximately twice as abundant (compared to the internal wave phase) and formed a thin layer that spanned approximately 3 km horizontally and was located a few meters shallower than the chlorophyll-*a* maximum. This is consistent with other high-resolution observations showing the vertical separation of zooplankton thin layers and phytoplankton during daylight hours (McManus et al. 2005; Holliday et al. 2007). There are three possible explanations for the decrease in abundance between stratified and internal wave sampling: 1) the thin layer was advected closer to shore, 2) near surface mixing dispersed the thin layer both vertically and horizontally, or 3) the thin layer was an anomalous patch that was not sampled during the internal wave phase. Since we only sampled in two dimensions, the spatial extent of the patch perpendicular to the transect was unknown, and therefore it is not possible to know if this was simply an anomalous patch with a very small dimension perpendicular to the transect path. To ascertain if advection of the layer was possible, an estimate of wave

phase speed is necessary, but our sampling scheme did not allow us to make this calculation. Nonetheless, if onshore advection were the cause, the patch would have to have been advected at a minimum speed of 56 cm s^{-1} starting at onset of the flood tide, which is faster than published internal wave speeds (Lai et al. 2010) and maximum surface tidal currents in this area (Blumberg et al. 1993). Results of this study showed reduced copepod abundance within the internal wave packet, consistent with previous research that documented internal wave driven mixing of plankton patches (Haury 1983; Sevadjian et al. 2012); therefore, it is more likely that mixing led to the dispersal of the thin layer.

Internal waves appeared to reduce copepod average abundance and increase their variability. In relation to the internal wave packet, copepod concentrations were highest in areas that the packet had already passed through and lowest within the packet (despite high chlorophyll-*a* fluorescence within the packet). Mixing within the packet could be driving the reduced abundance of copepods that then swarm together after the wave energy has passed to exploit small scale food patches. The thermocline was shallower in front of the internal wave packet, and deeper waters richer in oxygen were present near 10 m depth. The shoaling thermocline is a likely mechanism for pushing copepods out of this area of the water column, leading to low abundances before the internal wave packet arrived.

In addition to the generally high abundances of copepods in the stratified phase, fish larvae had a higher positive correlation with copepods on the fixed depth transect (~10 m depth) compared to the internal wave fixed depth transect. From the perspective of food concentrations, therefore, stratified conditions may allow more fish larvae to

experience favorable feeding environments due to decreased mixing. Lasker (1975) conducted lab and field experiments demonstrating that first feeding anchovy larvae had higher survivorship when ocean conditions were stratified. Although Lasker's (1975) study occurred in the wind-dominated upwelling system of the eastern Pacific, similar "stable events" in other systems could lead to higher concentrations of prey for larval fishes, and the results of our study suggest this can happen in relation to internal wave activity.

Negative correlations of copepods with predator zooplankton potentially support the idea of avoidance behavior and highlight the importance of measurement scales. Copepods, lobate ctenophores, and unknown ctenophores were all more abundant in zones after the internal wave packet had passed, but spearman correlations showed a negative association of copepods with these two ctenophore groups. The seeming contradiction is resolved by examining the scales of each measurement: the Spearman correlations made on a 1 m^3 scale show a negative association, while averaging over the entire "after" section of the internal wave packet shows positive association. Predation avoidance of copepods has been documented in other studies (Bollens et al. 1992; Carr and Pitt 2009), and the copepod sensory appendages and overall morphology suggest strong selection for predation avoidance (Kiørboe 2008). The results of our study further support the idea that organism behavior highly influences fine-scale distributions.

Predator zooplankton

One of the most noticeable differences in the vertical distribution of predator zooplankton between the two sampling periods was the shift in depth of the large

aggregation of lobate ctenophores and *Euplokamis* spp. ISIIS sampled a minimum of 5 m from the bottom, and during the stratified phase of sampling, there are indications that gelatinous zooplankton were aggregating near the bottom in a region we could not sample. One well-documented consequence of internal wave activity in coastal environments is the resuspension of sediments (Johnson et al. 2001) and bottom transport offshore (Butman et al. 2006). Cydippid ctenophores, such as *Euplokamis* spp., have been observed avoiding zones of the water column with high concentrations of particulates or diatoms, presumably to minimize adhesion of undesirable materials to their colloblasts (Malkiel et al. 2006). Sediment resuspension as would occur with the passage of internal waves, therefore, could drive *Euplokamis* spp. and other ctenophores away from the bottom. Sampling for the internal waves began at 1630 (sunset typically around 2000), so light levels are an unlikely explanation for the vertical displacement of these organisms.

The zone of the fixed depth transects (near thermocline, ~10 m) corresponded to some of the lowest concentrations of predator zooplankton. This is in contrast to some well-documented patterns of gelatinous organisms aggregating near density discontinuities (Graham et al. 2001; Jacobsen and Norrbin 2009; Frost et al. 2010). The pycnocline zone of the water column was dominated by phytoplankton (chlorophyll-*a*), small chaetognaths, and decapod shrimps, with shrimps potentially grazing the abundant phytoplankton. Aggregations at density discontinuities have been suggested as a passive mechanism of gelatinous zooplankton aggregation, and the observations of ISIIS at Stellwagen Bank suggest that behavior of the zooplankton can have a profound effect on whether or not they aggregate in a density discontinuity. In a similar manner that gelatinous predators were likely driven off the bottom from resuspended sediment, large

numbers of diatom chains present at the pycnocline (qualitative, not enumerated by the automated counter) could have induced avoidance behavior of this zone of the water column. The zone of the internal wave fixed depth transect that had already been mixed by the internal wave packet was the zone where gelatinous predators were abundant. This vertical mixing is likely responsible for overall predator zooplankton abundances that were twice as high during the internal wave vs. stratified fixed depth transects.

Predator zooplankton, including several different gelatinous taxa, were dominant in deeper waters sampled and generally not in close proximity to aggregations of copepods, the preferred prey item for many of these organisms. This is similar to findings from plankton imaging in a different oceanographic environment, Monterey Bay, in which many gelatinous taxa aggregated at depth (Greer et al. 2013) while copepods remained at the surface a few meters above the chlorophyll-*a* maximum. It must be noted, however, that copepods are present at all depths of the water column, so these gelatinous organisms either do not require aggregated food resources to survive or vertically migrate to the surface at night to feed on dense patches of prey. Diel vertical migration studies would shed light onto this predator-prey relationship.

Trophic interactions in the vertical and horizontal

The strong vertical structure in the biota of Stellwagen Bank has many implications for predator-prey interactions and the life cycle of fishes. Based on the distribution of prey and larval fishes, most larvae should experience much higher than average concentrations of copepod prey, especially within the shallowest 5 m of the water column. Potential predators were by far most abundant in a portion of the water column

that was virtually uninhabited by larval fishes; however, *Beroe* spp., hydromedusae, and lobate ctenophores were present near the surface, and because of this, these taxa can be considered to be more likely candidates for predators of larval fishes than *Euplokamis* spp., which, although abundant, almost exclusively occupied waters > 15 m deep. In addition, small larvae similar to the ones present near surface have been shown to be more vulnerable to predation by gelatinous zooplankton (Bailey and Batty 1984; Titelman and Hansson 2006). Some have argued that lobate ctenophores exhibit minimal predatory impact on larval fishes (Jaspers et al. 2011), but these calculations were based on estimated predator concentrations orders of magnitude lower than found in this study. It is unknown to what extent larvae can detect and avoid the surface-dwelling predators, or if the predator field changes at night through vertical migration.

Changes in the correlations among concentrations of different taxa in the horizontal dimension were associated with the presence of internal waves. Internal wave activity may reduce the concentration of prey on scales relevant to larval fishes (1-10 m), especially within the internal wave packet itself, as demonstrated by the 2.8 times higher copepod concentration in the stratified phase. When internal waves were present, larval fishes were more highly correlated with lobate ctenophores (also *Beroe* spp. and unknown ctenophores) and were less correlated with copepod prey than during the stratified conditions. The area of the fixed depth transect that had already been mixed by the internal waves likely heavily contributed to these higher correlations between larval fishes and zooplankton predators because abundances of both fish larvae and gelatinous zooplankton were high.

Considering both the horizontal and vertical dimensions, these analyses suggest that overall trophic conditions for larval fishes may be less favorable for survival during the propagating internal waves. The thermocline region sampled by fixed depth transects represents a vertical minimum in predator concentration but still has fairly abundant copepod prey, making it an ideal habitat for larval fishes. Oscillations of the thermocline caused by the flood tide interaction with Stellwagen Bank and subsequent internal hydraulic jump alter this habitat by vertically transporting zooplankton predators and dispersing patches of prey in both the vertical and horizontal dimensions. A shoaling thermocline in front of the propagating internal waves brings deeper water ctenophores, such as *Euplokamis* spp., and larger fish larvae into shallower waters, and restricts the depths of smaller larval fishes to near surface. The predictable summertime changes between stratified and internal wave conditions suggest semi-diurnal (hrs) oscillations in the drivers of plankton distributions. The ebb tide (stratified) is dominated by behavior of organisms where patches can form and correlations between taxa occupying similar depths are high, whereas internal waves are characterized by physical forcing that redistributes organisms vertically, bringing together organisms that are vertically separated under stratified conditions.

Fine-scale spatial relationships provide insights into potential trophic interactions relevant to larval fish survival. Larval fishes in our study aggregated in zones where copepods were abundant, suggesting, as has been previously hypothesized, that larvae experience much higher than average concentrations of prey. Predator zooplankton tended to reside deeper in the water column, and may, through vertical migration, be more important predators at night. Fine-scale correlations in the horizontal dimension

revealed that during internal wave propagation larval fishes were exposed to reduced food resources and higher abundances of potential predators. Combined, these data suggest that stratification in the Stellwagen Bank region is more favorable to larval fishes that require high concentrations of food; however, turbulence associated with the internal wave packet could improve plankton encounter rates to increase feeding (Rothschild and Osborn 1988; Kiørboe and MacKenzie 1995; MacKenzie 2000). More studies over longer time scales, perhaps utilizing a Lagrangian reference and larval condition metrics, will enable an assessment of the impact of stratification/mixing on larval fish survival. Optical systems, such as ISIIS, provide information on scales relevant to individuals to improve our understanding of processes contributing to population variability in the ocean.

Tables

Table 3.1. Copepod counter accuracy as verified by human identification for 10 m depth bins. Each particle enumerated by the counter was classified into one of six categories: copepods (true positive), marine snow, shrimp, jelly parts, appendicularians, and double counts (two copepods overlapping and counted as one particle).

	0 - 10 m	10 - 20 m	20 - 30 m	30 - 40 m	40 - 50 m
copepods	2383	2390	2582	2256	2027
marine snow	34	24	103	192	298
shrimp	0	105	9	5	5
jelly parts	26	8	28	26	6
appendicularians	2	6	24	245	189
double count	8	0	0	0	0
accuracy	0.9746	0.9435	0.9403	0.8282	0.8028

Table 3.2. Larval fish patchiness and prey environment using 1 m^3 sample sizes for the four different transects under stratified and internal wave conditions.

Water column Sampling Approach	Stratified profiles	Internal waves profiles	Stratified fixed depth	Internal waves fixed depth
Average copepod concentration	7496.326	5551.054	7109.010	2464.862
Standard error	226.688	52.865	71.037	19.429
Copepod patchiness	8.517	1.645	1.682	1.463
Larval patchiness index	5.2652	6.8700	1.7200	2.2431
Percent of larvae above average prey concentration	35.76	59.77	59.37	49.46
Percent of larvae in double average prey concentration	21.5	39.94	16.19	18.28
Percent of larvae in 5 times average prey concentration	13.95	7.08	1.90	0.43
Percent of larvae in 10 times average prey concentration	9.59	0	0	0

Figures

Figure 3.1. Map of the transect locations during stratified and internal wave phases of sampling. Bathymetry contours are shown in blue with color corresponding to depth.

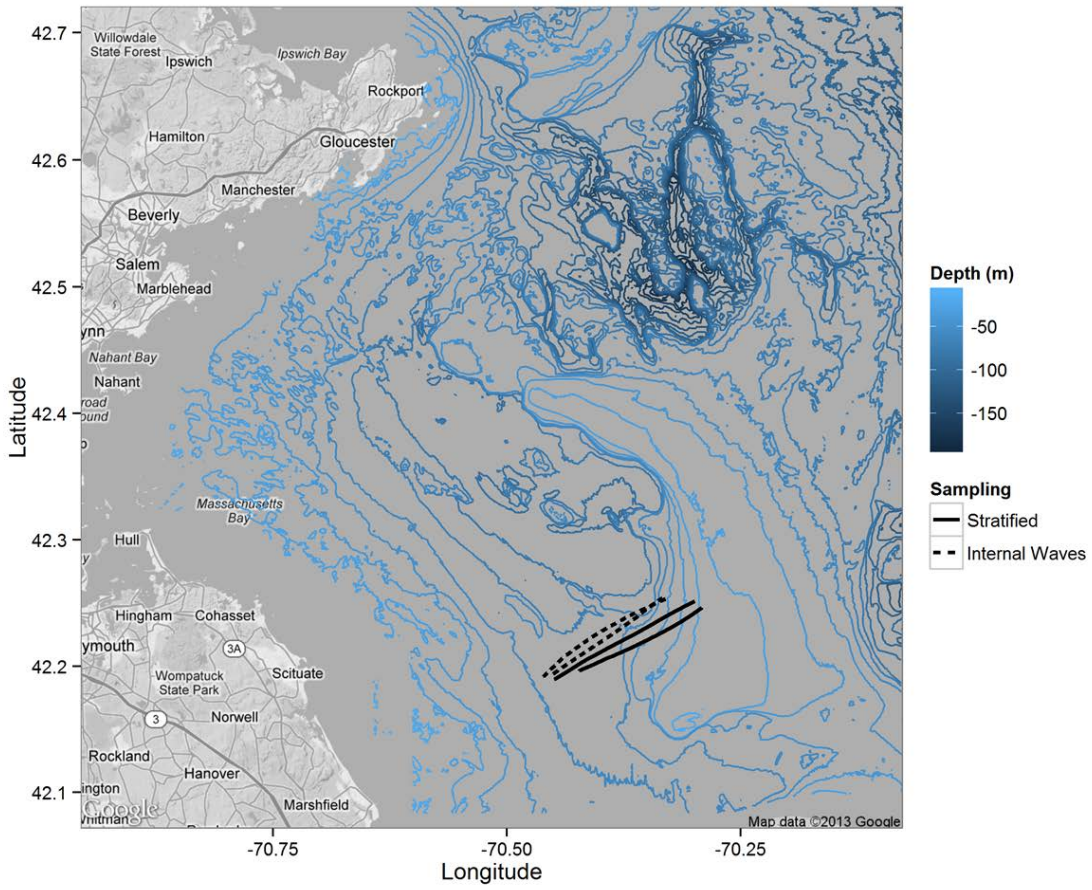

Figure 3.2. A) Physical properties of water sampled during fixed depth transects. First panel shows the depth of the ISIIS vehicle for the samples B) Close up of the internal wave packet as determined by chlorophyll-*a* fluorescence and associated power spectrum.

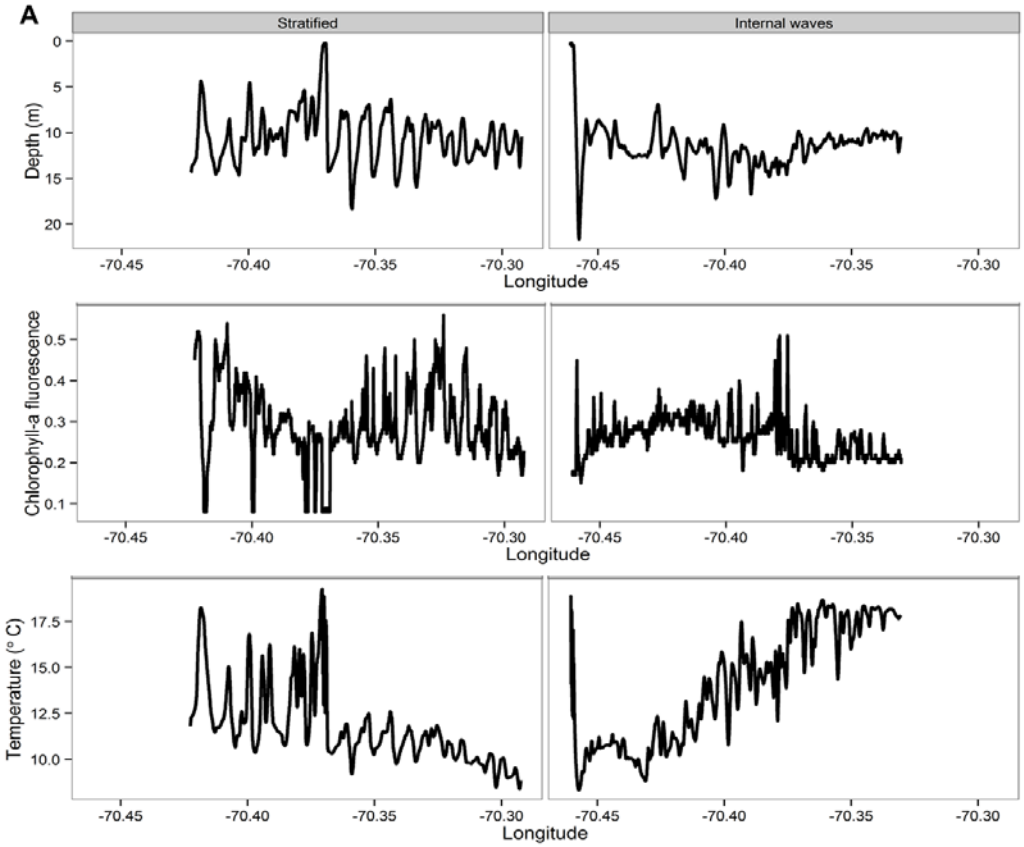

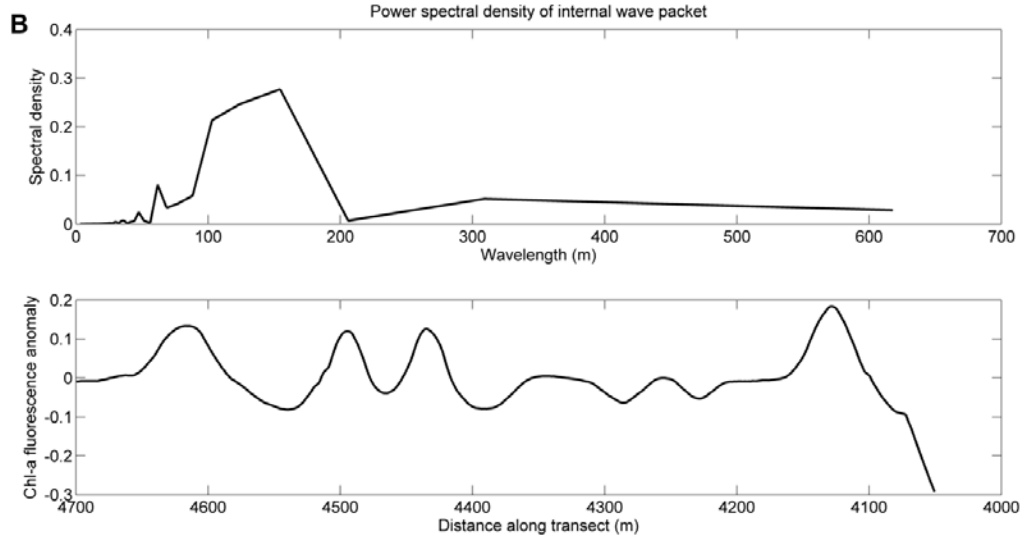

Figure 3.3. Larval fishes and zooplankton predators imaged with ISIIS A) *Merluccius* spp., B) Pleuronectiformes, C) *Euplokamis* spp., D) *Urophycis* spp., E) Labridae, F) Ophidiidae, G) Lobate ctenophore (*Bolinopsis* spp.), H) *Tomopteris* spp., I) Hydromedusa *Clytia hemisphaerica*

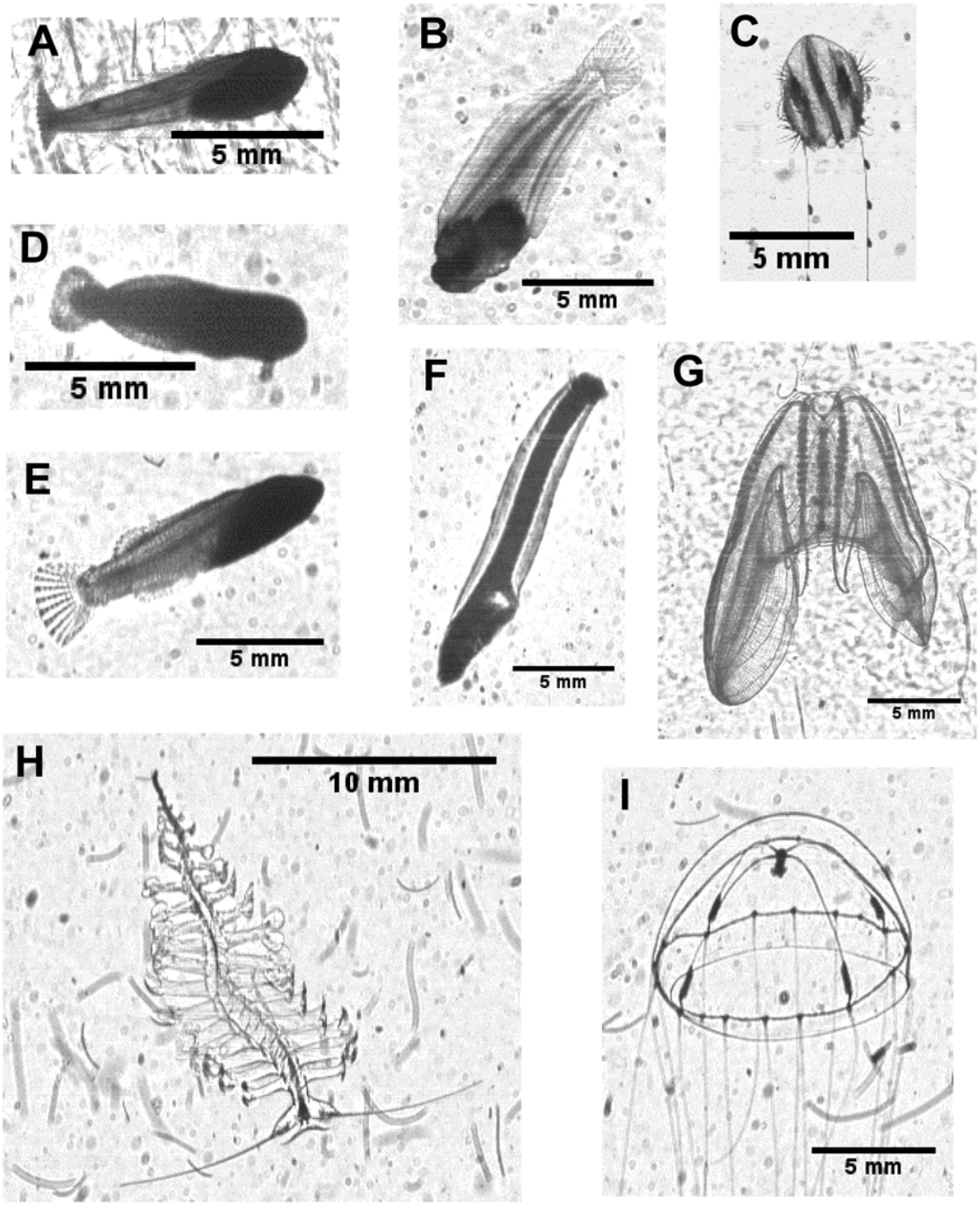

Figure 3.4. Vertical distribution of fish larvae during the different phases of sampling. Bars are stacked to give the total concentration of fish larvae in each 1 m depth bin.

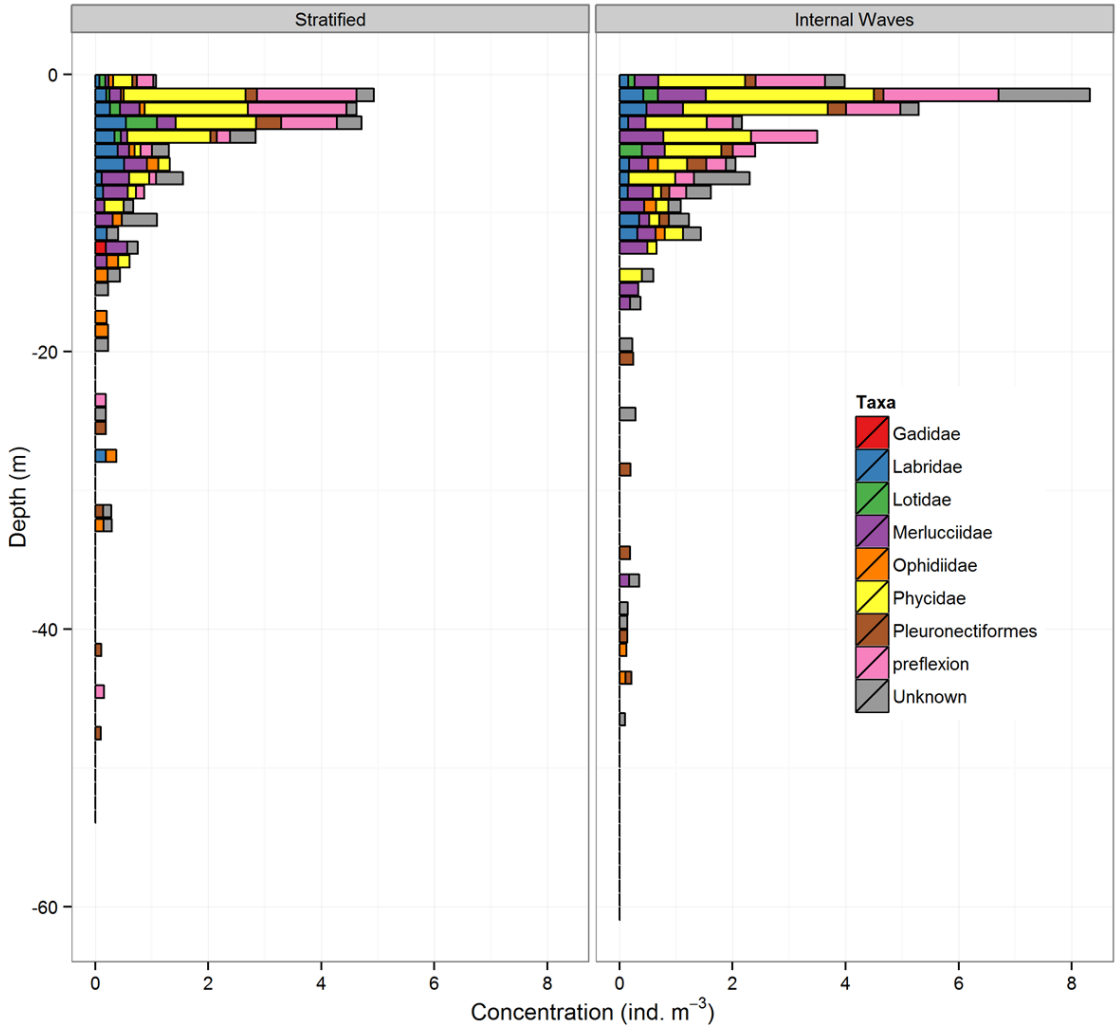

Figure 3.5. Vertical distribution of fish larvae in relation to size.

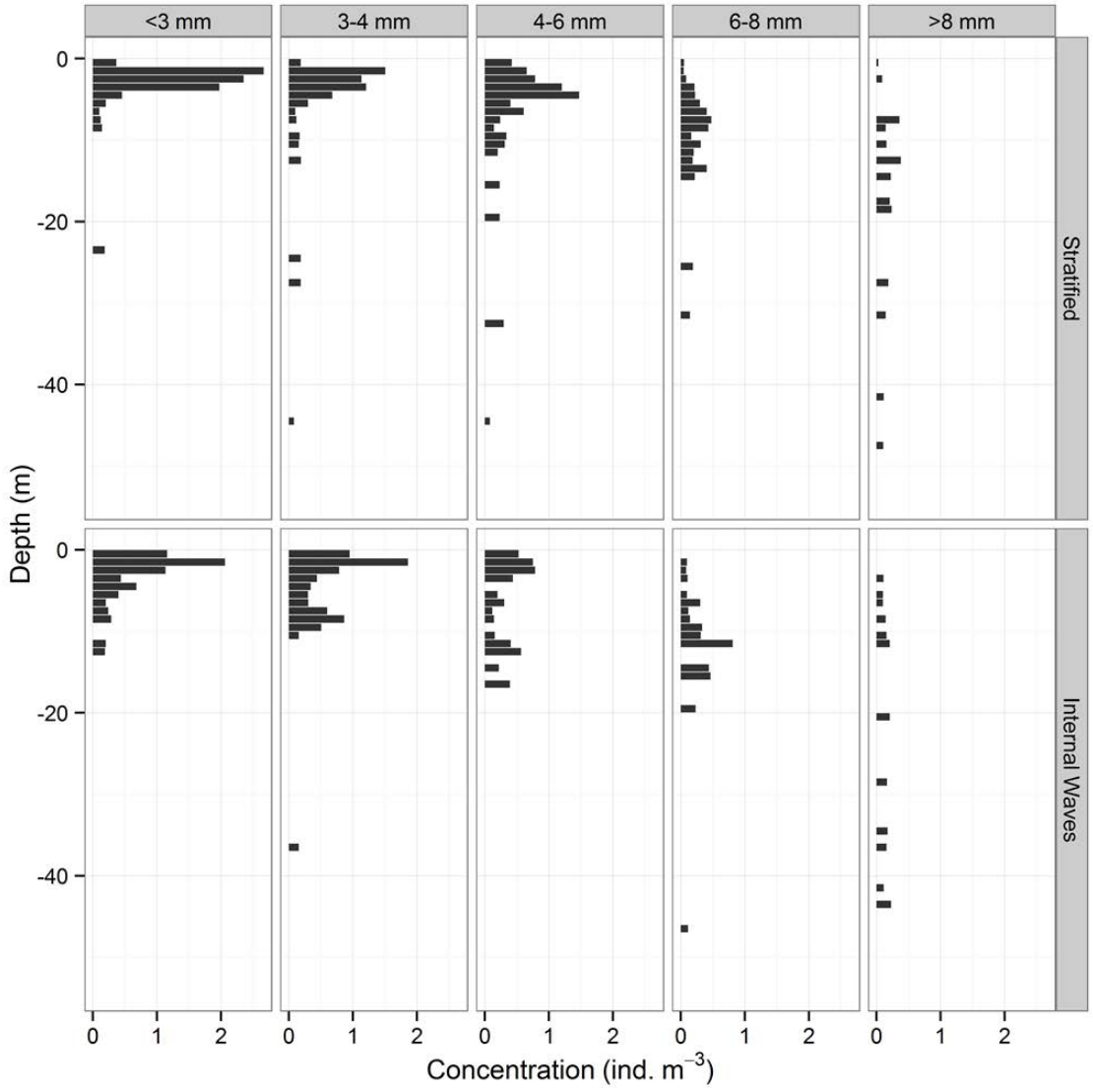

Figure 3.6. A) Distance to next encounter (DNE) for fish larvae in A) Stratified and B) Internal wave sampling phases. Black line shows the average DNE of 100 trials of a simulation of randomly distributed group of points along the transect. Dotted lines represent ± 1 standard deviation. C) Average linear patch size of fish larvae with varying definitions of Dmax (the maximum distance of an organism from its next neighbor to be considered to be within a patch).

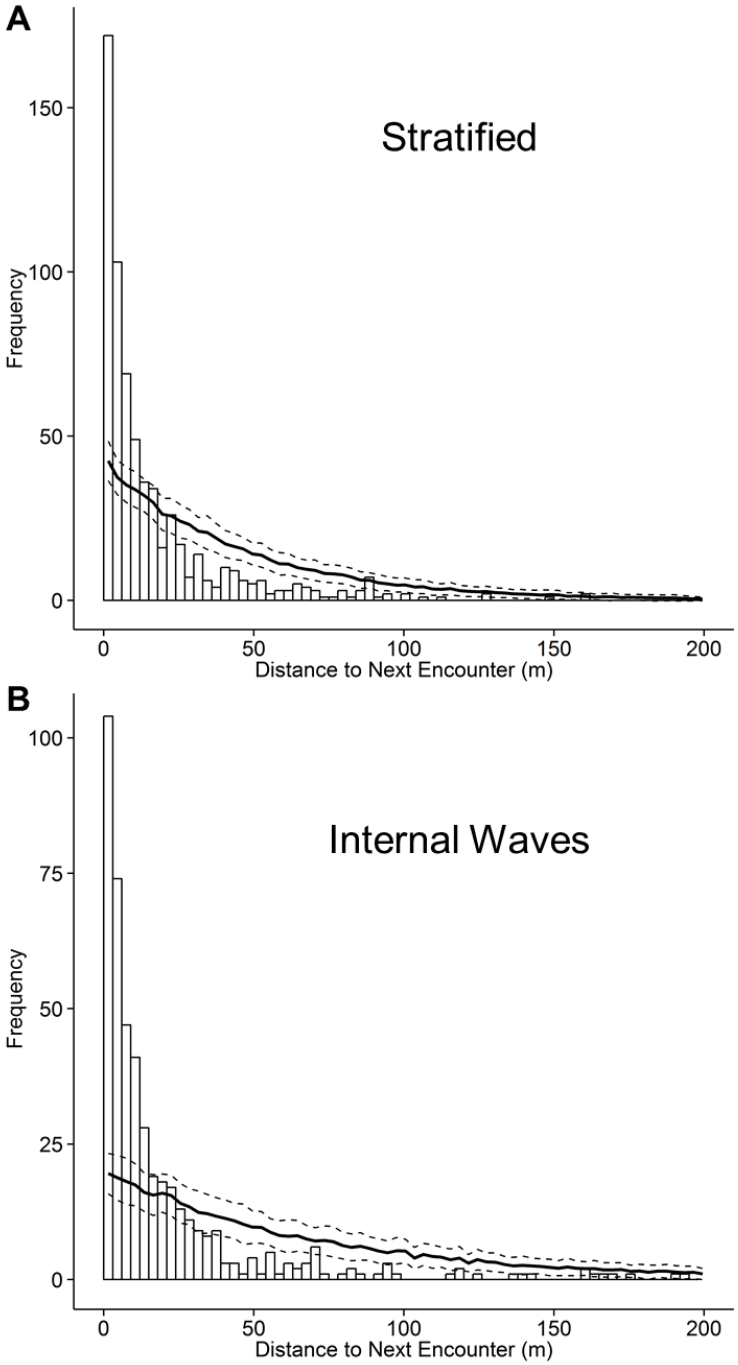

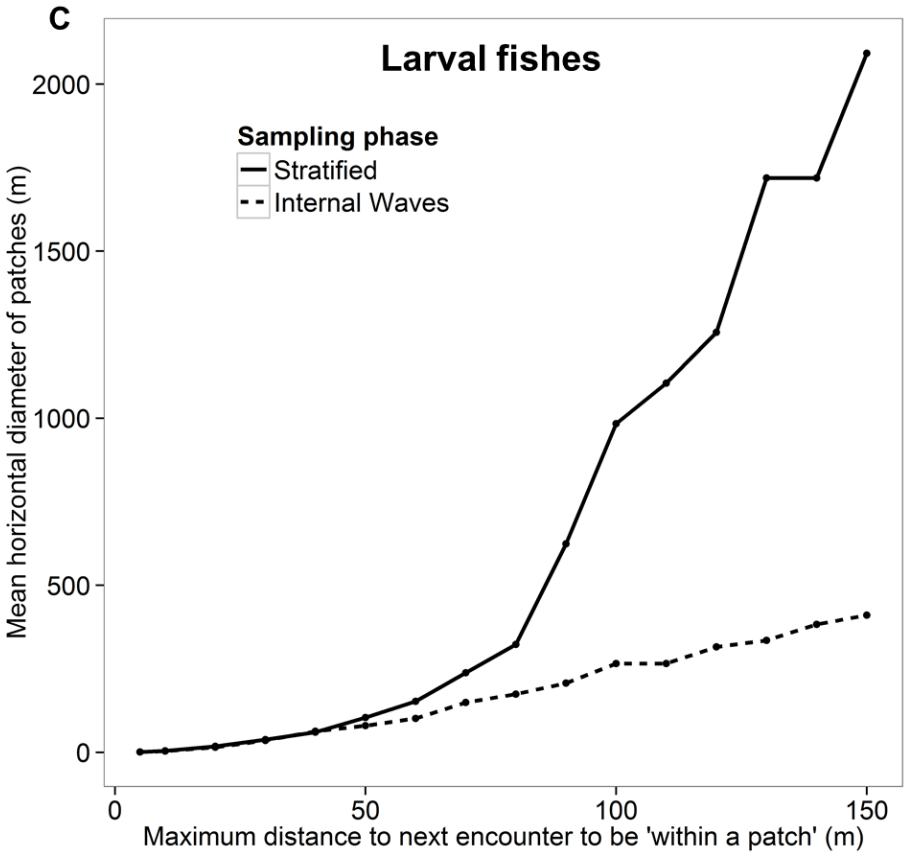
C
Larval fishes
Sampling phase
Stratified
Internal Waves
Mean horizontal diameter of patches (m)
2000
1500
1000
500
0
0
50
100
150
Maximum distance to next encounter to be 'within a patch' (m)

Figure 3.7. Lloyd's patchiness vs. size relationships for larval fishes in the four transects performed during internal waves (IW) and stratified conditions near Stellwagen Bank.

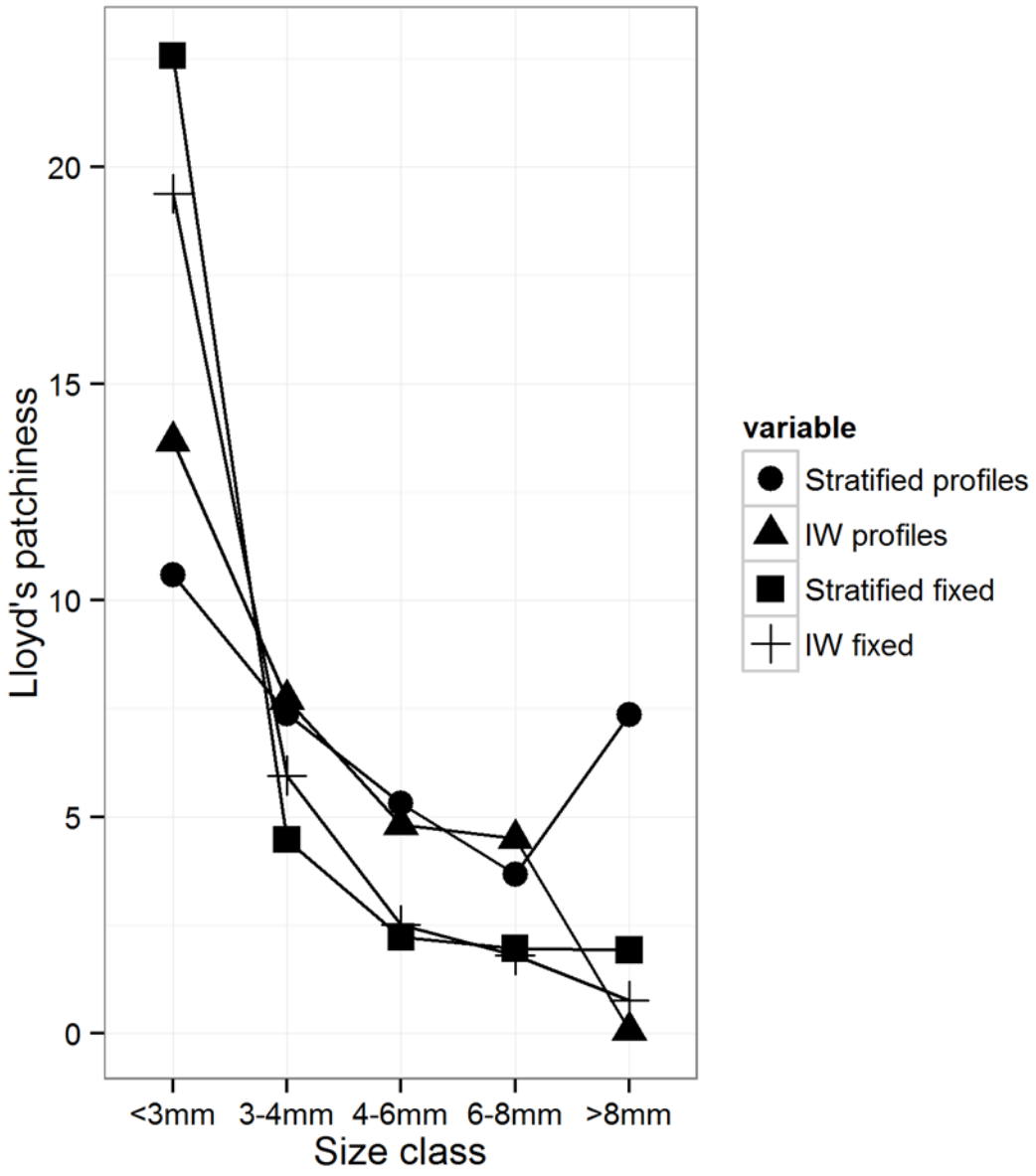

Figure 3.8. A) Vertical distribution of copepods with errorbars representing 1.96 standard error (SE) of the concentration. Horizontal lines represent the mean depth of the chlorophyll-*a* maximum with 1.96 SE of the depth indicated by dashed lines B) Copepod concentration on the three vertical profiles taken from offshore Stellwagen Bank. Results show a thin layer spanning approximately 3 km. The 0.3 and 0.4 volt contours of chlorophyll-*a* fluorescence are shown in black.

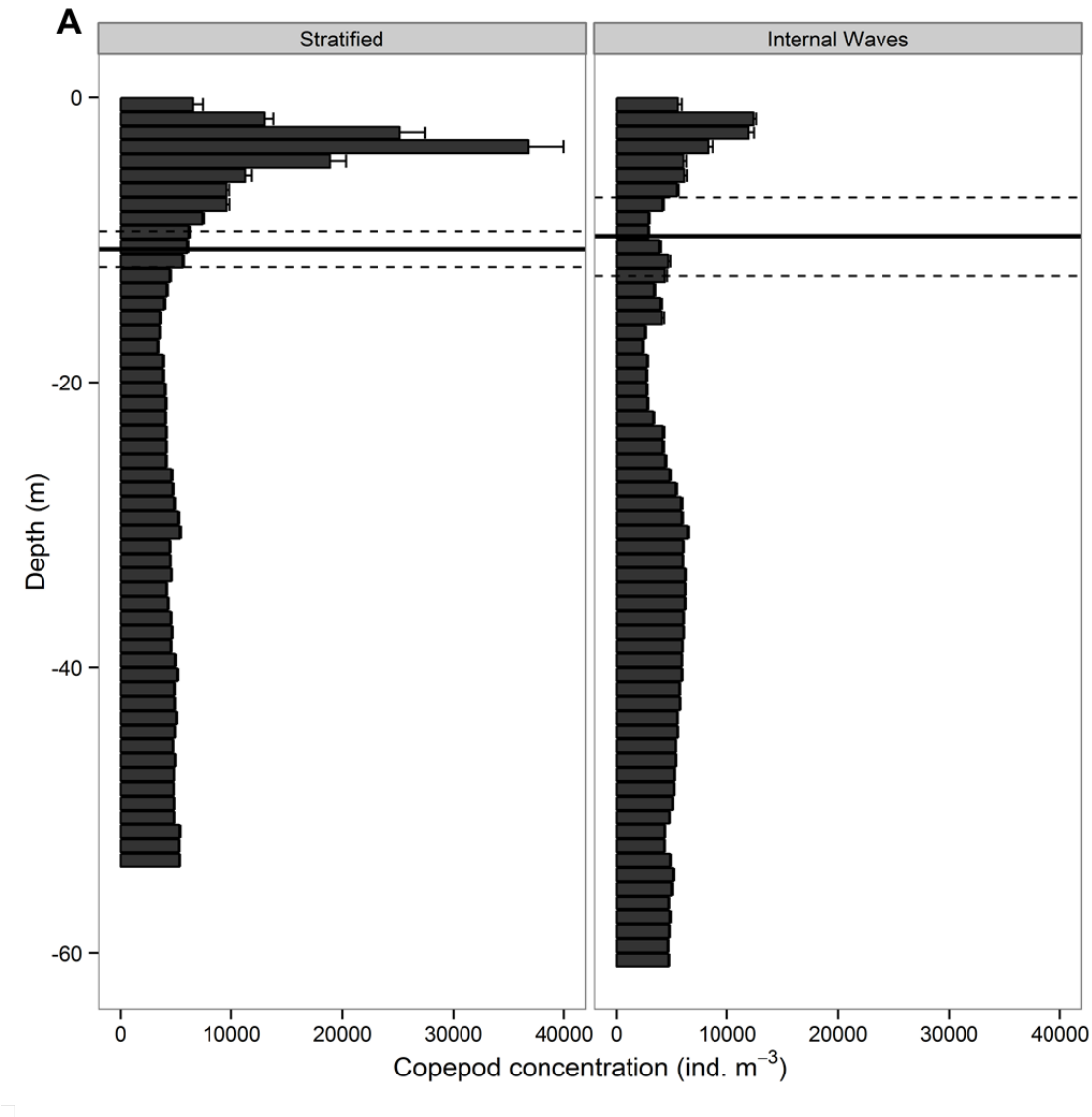

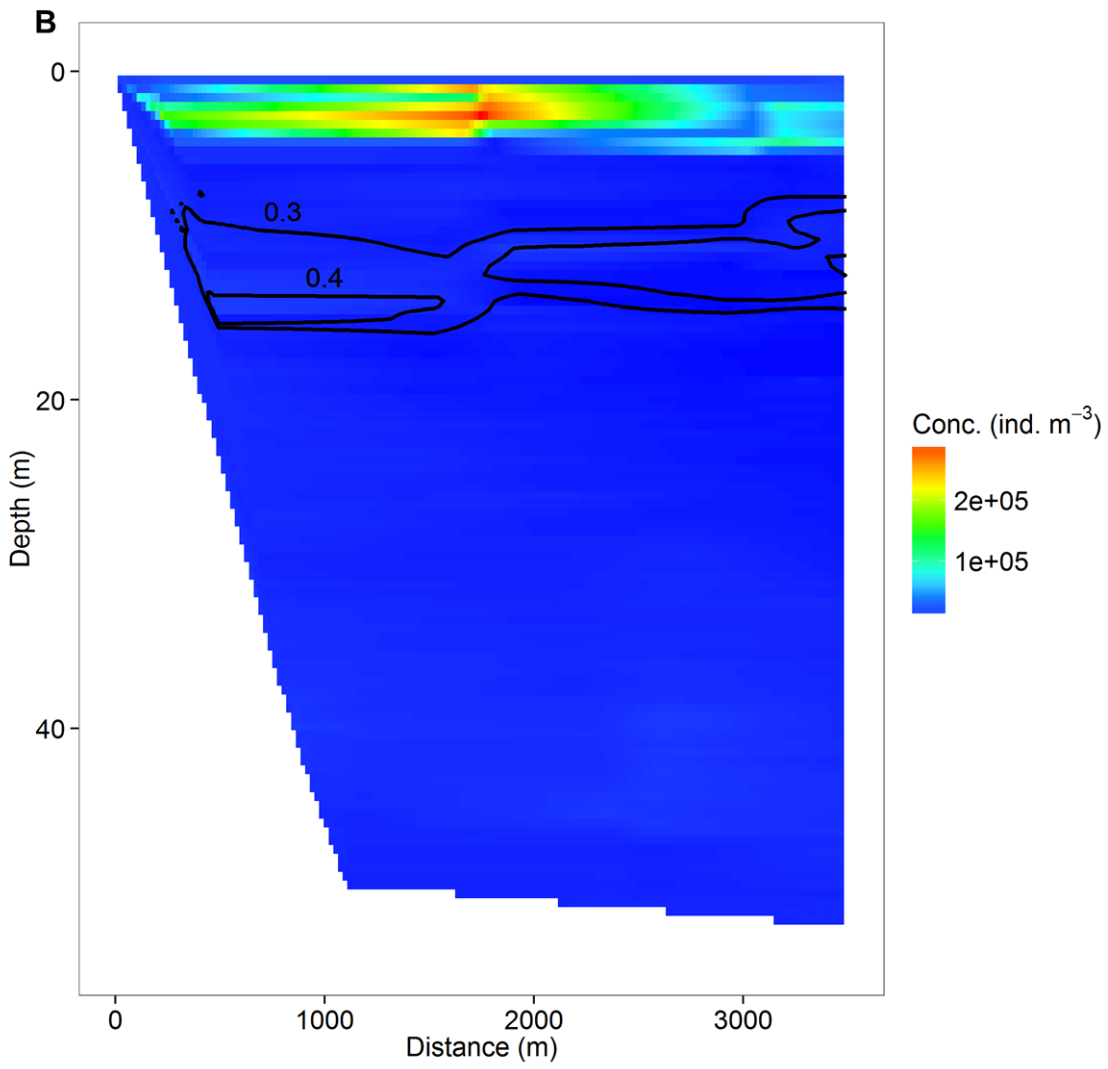
B
0
20
40
Depth (m)
0.3
0.4
0
1000
2000
3000
Distance (m)
Conc. (ind. m^{-3})
2e+05
1e+05

Figure 3.9. Vertical distribution of predator zooplankton in the different phases of sampling. Bars are stacked to give the total concentration of predator zooplankton in each 1 m depth bin.

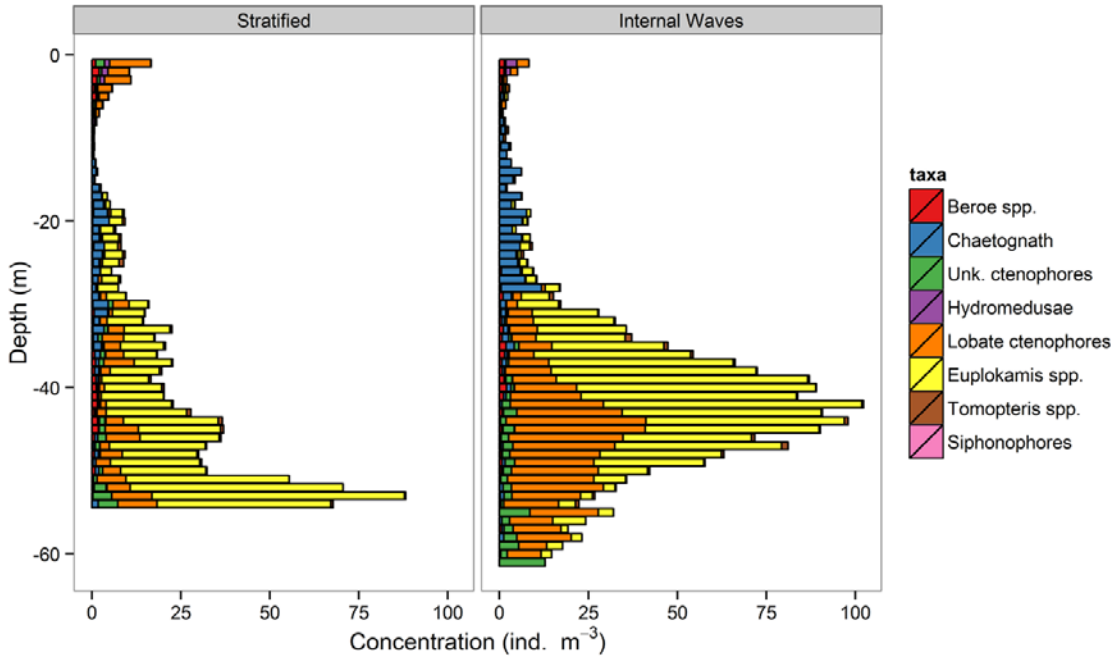

Figure 3.10. A) Location of the six most common predator zooplankton on the fixed depth transect during internal wave propagation. The dotted lines denote the area in which the internal wave packet was present during sampling (propagates to the left). B) Average linear patch size predator zooplankton with varying definitions of Dmax (the maximum distance of an organism from its next neighbor to be considered to be within a patch).

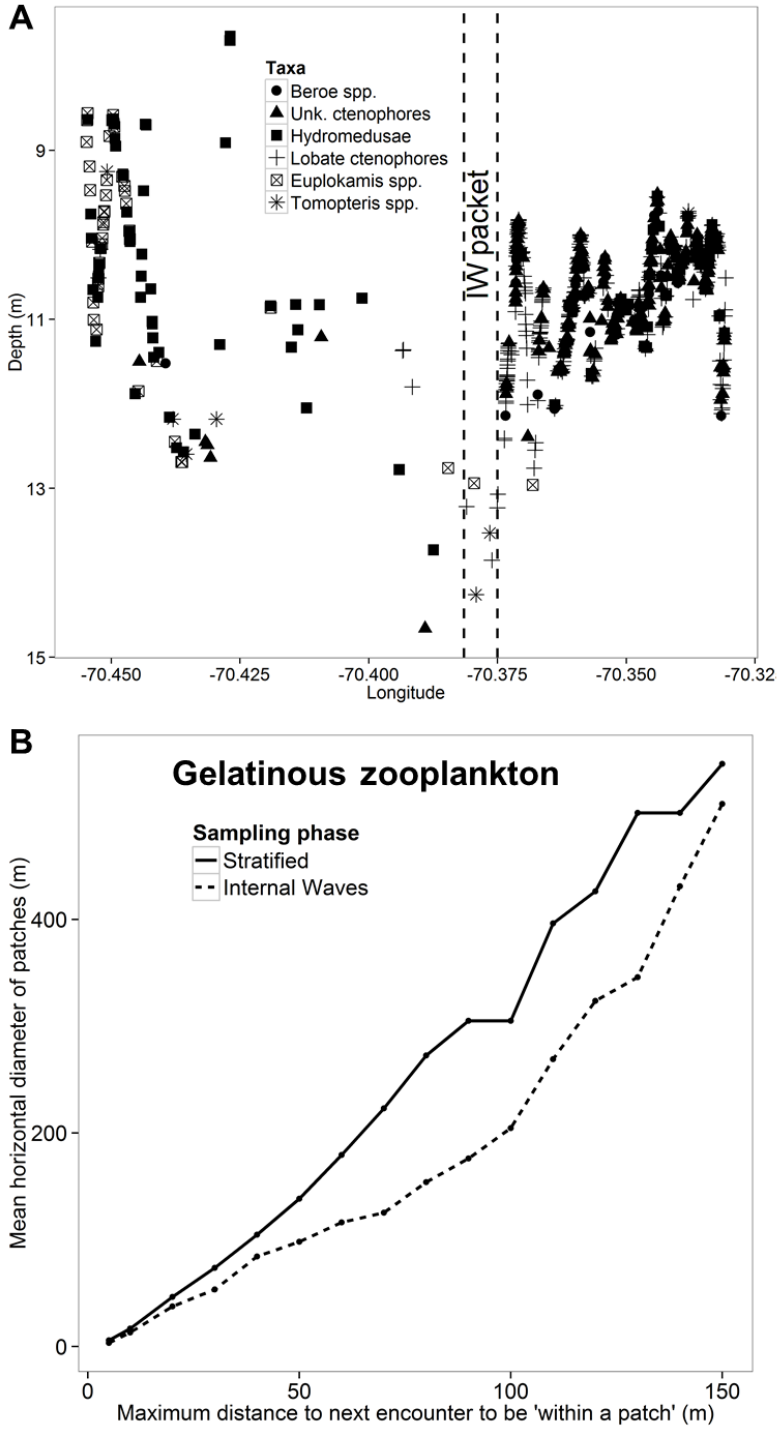

Figure 3.11. Spearman correlation coefficients for 1 m^3 binned counts of organisms along fixed depth transects for the (A) stratified and (B) internal wave phases of sampling.

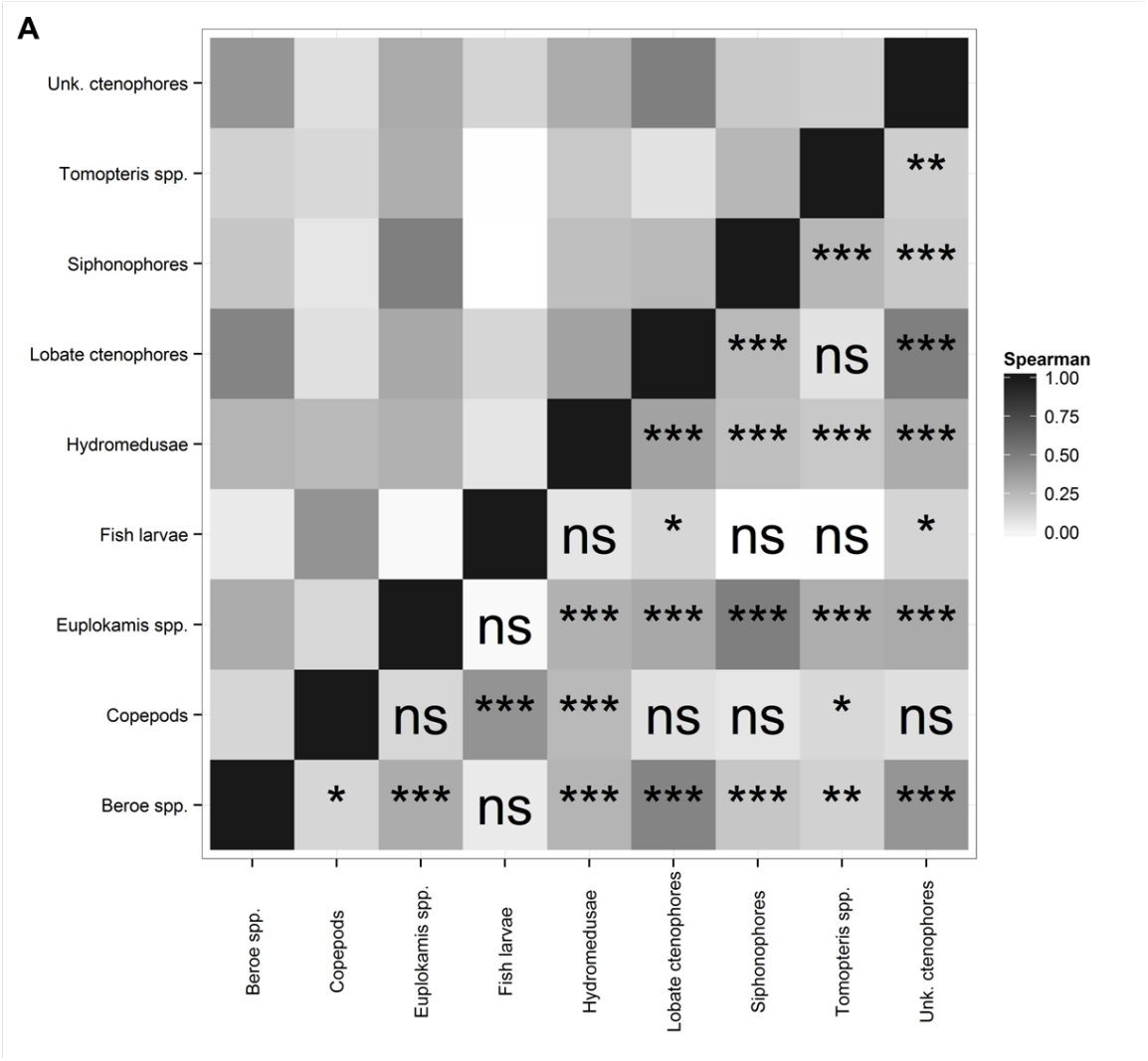

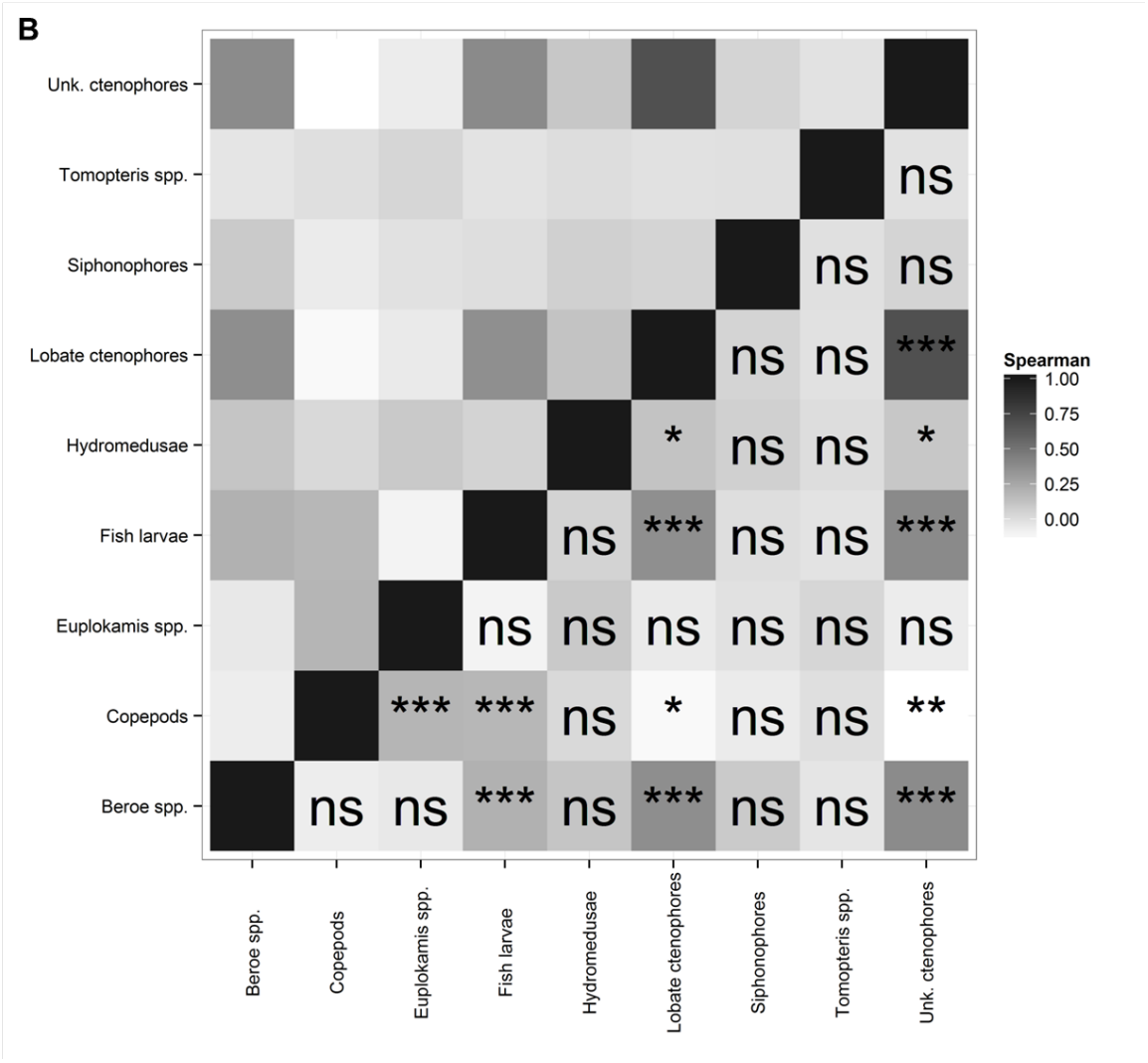
B
Unk. ctenophores
Tomopteris spp.
Siphonophores
Lobate ctenophores
Hydromedusae
Fish larvae
Euplokamis spp.
Copepods
Beroe spp.
ns
*
***
**
Spearman
1.00
0.75
0.50
0.25
0.00

Figure 3.12. A) Chlorophyll-*a* fluorescence (Chl-a) and copepods in different zones of the internal wave fixed depth transect. "After" denotes area through which the internal wave packet had presumable passed, while "before" denotes zones that had presumably not yet been affected (yet) by the internal waves. B) Relationship of larval fish concentration to copepod concentration in different sections of the internal wave fixed depth transect. The size of the point represents the average standard length of larvae in each section.

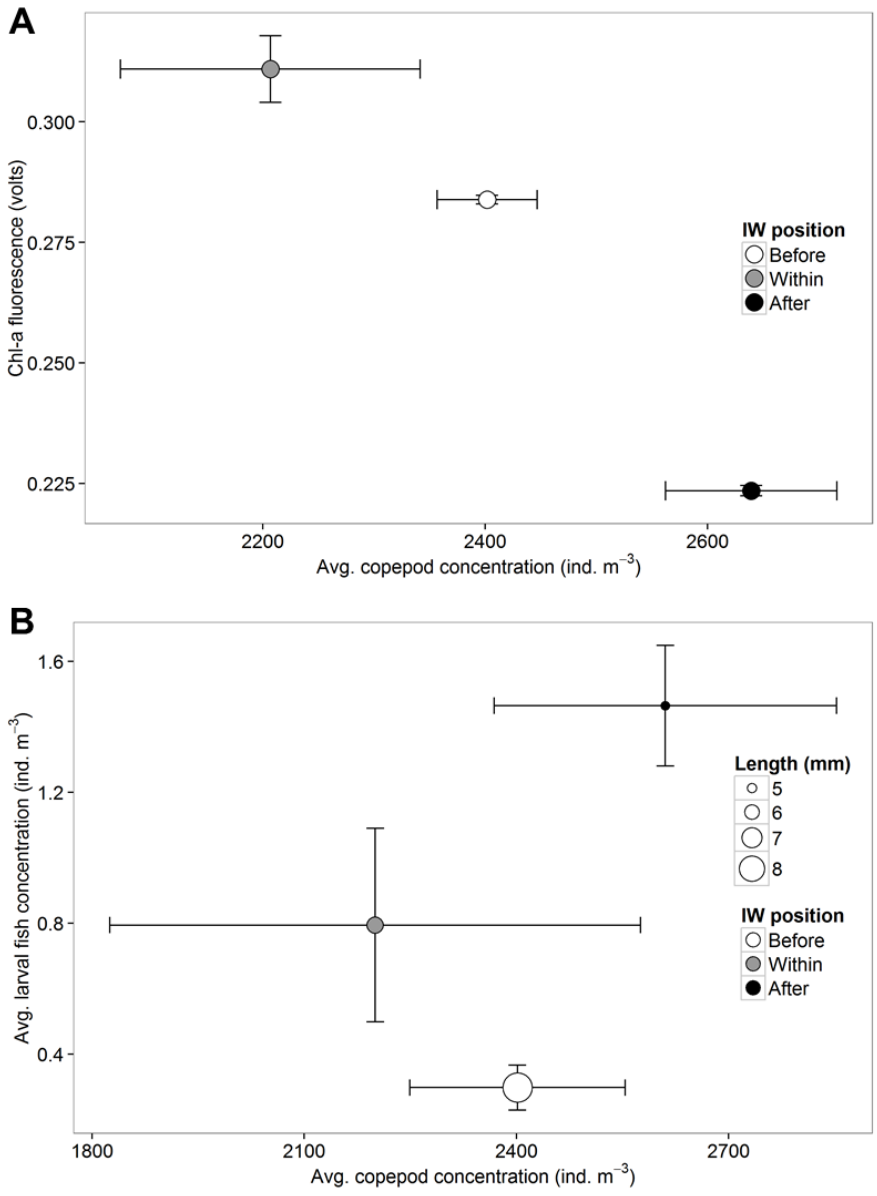

CHAPTER 4: FINE-SCALE PLANKTONIC HABITAT PARTITIONING AT A SHELF-SLOPE FRONT REVEALED BY A HIGH-RESOLUTION IMAGING SYSTEM

Shelf-slope fronts represent productive regions of the ocean, but predator-prey interactions within these features are poorly understood partially due to coarse-scale and biases of net-based sampling methods. We used the *In Situ* Ichthyoplankton Imaging System (ISIIS) to sample across a shelf-slope front near Georges Bank on two separate sampling days in August 2010, capturing ~800,000 images with fine-scale environmental data (temperature, depth, salinity, chlorophyll-*a* fluorescence). Salinity defined the transition from shelf to slope water, with isopycnals sloping vertically, seaward, and shoaling at the thermocline, consistent with upwelling characteristics documented in previous studies of shelf-slope fronts during the summer. Zooplankton and larval fishes were abundant on the shelf side of the front and displayed taxon-dependent depth distributions, but were much less common in the slope waters. Supervised automated particle counting showed small particles with high solidity, verified to be zooplankton (copepods and appendicularians), aggregating near surface above the front, potentially in the vicinity of the frontal jet. Salps were most abundant in zones of intermediate chlorophyll-*a* fluorescence in shelf waters, distinctly separate from high abundances of other grazers, and were found almost exclusively in colonial form (97.5%). Distributions of gelatinous zooplankton differed among taxa but tended to follow isopycnals. Such fine-scale sampling reveals distinct habitat partitioning of various planktonic taxa, which results from a balance of physical and biological drivers in relation to the front.

Background

Planktonic organisms experience environmental gradients that likely influence the processes of aggregation, dispersal, and differential survival, resulting in plankton patchiness (Steele 1978). Sharp gradients in temperature and salinity typically occur in the vertical direction; the subject of numerous recent studies using high frequency sampling (Dekshenieks et al. 2001; McManus et al. 2005; Greer et al. 2013). Strong horizontal gradients in water column properties can also occur, but are typically confined to areas of the ocean where two different bodies of water meet, known as fronts. Though not exclusively so, fronts are often associated with a variety of ocean topographies such as seamounts, canyons, and shelf-breaks (see Genin 2004 for review). Despite their prevalence, the role of fronts in structuring plankton communities at fine scales (1 m to 10 m) relevant to predator-prey interactions is poorly understood.

Shelf-slope fronts are common along the western shelves of the world's oceans (Mann and Lazier 2006) and serve as the boundary between relatively fresh shelf water and salty slope water (Houghton 1997). These fronts are favorable habitat for a variety of organisms, having been shown to be associated with increased productivity in phytoplankton, zooplankton, and fish (Fournier et al. 1977; Mann and Lazier 2006). To explain shelf-slope front productivity, Chapman and Lentz (1994) created a numerical model that described the circulation and predicted that bottom boundary convergence maintained the stability of the front. The convergence leads to upward flow of water along seaward sloping isopycnals, which increases nutrient input into near surface waters and consequently, phytoplankton productivity (Gawarkiewicz and Chapman 1992).

Experimental dye injections into the bottom boundary layer confirmed that convergence and along-isopycnal upwelling occurs in the field (Houghton 1997).

Upwelling flows at the shelf-break enhance biological productivity for a variety of taxa. For primary consumers, upwelling at the shelf-break leads to phytoplankton production and a favorable feeding environment for a variety of grazers including salps, copepods, and appendicularians. For larval fishes, fronts can serve as a concentrating mechanism to enhance access to high abundances of these grazers as prey (Miller 2002; Bakun 2006). Fronts also can concentrate potential predators of larval fishes, such as hydromedusae and ctenophores (McClatchie et al. 2012). Many of these osmoconformers actively reduce their swimming speed and aggregate near salinity gradients, which are a characteristic feature of the shelf-slope front (Graham et al. 2001; Jacobsen and Norrbin 2009). Salps, unlike hydromedusae and ctenophores, are bacteria and phytoplankton grazers that occupy a similar trophic niche as prey of larval fishes (copepods and appendicularians) but have reproductive rates similar to bacteria, much faster than copepods and appendicularians (Heron 1972; Alldredge and Madin 1982). Therefore, salps could have an indirect negative impact on larval fishes by quickly consuming phytoplankton in a zone that is potentially favorable to secondary production of larval fish food sources (copepods and appendicularians).

Most studies of planktonic organisms around frontal features have examined mesoscale patterns, detecting changes in average zooplankton and larval fish concentrations on either side of a front (Govoni and Grimes 1992; Kingsford and Suthers 1994; Nielsen and Munk 1998). While these studies are useful in describing the shifts in plankton communities at fronts, they do not reveal much about small scale structure

relevant to predator-prey interactions. The interactions of predators and prey at these fronts are largely unknown mainly because spatio-temporal patterns have not been resolved on the relevant scales of these associations. Small scale feeding environments have been shown to be extremely important to larval fish survival (Vlymen 1977; Davis et al. 1991), yet remain a critical gap in our knowledge of the biological impact of many oceanographic features. In addition, the diversity of grazers and the biases of net based sampling systems to crustacean zooplankton (Alldredge and Madin 1982; Remsen et al. 2004) obscure the fine-scale distribution of grazers and potential predators, thereby limiting the detectability of zones of the water column potentially favorable to larval fish feeding and survival.

New imaging technology is addressing some of the fundamental issues with sampling larval fishes and the surrounding biological community by quantitatively describing plankton in relation to fine-scale environmental variables that characterize shelf-slope boundaries. A distinct advantage of optical systems is the ability to automatically count and size marine particles using computer software. Particle size and abundance provides a suite of information relating to trophic interaction, reproduction, and carbon export to deeper waters (Sheldon et al. 1972; Woodward et al. 2005; Stemmann and Boss 2012). In addition, the metric equivalent spherical diameter (ESD) commonly used in particle size estimation may not be applicable in coastal waters where particles (marine snow) vary in shape, composition, and optical properties (Kranck and Milligan 1991). The *In Situ* Ichthyoplankton Imaging System (ISIIS) combined with image analysis software allows for the automated counting, sizing, and simple feature extraction of particles, while providing the resolution adequate for the identification of

many specimens to the family or genus level. The central goal of this study was to quantitatively describe the fine-scale abundances of larval fishes, gelatinous zooplankton, and particles of different size classes and composition, and use this high resolution data to better understand biological interactions at the shelf-slope front.

Methods

Imaging system

The *In Situ* Ichthyoplankton Imaging System (ISIIS) was used to quantify a variety of planktonic organisms in the size range of 680 μm to 13 cm. ISIIS utilizes a Piranha II line scan camera (Dalsa) to shoot a continuous image with a scan rate of 36000 lines s^{-1}. The images are produced by projecting collimated light across an imaged water parcel, and plankton blocking the light source are imaged as shadows, allowing for a range of transparent (gelatinous) and opaque (crustaceans) organisms to be imaged with no discernible bias in detectability (Cowen and Guigand 2008; Cowen et al. 2013). Although ISIIS shoots a continuous image, software (Boulder Imaging, Inc.) breaks up the image into 13 cm * 13 cm frames with a 40 cm depth of field. At typical tow speeds of 2.5 m s^{-1}, it takes approximately 7.7 s to sample 1 m^3 of water. ISIIS was also equipped with motor actuated fins for depth control, a Doppler velocity log (600 micro, Navquest) and environmental sensors including a conductivity, temperature, and depth sensor (CTD) (SBE 49, Seabird electronics) and fluorometer (ECO FL (RT), Wetlabs chlorophyll-*a* fluorescence). The CTD and fluorometer sampled ~30 cm and ~1 m above the imaged water parcel, respectively.

Sampling scheme

Two ISIIS transects were performed in the same location on separate sampling days in August 2010, beginning on the shelf in waters approximately 75 m deep during different stages of the tidal cycle. The transect on August 27 was performed between 0710 and 1348, spanning 60.1 km, while the transect on August 29 was slightly shorter, lasting from 1656 to 2248 for a total distance of 52.7 km. The August 27 transect was performed during the flood tide, and the August 29 transect was during ebb tide, though tides were expected to have little effect on this spatial scale. Transects occurred in the shelf-break zone east of Georges Bank, off the coast of Massachusetts, USA, where there are consistent horizontal gradients in salinity and temperature (Fig. 4.1).

Bongo net samples

After each ISIIS transect, 3-4 net tows using a 61 cm bongo sampler with 335 μm mesh size were performed along the transect path at approximately evenly spaced stations. A flowmeter was attached in the center of the bongo mouth opening to quantify the volume of water filtered by the net. A CTD (SeaCAT SBE 19) was also attached to the tow wire above the bongo net to measure environmental variables and real time depth of the sampler during deployment. The bongo tows were conducted following the method of Jossi and Marak (1983). For each tow, the wire was paid out at a rate of 50 m min^{-1} to a depth of ~5 m above the bottom. The wire was then retrieved to the surface obliquely at 20 m min^{-1} while the ship was moving at 0.75-1 m s^{-1}. At the end of each tow, the bongo net was brought onboard and samples were rinsed onto a 333 μm sieve, and then preserved in 95% ethanol. After 24 hours, sample ethanol was replaced with fresh 95%

ethanol to enhance preservation. Samples were then shipped to the Plankton Sorting and Identification Center in Szczecin, Poland for sorting, identification, and measurement.

Image processing

ISIIS images were viewed and analyzed in ImageJ (v1.46r, Rasband 1997-2013). Prior to analysis, images underwent a standard 'flat-fielding' procedure to remove background variation and vertical lines from the line scan imaging. Transects were viewed in their entirety, and larval fishes were identified to the family level and measured. For each ISIIS downcast, gelatinous organisms, including salps, hydromedusae (*Clytia hemisphaerica* and *Persa incolorata*), ctenophores (Lobate ctenophores and *Beroe* spp.), and siphonophores, were identified to the lowest taxonomic level possible (typically at least to family level). For the colonial salps, counts of organisms per colony were made, and it was noted if only part of the colony was in the image frame.

Counts of particles (predominantly diatoms and marine snow) were made using a custom ImageJ macro, which automated a series of tasks. The program first thresholded the 8-bit grayscale image by converting pixels with a gray level ≤ 170 to black and > 170 to white. Then, utilizing ImageJ's 'Particle Analyzer,' particles were enumerated in three different size classes based on pixel area of the particle corresponding to different plankton groups. Size was measured using the cross-sectional area (in pixels) measured by the number of white and black pixels within a black pixel contiguous border. The size classes were defined by running the particle counter on human identified images, and making size classes based on differences in the taxon-specific size frequency histograms

(see Appendix A). The 100-400 pixel size class (0.25-1.00 mm^2 cross-sectional area) corresponded mostly to diatom chains, small copepods, and small marine snow aggregates. The 401-1200 pixel size class (1.003 – 3.000 mm^2 cross-sectional area) consisted of larger copepods, appendicularians, and large marine snow aggregates. Particles in the 1201-5000 pixel size range (3.003 – 12.500 mm^2 cross-sectional area) targeted chaetognaths and shrimps (and the occasional fish larva). To further differentiate between particles within size class, a solidity metric was used to distinguish organisms with an exoskeleton (high solidity) and loosely aggregated diatom flocs (low solidity).

$$\text{Solidity} = D/C \qquad \text{(eq. 1)}$$

Where D is the area of black pixels within the object (after thresholding) and C is the total cross-sectional area of the entire object including the white and black pixels inside of a black pixel perimeter. Crustaceans, with their opaque exoskeletons, have solidity near 1, while diatom aggregates with uneven gray level in the images will have lower solidity (~0.2).

Image histogram statistics for each frame were used to remove images that likely had erroneous counts. Images with mean pixel gray levels of < 221 and pixel standard deviation > 42 contained artificially inflated particle counts and were discarded. Even with this filtration procedure, many of the images after the front had artifacts from passing through strong density discontinuities. The use of solidity to distinguish these artifacts from actual particles was tested by manually examining portions of the water column with different particle solidities.

Data analysis and statistics

ISIIS sensor data (temperature, salinity, chlorophyll-*a* fluorescence) underwent processing for quality control and interpolation. 134 chlorophyll-*a* readings and two temperature readings were removed because measurements were erroneous. Directional variograms (vertical and horizontal) were used for interpolation of the sensor data and particle counts. Directional variograms and interpolation was accomplished in R (v2.15.2) with use of the packages "sp" (Pebesma and Bivand 2005; Bivand et al. 2008), "gstat" (Pebesma 2004), and "Akima" (Akima et al. 2013). Kruskal-Wallis tests were used to assess the larval fish taxonomic differences in depth.

A logistic Generalized Linear Models (GLM) with logit link function was used to examine the power of environmental variables to explain the probability of salp presence/absence. Logistic GLMs require a response variable that is binary or a proportion between 0 and 1 and can elucidate variables associated with changes in this response. The response variable was salp presence/absence with relative chlorophyll-*a* fluorescence and distance to the front as predictor variables. The front was located by visually inspecting the point where isopycnals reached their closest vertical distance. Salps from both sampling days were pooled and placed into 1 m^3 bins, and environmental variables were averaged for each bin. The model was fit in R (v2.15.2, R Core Team) and assessed using Aikake's information criterion (AIC).

Results

Mesoscale (bongo) sampling for fish larvae

The abundance of larval fishes captured in the bongo nets showed dramatic differences between the two sampling days. On August 27, a total of 23 larvae were captured (0.03 ind. m^{-3}), while on August 29, 123 larvae were captured (0.17 ind. m^{-3}), including 61 individuals on the most inshore bongo sample (0.483 ind. m^{-3}, Fig. 1). Bongo samples were dominated by *Urophycis* spp. and *Merluccius bilinearis* (47.9% and 33.6%, respectively). Salps were also abundant in the bongo nets on the shelf side of the front, but were not quantified.

Fine-scale physical setting

The sampling area was marked by strong shifts in temperature and the vertical positioning of isotherms. The temperature on the shelf edge below the pycnocline was 9-10°C. This cold water had moved shoreward on August 29, relative to its August 27 position, possibly due to the August 29 transect beginning at high tide. Waters on the shelf tended to be cooler at the surface and less thermally stratified compared to the slope waters. Moving offshore, isotherms tended to shoal near the pycnocline, forming highly stratified waters near the shelf edge and slope (Fig. 4.2A).

Changes in salinity were the most apparent physical characteristic defining shelf and slope waters at the front. Isohalines sloped seaward, and salinity intrusions of slope water onto the shelf occurred along the pycnocline (Fig. 4.2B). Higher salinity levels were seen on August 29, potentially due to the movement of colder slope water onto the shelf. In addition, higher surface salinity gradients were seen on this day of sampling.

The combination of temperature and salinity created shifts in water density that were closely connected to the vertical and horizontal distribution of chlorophyll-*a* fluorescence. Similar to isotherms, isopycnals shoaled as the 12°C isotherm reached its shallowest depth of 15-20 m. Most of the relatively high chlorophyll-*a* fluorescence above 0.2 volts was contained between the 23.3 and the 24.7 isopycnals, with generally lower and a much more limited vertical extent of chlorophyll-*a* fluorescence in the stratified slope waters. Isopycnals generally sloped seaward in a similar direction to isohalines, but, unlike isohalines, flattened out when reaching ~25 m, a depth where the vertical temperature and density gradients were sharpest (Fig. 4.2C).

Particle distributions and solidity

Particles in the 100-400 (0.25-1.00 mm^2 cross-sectional area) pixel size range generally consisted of small diatom aggregates and small copepods, and particle solidity was used to distinguish between these groups (Fig. 4.3). Particles were most abundant before convergence of isopycnals (i.e. the shoreward side of the front) and overlapped with the distribution of chlorophyll-*a* fluorescence (Fig. 4.4A). The solidity metric revealed strong changes in the dominant constituents of these particles. Particles with low solidity were found within areas of high chlorophyll-*a* fluorescence and were visually confirmed to be dominated by diatoms. A subsurface layer of high solidity occurred a few meters above the convergence of isopycnals on both sampling days, and was dominated by copepods with very few diatoms imaged in this area. Appendicularians were also common in this surface layer, especially on August 27, but many occupied a larger size class. Particles in deeper waters (> 30 m) with high solidity were mostly dark

colored marine snow, with very few copepods. The 100-400 pixel size class was contaminated with image artifacts near strong density gradients (caused whirls in the images). These artifacts were counted as particles in zones of strong density stratification, which occurred almost exclusively after the front. The artifacts are indicated by solidity near 0.6 and proximity to several isopycnals, which occurred most often in the stratified slope waters (offshore sporadic high counts Fig. 4.4A).

Particles from 401 to 1200 pixels (1.003 – 3.000 mm^2 cross-sectional area) were mostly larger diatom aggregates, larger copepods, and appendicularians. The highest abundance of these particles also occurred near the chlorophyll-*a* maximum, with twice the maximum abundance occurring on August 29 compared to August 27 (Fig. 4.4B). August 27 showed more size separation, with particles in the 401-1200 pixel size range being more abundant close to the front and near surface, corresponding with zooplankton aggregations. Particle solidity measurements provided further evidence of crustaceans and appendicularians aggregating near surface above the isopycnals convergence. The chlorophyll-*a* maximum was dominated by loose diatom aggregates (low solidity), and deep waters on the shoreward side of the front were once again populated by dense marine snow aggregates (high solidity).

Particles in the size range of larger zooplankton (chaetognaths and shrimps) between 1201-5000 pixels (3.003 – 12.500 mm^2 cross-sectional area) were also dominated by aggregates, but showed different patterns in relation to the zone of high chlorophyll-*a* fluorescence between the sampling days. On August 27, most of these large particles were aggregated near the front, but on August 29, the particles were most abundant in the same area as the other particle size classes and zone of high chlorophyll-*a*

fluorescence (Fig. 4.4C). There was also a trend towards decreased solidity on August 29 compared to August 27. Similar to the other particle size classes, the solidity was lowest in areas where chlorophyll-*a* fluorescence was highest, indicative of large diatom aggregates in this zone.

Fine-scale larval fish abundance and distribution

In total, 223 larval fishes were found in ISIIS images on the two sampling days, dominated by the families Merlucciidae (48.4%) and Phycidae (23.3%) (see Fig. 4.5 for example images) and confined to the shelf side of the front (Fig. 4.6). A portion of the larval fishes were not identifiable (12.1%) due to orientation and/or lack of detectable features, while 9.9% were preflexion larvae. Families under the order Pleuronectiformes were pooled due to low abundances. Merlucciidae and Pleuronectiformes larvae occupied significantly deeper waters than other taxa (Kruskal-Wallis test, $P<.0001$). Phycidae larvae were significantly shallower (Kruskal-Wallis test, $P<.0001$) (Fig. 4.7), with preflexion larvae were found in waters slightly deeper than Phycidae. Unlike the bongo sampling, no difference in larval fish abundance was found between the two sampling dates; however, the first ISIIS profile on August 29 contained a concentration of 0.740 ind. m^{-3}, corresponding to the same area of high abundances detected by the bongo net (0.483 ind. m^{-3}).

Temperature/salinity diagrams in the context of larval fish presence/absence showed larval fishes occupying a fairly narrow range of salinity (almost absent when salinity > 33) but a larger range of water densities (Fig. 4.8). The 23.3 isopycnal was the only one along which larvae were found across a range of salinities on both sampling

days. Larval fishes were found in zones where chlorophyll-*a* fluorescence and particle abundance were high (on the shoreward side of the front).

Salp abundance and distribution

A total of 49,161 salps, consisting of *Thalia democratica*, were found in the images, with 97.5% of those individuals being in colonial form. The highest abundances of salps occurred in shelf waters with intermediate levels of chlorophyll-*a* fluorescence, usually several meters shallower than the chlorophyll-*a* maximum on each profile (Fig. 4.9). Salps reach concentrations of over 5000 ind. m^{-3}on several occasions, but were most concentrated on August 29, which had higher peak chlorophyll-*a* fluorescence. A few individuals were found in very deep waters (>70 m) and were likely dead or decaying since phytoplankton abundance in this area was low and dominated by dense marine snow aggregates.

A logistic regression revealed a significant impact of chlorophyll-*a* fluorescence and distance to the front on the probability of salp presence (Table 4.1). The model showed the highest probability of presence occurred at intermediate levels of fluorometry, similar to those found several meters above the chlorophyll-*a* maximum (Fig. 4.10). Salps were accurately predicted to be absent within and seaward of the front, regardless of the chlorophyll-*a* fluorescence in these zones.

Gelatinous zooplankton distributions

The most abundant gelatinous zooplankton other than salps were the hydromedusae *Clytia hemisphaerica* and *Persa incolorata*. Maximum concentration

detected for these two species was 167 ind. m^{-3} and 90 ind. m^{-3}, respectively. Distributions of the hydromedusae tended to follow isopycnals, with highest abundances between the 23.8 and 23.3 isopycnals. Both species were absent seaward of the front (Fig. 4.11A, B).

Ctenophores and siphonophores displayed a remarkably different distribution from the hydromedusae, with the two ctenophore groups occupying opposite extremes in depth, but, like other zooplankton, were most abundant on shoreward of the front. Lobate ctenophores, consisting mostly of *Bolinopsis* spp., were common in surface waters and showed signs of limited depth distribution based on the 23.3 isopycnal (Fig. 4.11C). The miscellaneous ctenophores, mostly consisting of *Beroe* spp., were more common in deeper waters, and spatial patterns did not follow isopycnals (Fig. 4.11D). Siphonophores were much less abundant overall, but aggregated at the surface near the front on August 29 (Fig. 4.11E).

Discussion

Distributions of larval fishes, fluorescence, diatom aggregates, and gelatinous zooplankton near a shelf-slope front showed strong vertical patterns often associated with isopycnals. Fine-scale abundances in the horizontal direction showed elevated abundances in the shelf waters with almost complete absence of organisms in the stratified slope waters. Particles of varying composition showed distinct associations with certain portions of the front. Copepods aggregated at the surface near the convergence of isopycnals, and a large number of particles were found underneath the front, potentially contributing to the export of organic material into deeper waters. Previous studies of

shelf-slope fronts have not documented these detailed associations because of coarse sampling resolution (Fernandez et al. 1993; Munk et al. 2003; Albaina and Irigoien 2004) or inability to detect gelatinous organisms in these features that, based on high abundances, are likely important grazers (salps) and larval fish predators (hydromedusae and ctenophores). This and previous studies of fine-scale features demonstrate the importance of fine-scale environmental heterogeneities in determining the abundance and spatial extent of many zooplankton taxa. The following discussion will transition from a description of the circulation at the front and move through the food web, starting with the distribution of chlorophyll-*a* fluorescence, diatom particles, and grazers, to larval fishes and zooplankton predators.

Physical environment at the front

Seaward sloping isopycnals merging near the pycnocline were consistent with previous studies at the shelf slope fronts. Upwelling of deep shelf water has been found to occur along these isopycnals (Marra et al. 1990) with an average upwelling velocity of 17.5 m d^{-1}, depending on the steepness of the isopycnal slope (Barth et al. 2004). The shoaling of isopycnals near 20-30m depth during the summer has been suggested as a mechanism for favorable cross-front exchange (Houghton et al. 1988), but our finding of very few zooplankton on the oceanic side of the front despite the presence of high salinity intrusions suggests that cross-shelf exchange of zooplankton only occurs during the passage of warm core rings (Houghton et al. 1986). Strong diapycnal velocities at shelf slope fronts indicate mixing across isopycnals (Houghton and Visbeck 1998; Barth et al. 2004), which may have been depicted in our images as whirls within the image near

density discontinuities. This diapycnal mixing also led to inflated particle counts in the highly stratified slope waters, particularly in the smallest size range (100-400 pixels). Flattening of isopycnals at the thermocline during the summer stratified months has been documented previously (Houghton et al. 1988; Barth et al. 2004), with strongest density changes containing intrusions of salty slope water onto the shelf (Gordon and Aikman 1981). Because many characteristics documented by ISIIS were consistent with previous studies of the shelf-slope front, it is likely that frontal circulation patterns, including bottom boundary convergence, upwelling along isopycnals, and a strong southward flowing frontal jet (Chapman and Lentz 1994; Houghton and Visbeck 1998; Mann and Lazier 2006), were occurring during this study.

Distribution of primary producers and particles

Diatoms and dinoflagellates are common summer phytoplankton prey on the shelf for a variety of grazers including salps, copepods, and appendicularians (Malone 1977). Physical coagulation of diatoms appeared to dominate in areas of high chlorophyll-*a* fluorescence, but the fluorescence signal was spatially distinct from the aggregations of grazers, which were in shallower waters. These shallow zones are potentially populated by dinoflagellates, which are too small to be imaged by ISIIS, as copepods have shown strong fine-scale spatial overlap with dinoflagellates near Georges Bank (Gallager et al. 2004). Diatoms, which were correlated with chlorophyll-*a* fluorescence, may not be nutritionally sufficient for copepods (Pierson et al. 2005a, b) and when present in high concentrations, can even have deleterious effects due to the production of toxic aldehydes (Miralto et al. 1999; Tosti et al. 2003; Leising et al. 2005).

Where light levels are favorable for phytoplankton growth, converging, upward sloping isopycnals should be associated with the input of nutrient-rich deep water (Marra et al. 1990). In the present study, however, chlorophyll-*a* fluorescence and peak particle concentrations did not occur in these areas, suggesting that the chlorophyll-*a* maximum is more related to the aggregation of sinking particles than the active growth and production of phytoplankton most favorable to zooplankton grazing. Elevated chlorophyll-*a* fluorescence inshore of the shelf-slope front has been documented occasionally (Marra et al. 1982, 1990), and our results suggest that the coagulation of diatoms at particular isopycnals could be responsible for this shift. This idea is supported by models of diatom coagulation, which predict particles will become more aggregated with depth (Alldredge and Gotschalk 1989), causing particle size to increase and reach a maximum at the base of the photic zone (Jackson 1990; Kiørboe et al. 1990). Further details on the surface circulation near the front and the stickiness of diatoms in this region could reveal the mechanism behind this phenomenon.

Copepods, appendicularians, and salps

Phytoplankton grazers (salps, copepods, and appendicularians) were mostly found in waters several meters above high levels of chlorophyll-*a*. While salps were more abundant shoreward of the front at intermediate levels of chlorophyll-*a* fluorescence, copepods and appendicularians were dominant in surface waters above the front, with no particular relationship to chlorophyll-*a* or hydrographic variables (other than depth). Ashjian et al. (2001) quantified fine-scale distributions of copepods using the Video Plankton Recorder (Davis et al. 1992, 2005) across Georges Bank, finding high

variability in abundances and little correlation with hydrographic variables, other than a slight negative correlation with chlorophyll-*a* fluorescence in the summer. Copepod behavioral experiments have shown that copepods are attracted to velocity gradients and show area-restricted searching (Woodson et al. 2005, 2007), potentially increasing their encounter rates with prey items in these zones. The surface waters have also been shown to have the highest mean current speed in this region due to the strong surface frontal jet (Aikman et al. 1988; Mann and Lazier 2006), and this zone has also been found to be populated with ciliates, another food item for copepods and potentially an understudied trophic link (Fernandez et al. 1993; Calbet and Saiz 2005). Gawarkiewicz et al. (1996) found highest along-isobath velocities at ~10 m in the frontal zone (0.51 m s^{-1}, perpendicular to our transects), which would be just below the layer of copepods found on August 29. If the upwelling does indeed bring elevated nutrients and favorable conditions for dinoflagellate and/or ciliate growth combined with strong current velocity gradients, the surface waters above the front could be an ideal habitat for copepods. Higher resolution observations of smaller plankton (< 400 μm) would be needed to confirm whether the surface waters above the front are populated with smaller phytoplankton or microzooplankton that may be more important to copepod growth than diatoms (Pierson et al. 2005; Calbet and Saiz 2005).

Shelf-slope fronts have been suggested as oceanographic features that would be particularly favorable for salp growth (Paffenhöfer and Lee 1987), and our results provide support for this idea based on observed concentrations of salps being an order of magnitude higher than in previous studies in this region (Atkinson et al. 1978; Bathmann 1988; Diebel and Paffenhöfer 2009). Salps are capable of daily population doubling

through asexual reproduction (Heron 1972) and are able to filter large volumes of water to ingest prey across a range of sizes. Concentrations of other grazers are often negatively correlated with salps (Fraser 1962; Berner 1967; Deibel 1980; Paffenhöfer et al. 1995), and our data revealed distinct spatial partitioning between salps and other grazer zooplankton.

The logistic GLM fit to salp presence/absence showed an affinity of these organisms to intermediate levels of chlorophyll-a on the shelf side of the front. When salps encounter particularly high concentrations of particles (and high chlorophyll-*a* fluorescence), their filters clog, stopping ingestion and greatly reducing their fitness (Alldredge and Madin 1982). Intermediate fluorescence levels (0.2 volts in our study) may therefore represent a "goldilocks" amount of phytoplankton: sufficient for growth but not so much as to clog filters and decrease feeding efficiency. The well-mixed surface waters are likely the site of growing diatoms which gradually coagulate and sink until reaching density discontinuities. The zones a few meters above the density discontinuities provide the opportunity of salps to feed before concentrations get too high near the pycnocline.

Zooplanktivorous gelatinous organisms

Gelatinous zooplankton were abundant on the shelf side of the front, with taxon dependent depth patterns often following isopycnal surfaces. The common hydromedusae sampled (*Clytia* spp. and *Persa* spp.) showed changes in their vertical distribution closely related to isopycnal depth. This is consistent with studies indicating that density discontinuities limit the movement of hydromedusae due to their inability to

osmoregulate (Arai 1976; Mills 1984; Graham et al. 2001). Ctenophores also followed isopycnals, but the two groups were separated by depth. Lobate ctenophores aggregated in the surface waters with particularly high abundances near the surface intersecting with the 23.3 isopycnal. Other ctenophores (mostly *Beroe* spp.) were concentrated at depth and tended to be most abundant near the 25.0 isopycnal and in areas of lowest particle abundance. These ctenophores are known to have high clearance rates, and could potentially feed on marine snow aggregates exported from above the thermocline, and large copepods, euphausiids, and lobate ctenophores that venture to deeper waters (Reeve and Walter 1978). Since some lobate ctenophores have been demonstrated to alter their swimming speed and vertical distribution in the presence of *Beroe* spp. predators (Titelman et al. 2012), the vertical separation between *Beroe* spp. and lobate ctenophores could indicate avoidance behavior or top down regulation.

Larval fish distributions and sampling technology

Fish larvae, many of which require copepods or nauplii for food, were found throughout the shallow shelf waters and were limited to relatively low salinities. Seaward of the converging isopycnals that marked the front, fish larvae were absent except for two individual Bothid larvae found near the surface. Due to the coarse resolution of most ichthyoplankton sampling, this strong association of larval distributions with particular physical features has not been previously documented. Phycidae larvae occupied the shallowest waters, and based on our particle counts and solidity measurements, likely had the highest probability of encountering zooplankton prey in this area. Merlucciidae larvae were found significantly deeper on both sampling days and are known to feed during the

daytime on copepods up to 700 μm in size (Sumida and Moser 1980; Cass-Calay 2003). The large eye lenses relative to the size of Merluciidae larvae suggests they are adapted to a wide range of light conditions (Morote et al. 2011), and therefore may rely on this stealthy behavior to feed successfully on lower concentrations of copepods at depth, whereas the distributions of Phycidae larvae suggests they may require high concentrations of prey. Taxon-specific differences in habitat requirements have been suggested in many studies showing that larvae of different species thrive under different physical regimes (Buckley and Lough 1987; Dower et al. 1998), but further study is required to determine if differences in food concentration affect species-specific condition.

High larval abundances appeared to be associated with zones of the water column where isopycnals intersected with the surface, and larval distributions tended to follow the sloping isopycnals. Many studies have shown larval behavioral changes or aggregation in the vicinity of temperature or density gradients, unrelated to the presence or absence of prey in these zones (Batty 1994; Lougee et al. 2002; Clay et al. 2004; Catalan et al. 2011). Since prey patches have been shown to aggregate at density discontinuities (Bjornsen and Nielsen 1991), occupying these zones increases the chances of encountering high concentrations of prey items. Specifically, the upward sloping isopycnals and diapycnal velocities may be sites of velocity gradients or increased turbulence, potentially favorable for prey encounters (Rothschild and Osborn1988; Kiørboe and MacKenzie 1995).

Larvae grow faster in warmer waters (Houde 1989; Pepin 1991; Buckley et al. 1999), but require adequate food resources to obtain this benefit. The slope waters had

the warmest surface waters, but were virtually devoid of zooplankton prey for the fish larvae. The cold pool, which had very few fish larvae, also had few potential prey items and unfavorable conditions for larval growth. Thus, it is not surprising, given the horizontal shifts in both physical and biological conditions, that the upper half of the water column on the shelf side of the front was most populated with larval fishes.

In their relationship to potential predators, fish larvae showed spatial overlap with gelatinous zooplankton, providing little evidence of avoidance of these predators. It is apparent from these distributions that the primary driver of larval fish distributions is the distribution of prey, as all taxa which feed on zooplankton were most abundant on the shelf side of the front. Given the extremely high concentrations of gelatinous zooplankton near aggregations of larval fishes, predator avoidance of these larvae on fine scales is likely a necessity. Controlled behavioral experiments would shed light onto how these larvae survive despite high concentrations of predators throughout their habitat.

The two sampling methods used for quantifying larval fishes showed distinct differences likely based on the timing of sampling and speed of instrument towing. Although ISIIS has shown favorable comparisons to bongo nets during night sampling of fish larvae (Cowen et al. 2013), this study represents the first day/evening comparison of sampling techniques in the same area. While ISIIS imaged roughly the same number of larvae during each of the two transects, bongo nets captured 5 times fewer larvae during the day sampling compared to the evening sampling. In the ISIIS images, larvae tended to be large (8.1 mm average standard length), so it is likely that many of these larvae were able to avoid the bongo nets during the day, but were unable to avoid ISIIS due to the fast tow speed (2.5 m s^{-1} vs. 0.75 m s^{-1} for the bongo). During the night, as in the Cowen et al.

(2013) study, the bongo nets and ISIIS detected similar concentrations. ISIIS may be a more effective ichthyoplankton sampler during daylight hours if the targeted larvae are older or have strong sensory and swimming abilities enabling net avoidance.

Detailed events at the shelf-slope front and future directions

High-resolution particle counts revealed high vertical and horizontal structure of plankton patchiness near shelf-slope fronts. The front itself clearly acted as a barrier to the movement of shelf water onto the slope, with strong stratification on the slope side of the front and very low abundances of plankton and particles. Patterns in sigma-t showed surface shoaling isopycnals at the front, likely related upwelling and increased productivity. At the front, there was an increased abundance of particles in deeper waters below the pycnocline, and also high abundances of zooplankton at the surface. The source of these particles is not known, but it could be a mixture of salp or copepod fecal pellets and dead or decaying diatom aggregates. These particles were only found on the shelf side, suggesting export into the shelf sediments, with little moving through slope waters. It is possible that internal waves could resuspend these sediments to transport this organic matter into the deep ocean (Butman et al. 2006).

The wealth of information provided by image data lends itself to the simultaneous study of many trophic levels at important physical features such as shelf-slope fronts. Combining ISIIS data collection with other traditional samplers, such as sediment traps, niskin bottle samples, phytoplankton sampling, and distributions of nutrients could reveal new biologically important information on fronts and other oceanographic features. Whether or not the general patterns found in this study are consistent seasonally is

unknown, but the future of optical system use is promising as automated image analysis techniques and data management capabilities improve.

Tables

Table 4.1. Model coefficients on logistic regression of salp presence/absence in relation to chlorophyll-*a* fluorescence and distance to the front. Negative distances are shoreward of the front and positive distances are seaward.

Formula: Presence/Absence ~ Fluor+Fluor^2+Distance to Front

Coefficient	Estimate	SE	Z value	Pr
Intercept	-8.012	2.812e-01	-28.50	***
Fluor	5.634e+01	3.688	15.28	***
Fluor^2	-1.419e+02	1.096e+01	-12.94	***
Distance to Front	-4.471e-05	2.517e-06	-17.76	***

Figures

Figure 4.1. Map showing the location of the two ISIIS transects sampled on the eastern side of Georges Bank, Massachusetts, USA. Inset map displays the location of the bongo samples with color corresponding to the concentration of fish larvae.

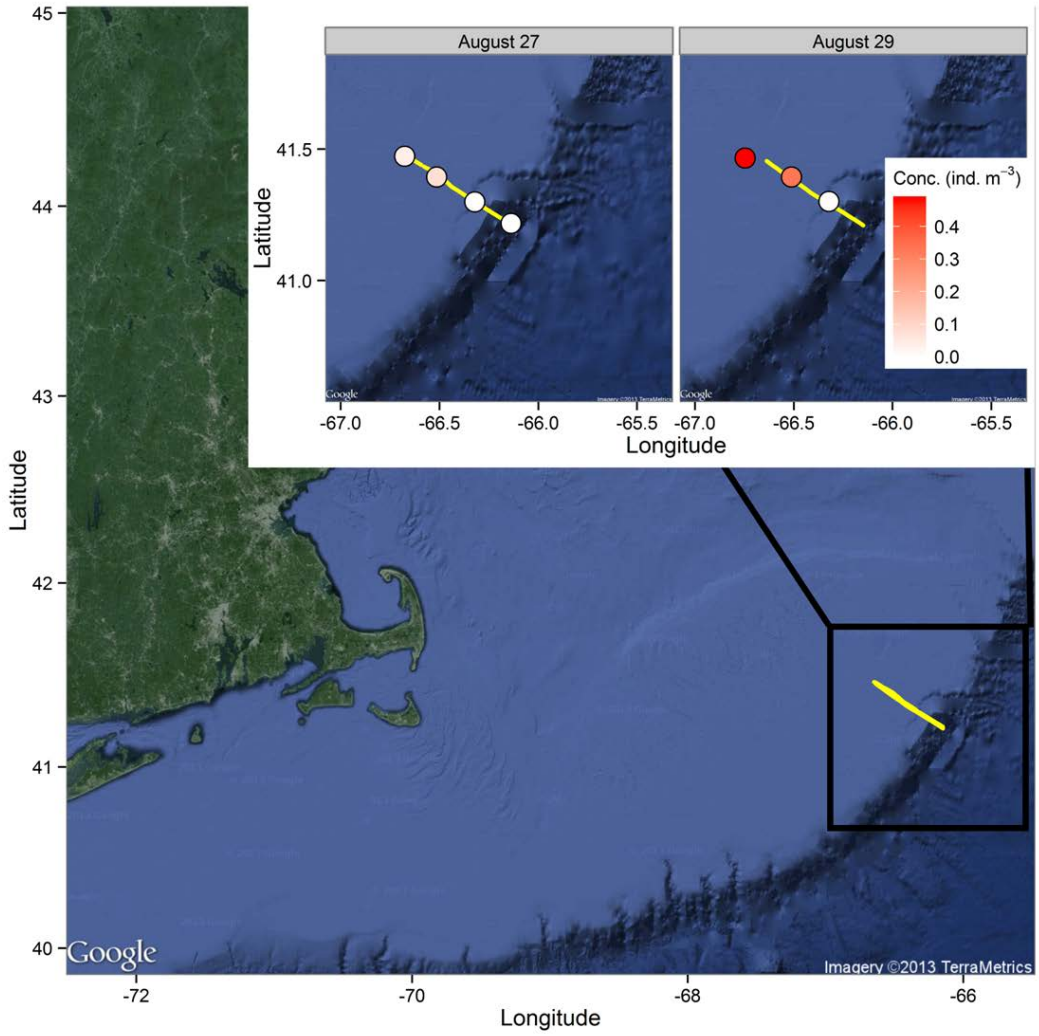

Figure 4.2. Environmental data collected with ISIIS sensors along two transects from northwest to southeast across a front. The smooth black line at the bottom of each panel shows the location of the bottom. A) Temperature with the 12 and 18°C isotherms in black B) Salinity with the 33 and 34 isohalines in black C) Chlorophyll-*a* fluorescence (volts) with the sigma-t contours shown in black (23.7, 24.0, 24.7, 25.3, 26.0 isopycnals). Location of the front is indicated by red arrows.

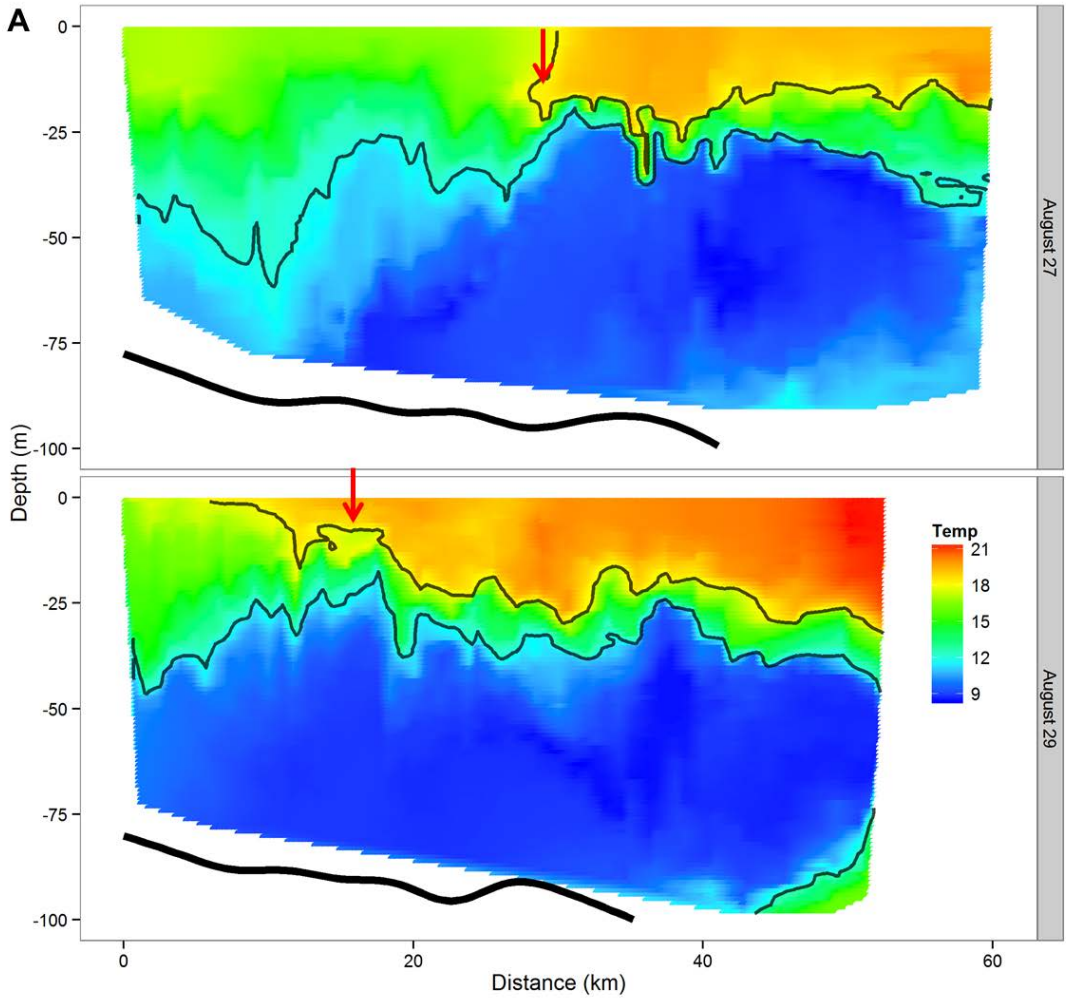

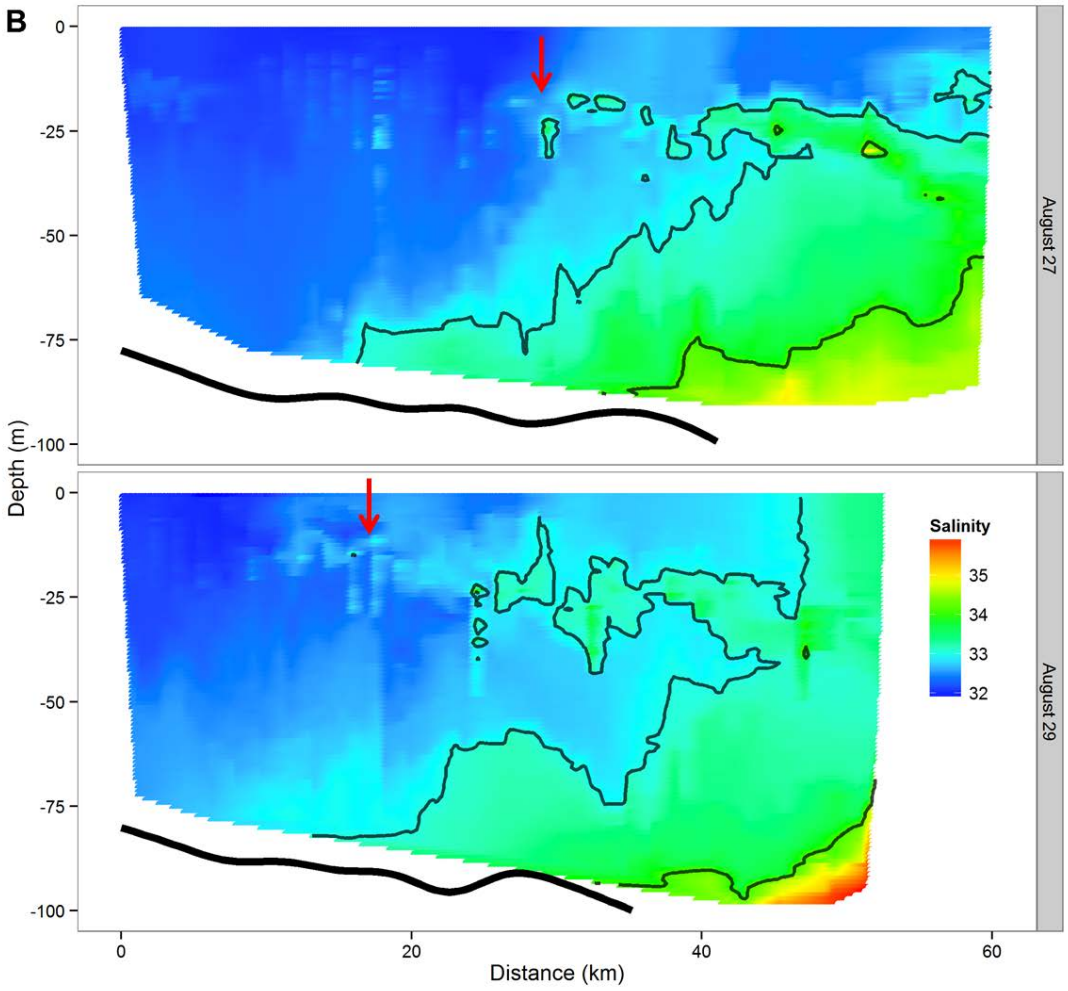
B
0
-25
-50
-75
-100
Depth (m)
August 27
August 29
Salinity
35
34
33
32
0
20
40
60
Distance (km)

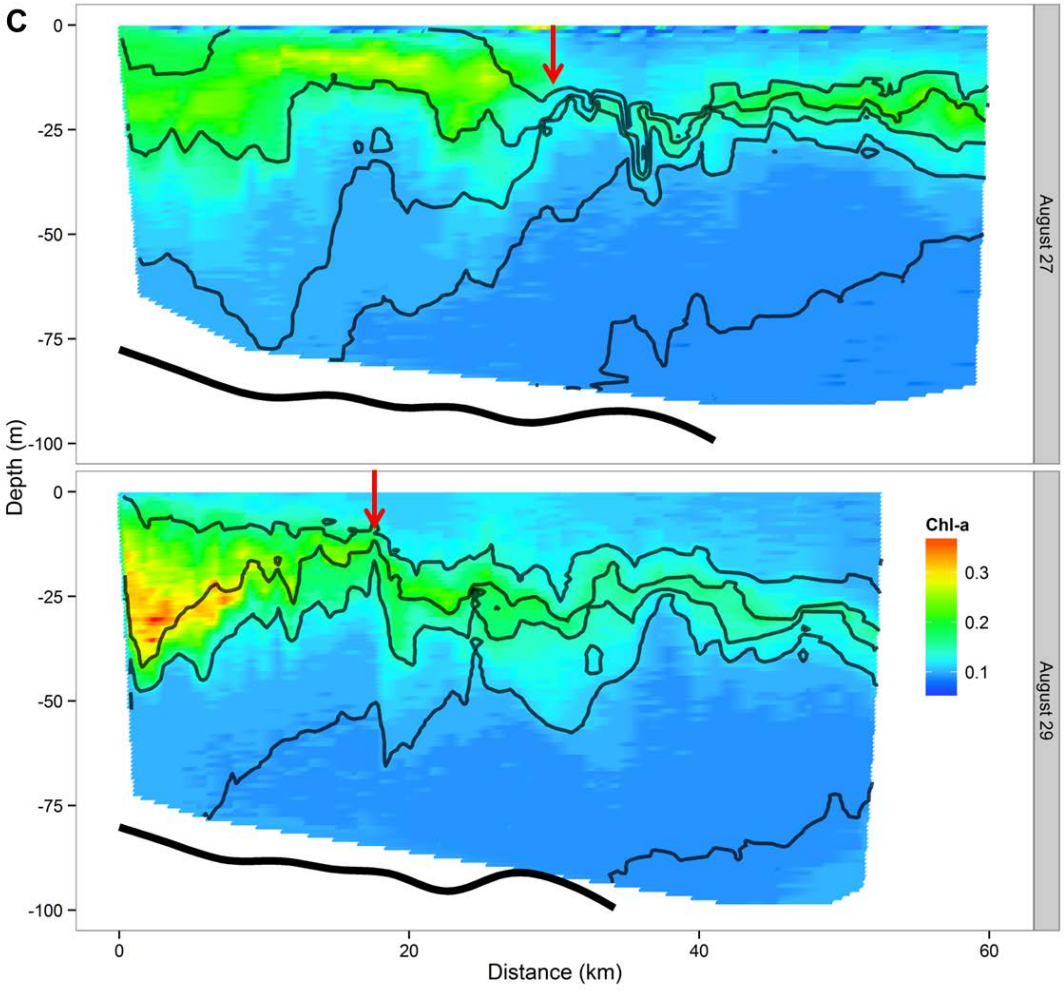
C
0
-25
-50
-75
-100
Depth (m)
August 27
August 29
Chl-a
0.3
0.2
0.1
0
20
40
60
Distance (km)

Figure 4.3. Example images from different parts of the water column with average particle solidity per frame: A) Near-surface copepod aggregations; B) near-surface mixture of zooplankton and diatom chains with two *Urophycis* spp. larvae; C) high concentrations of diatom chains in zone of high chlorophyll-*a* fluorescence; D) diatom aggregate formation at base of chlorophyll maximum; E) turbulence whirls and two euphausiids associated with slope water density discontinuities and low overall zooplankton abundance; and F) particles of unknown origin in deep waters (100 m)

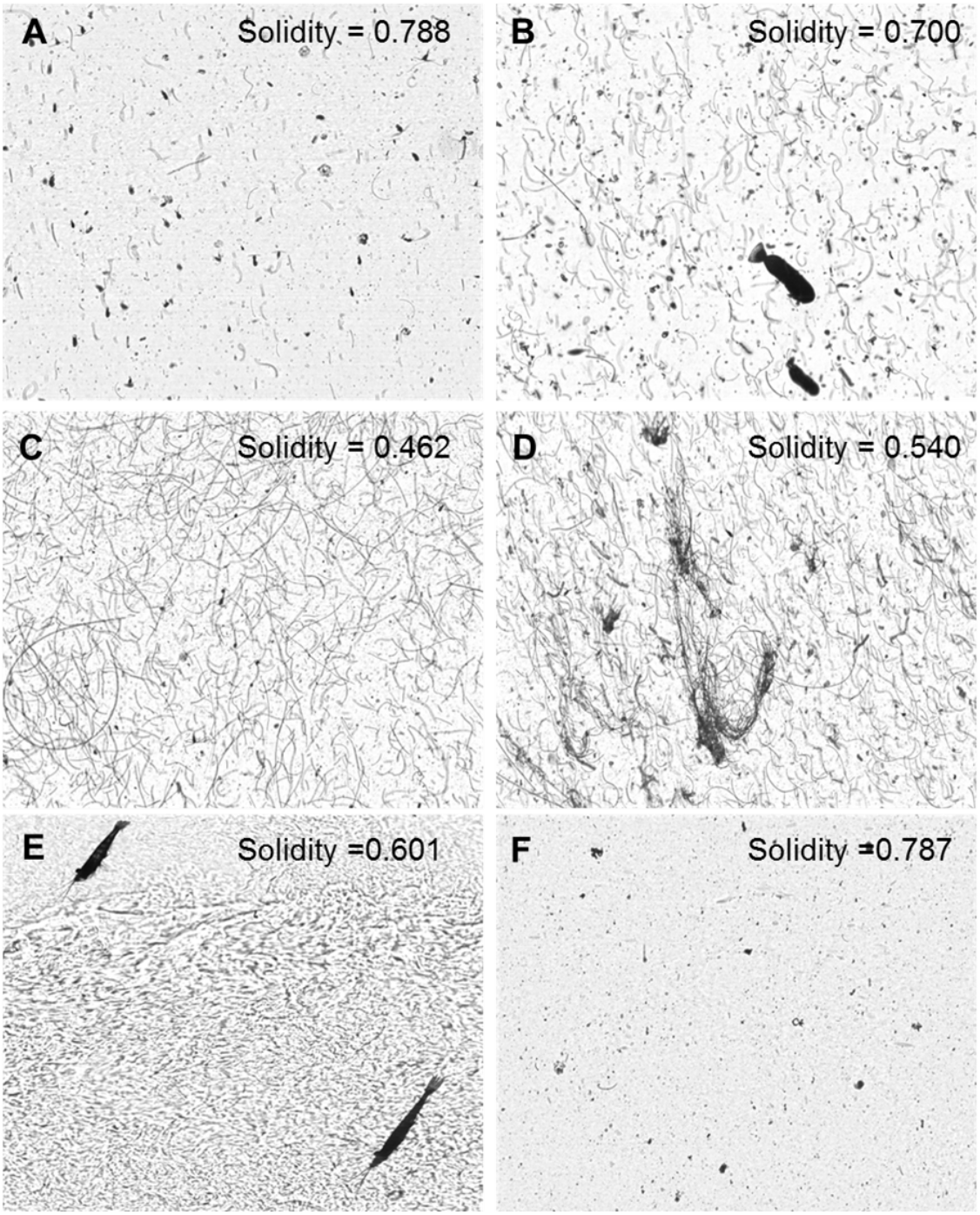

Figure 4.4. Particle counts in three different size classes and solidity of particles counted. The left panels show particle concentration with chlorophyll-*a* fluorescence drawn in black. Panels on the right show particle solidity above a certain minimum concentration for each size class with density contours drawn in black. The size of the point corresponds to particle concentration in that area. A) 100-400 pixel size class, B) 401-1200 pixel size class, C) 1201-500 pixel size class.

A

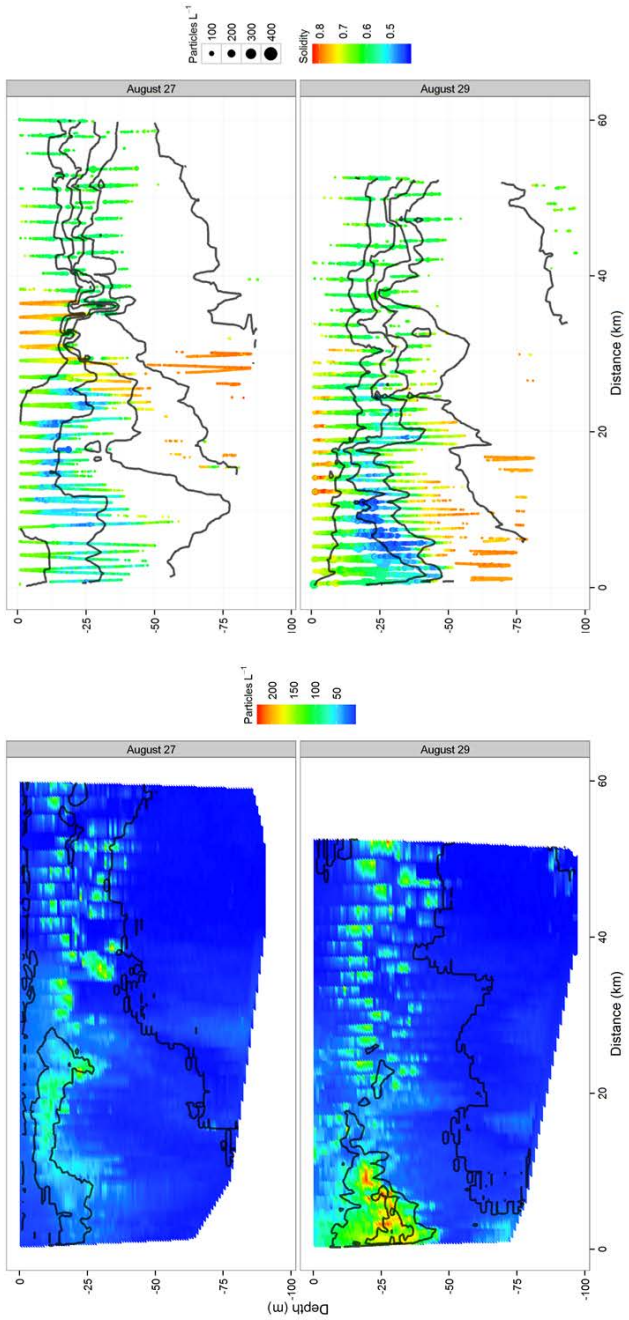

B

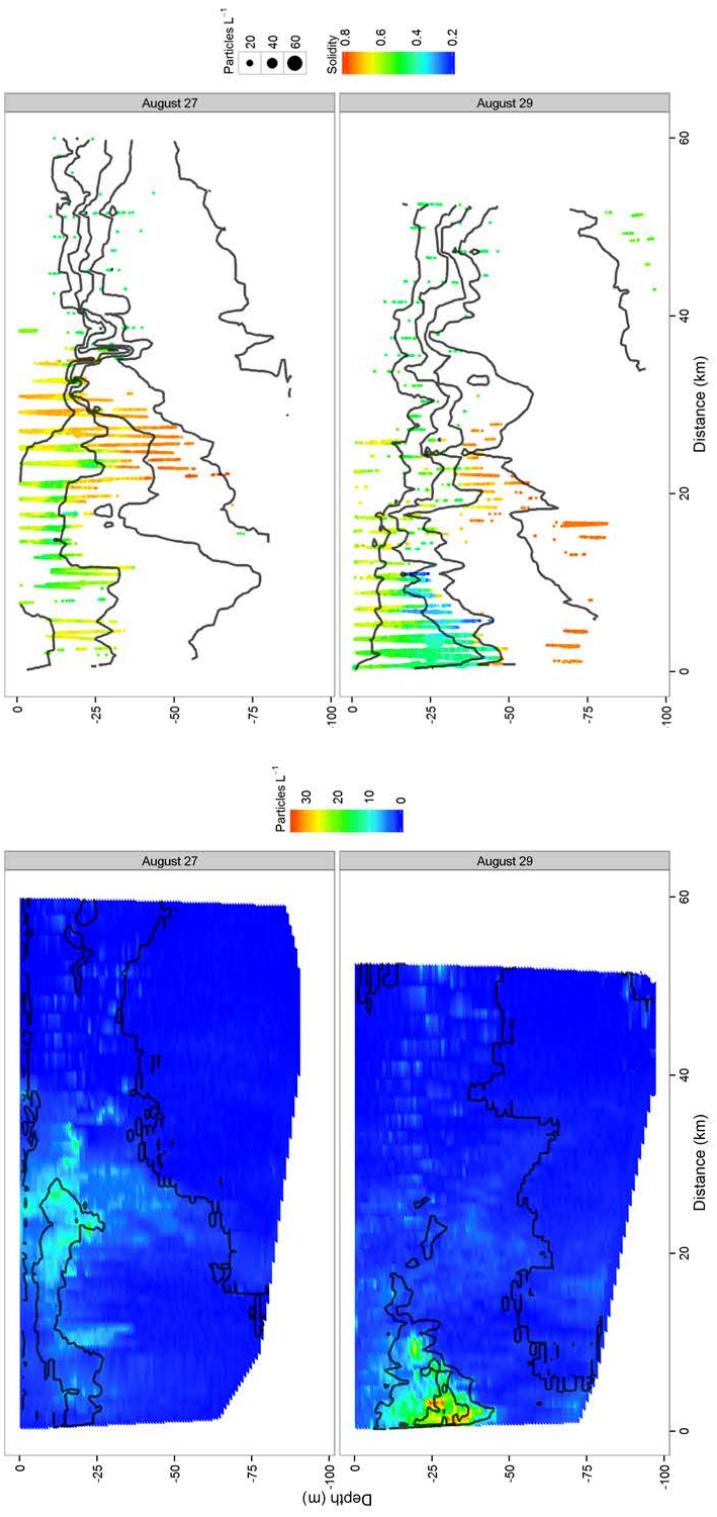
Particles L-1
20
40
60
Solidity
0.8
0.6
0.4
0.2
August 27
August 29
Distance (km)
0
20
40
60
0
-25
-50
-75
-100
Particles L-1
30
20
10
0
August 27
August 29
Distance (km)
Depth (m)

C

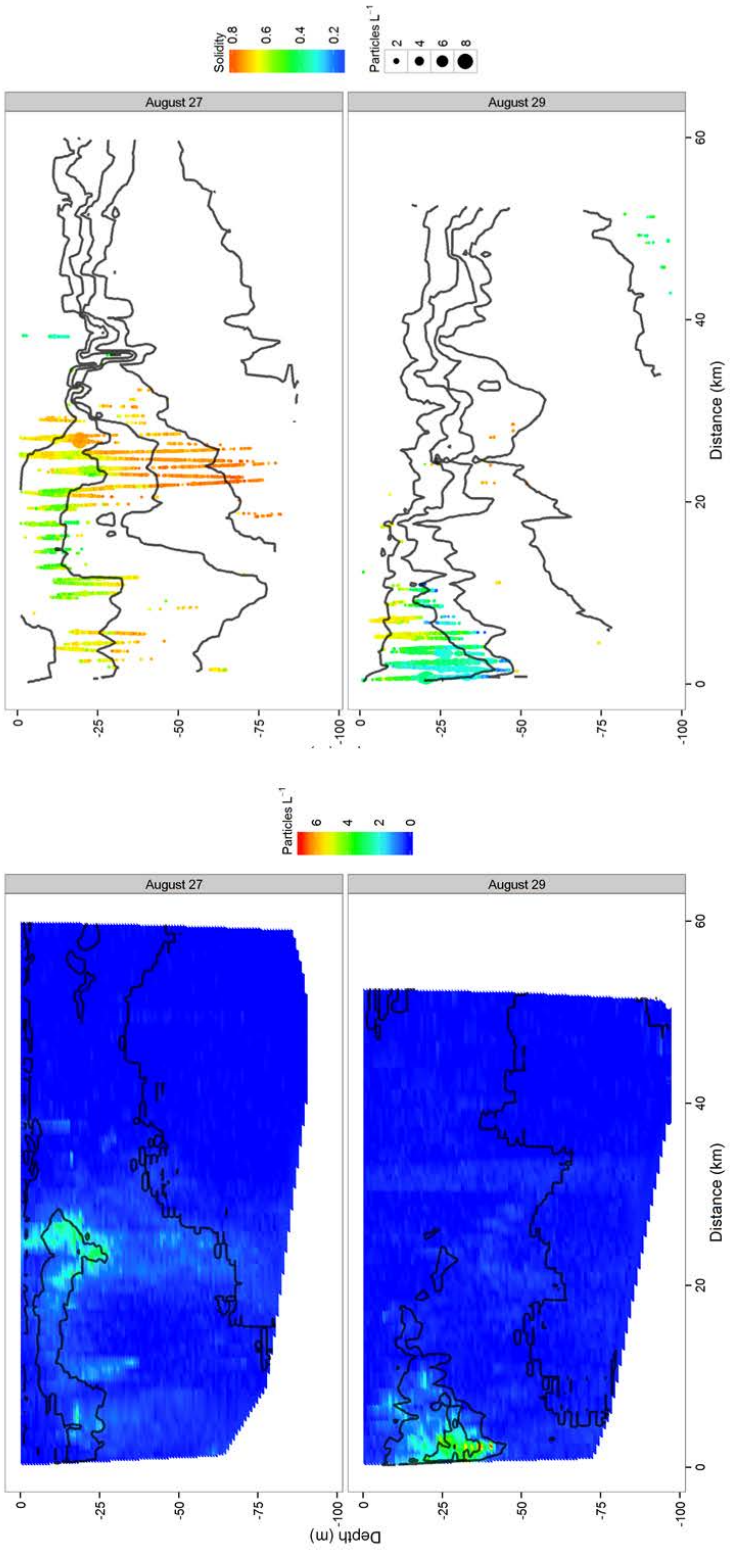
Solidity
0.8
0.6
0.4
0.2
Particles L⁻¹
2
4
6
8
August 27
August 29
Distance (km)
0
20
40
60
0
-25
-50
-75
-100
Particles L⁻¹
6
4
2
0
August 27
August 29
Distance (km)
Depth (m)

Figure 4.5. Example ISIIS images A) Phycidae larva B) Pleuronectiformes larva C) Two Merluccidae larvae D) *Clytia* spp. hydromedusa E) *Persa* spp. hydromedusa F) Lobate ctenophore (*Bolinopsis* spp.) G) Siphonophore H) *Beroe* spp. I) solo salp *Thalia democratica* J) *Thalia democratica* producing a new salp chain.

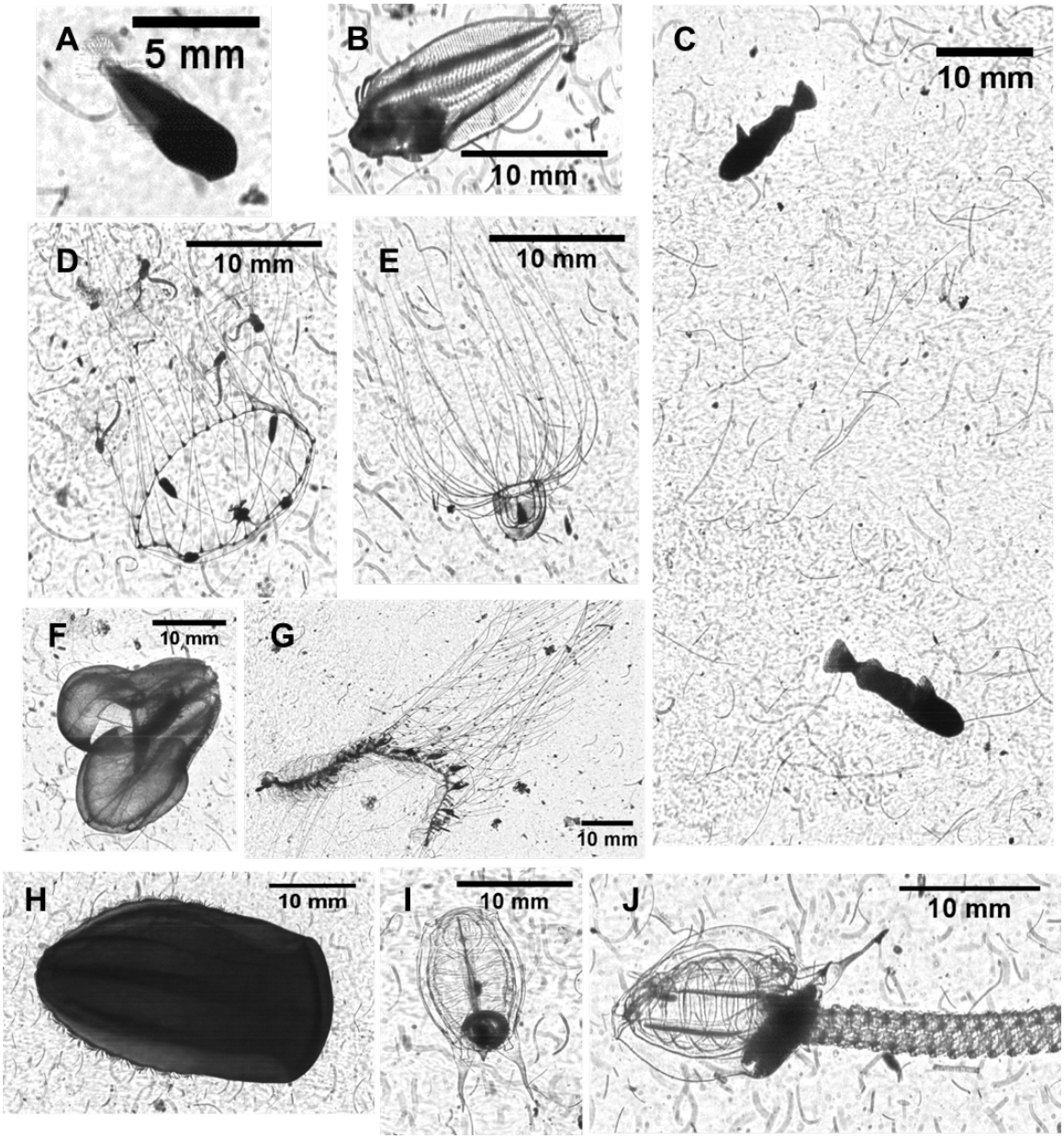

Figure 4.6. Location of fish larvae taxa in relation to density contours along transects sampled on two different days.

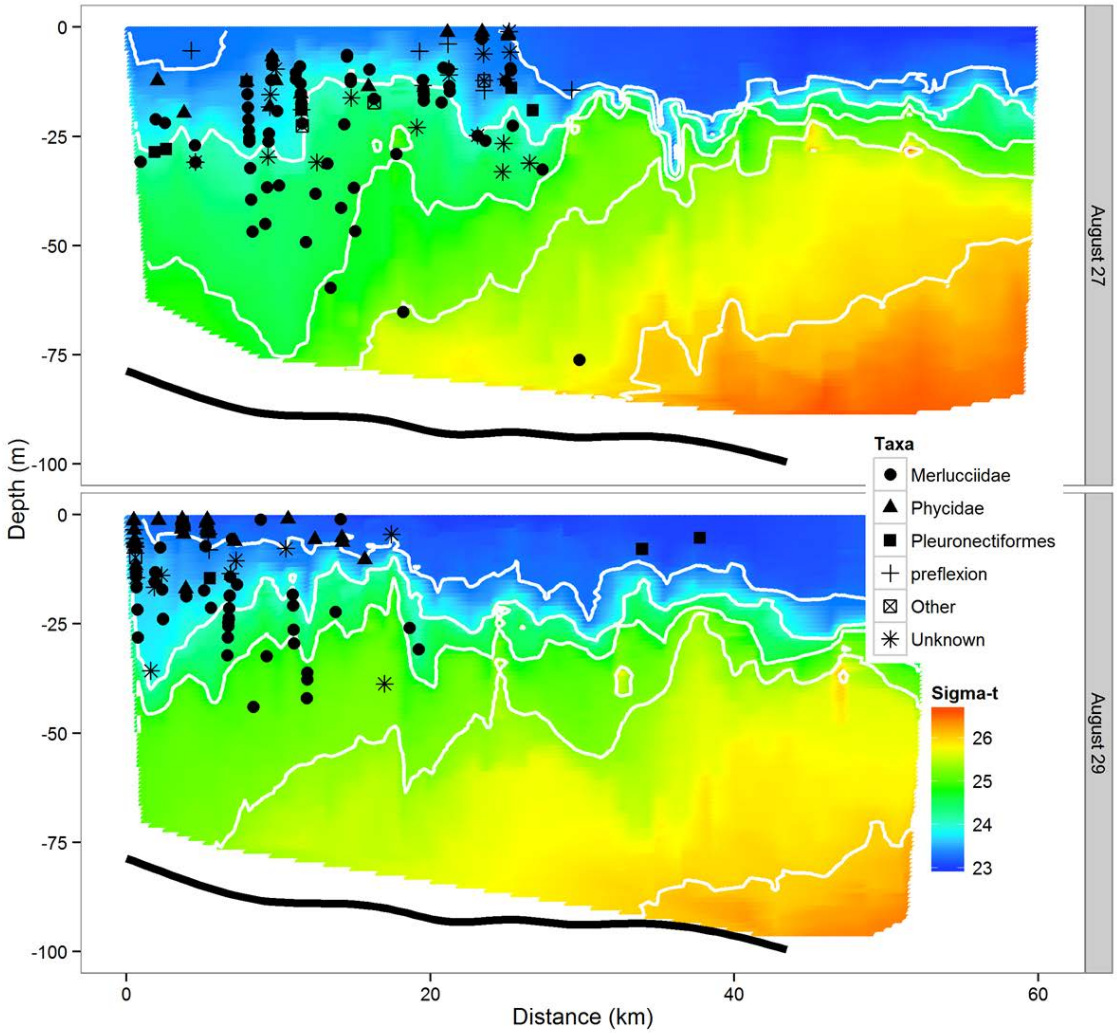

Figure 4.7. Mean depth and temperature occupied by each larval fish taxon (± 1.96 SE)

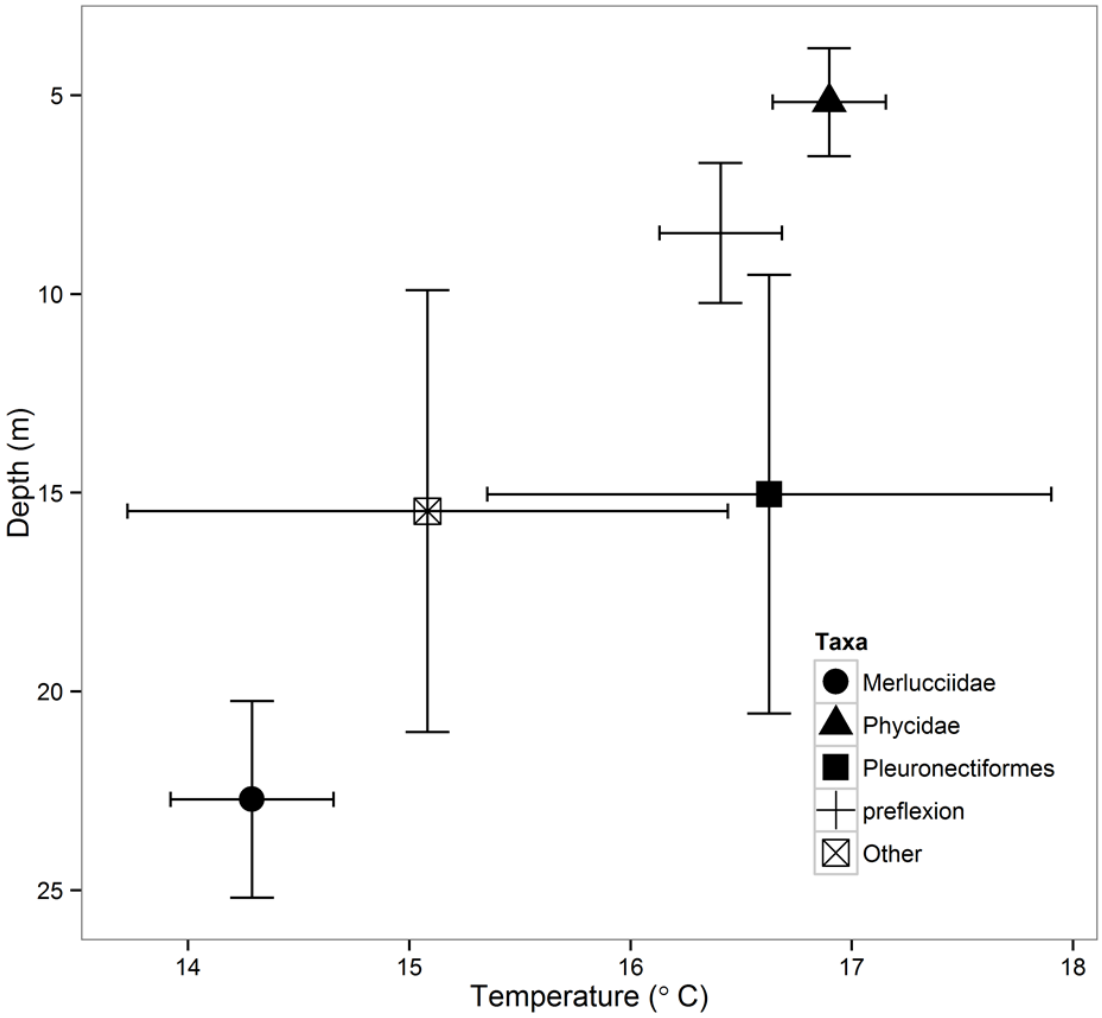

Figure 4.8. Temperature/salinity diagrams of waters sampled with and without fish larvae on each of the two sampling days. The color of each point corresponds to the chlorophyll-*a* fluorescence (volts). Lines are isopycnals.

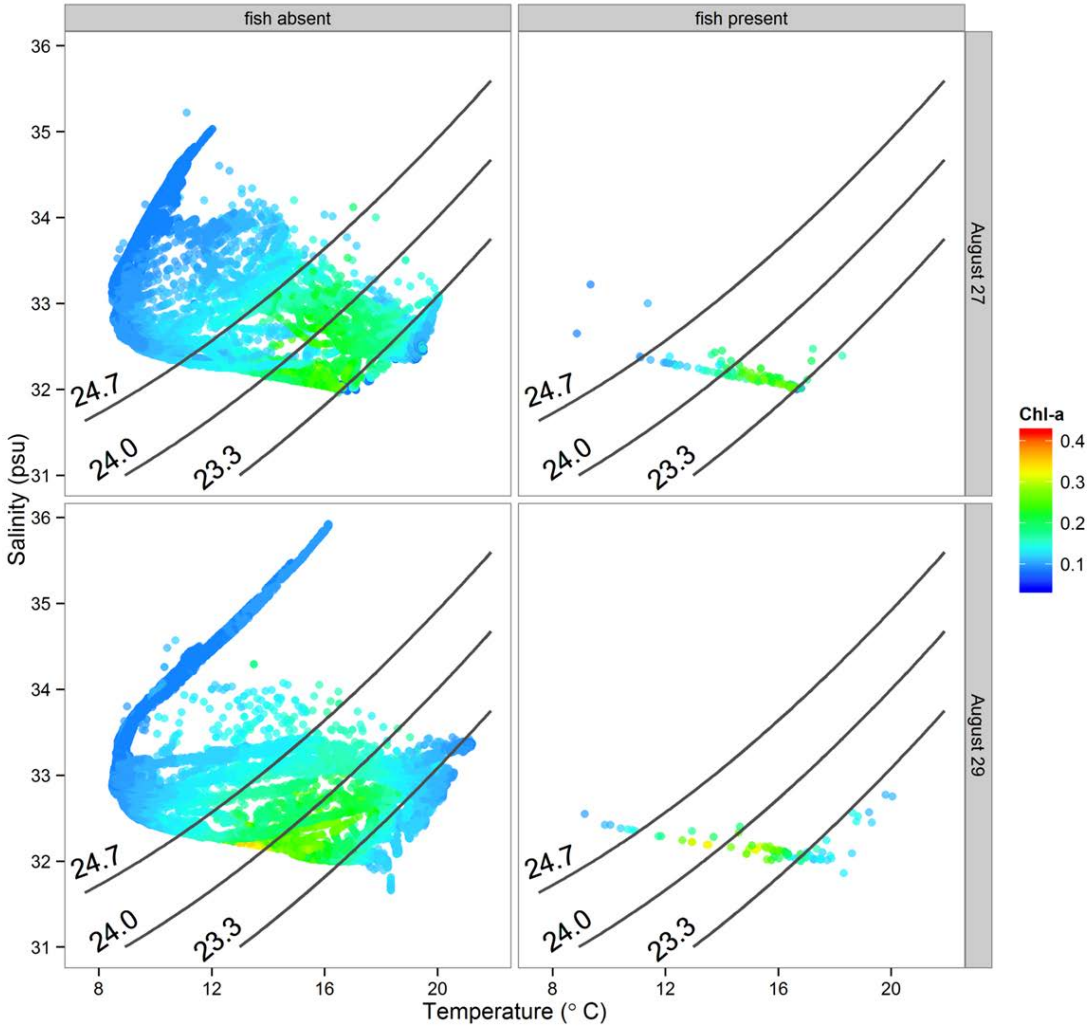

Figure 4.9. Fine-scale distribution of salps overlying chlorophyll-*a* fluorescence (volts). Chlorophyll-*a* contours are shown in white.

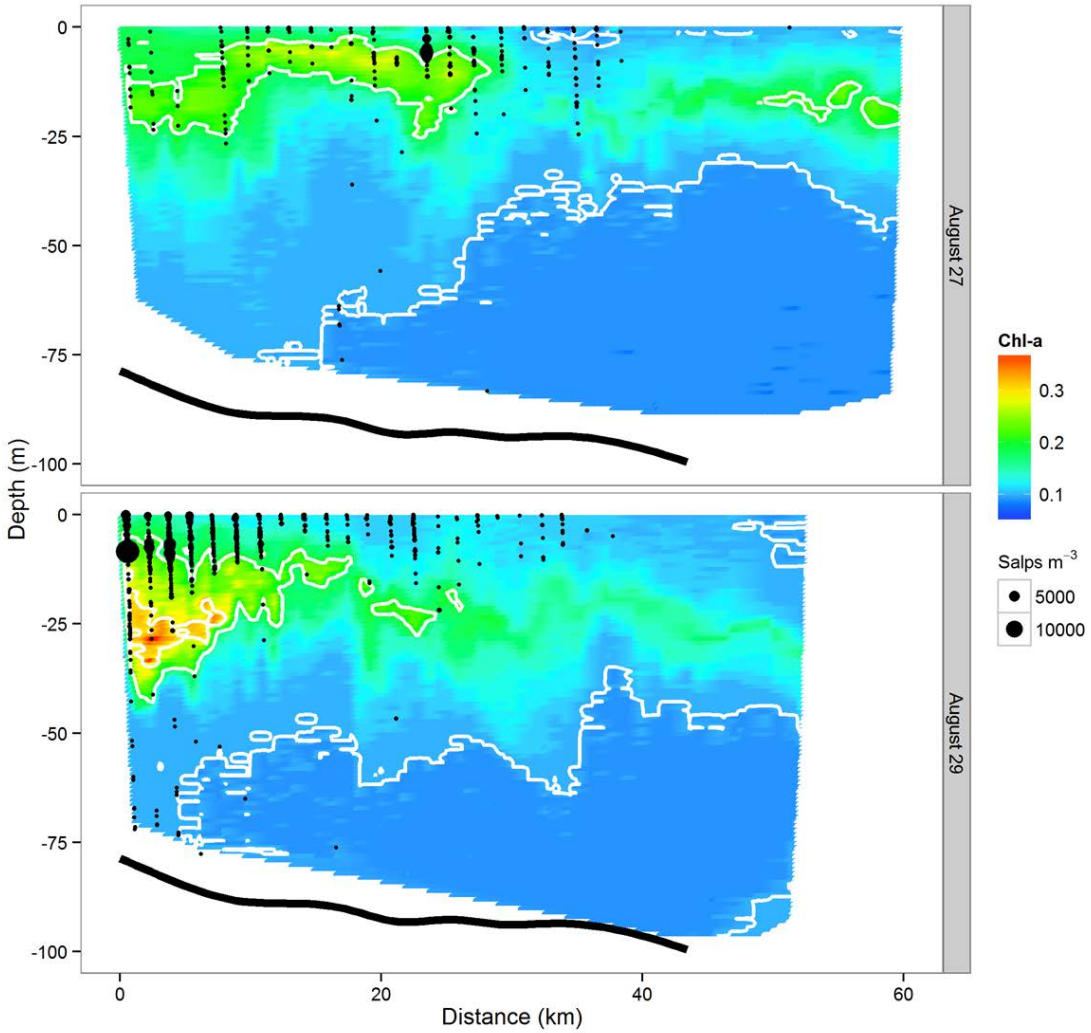

Figure 4.10. Results of a logistic generalized linear model for salp presence/absence in relation to distance to front and chlorophyll-*a* fluorescence. Negative distances to the front are on the shelf side and positive distances are in slope waters.

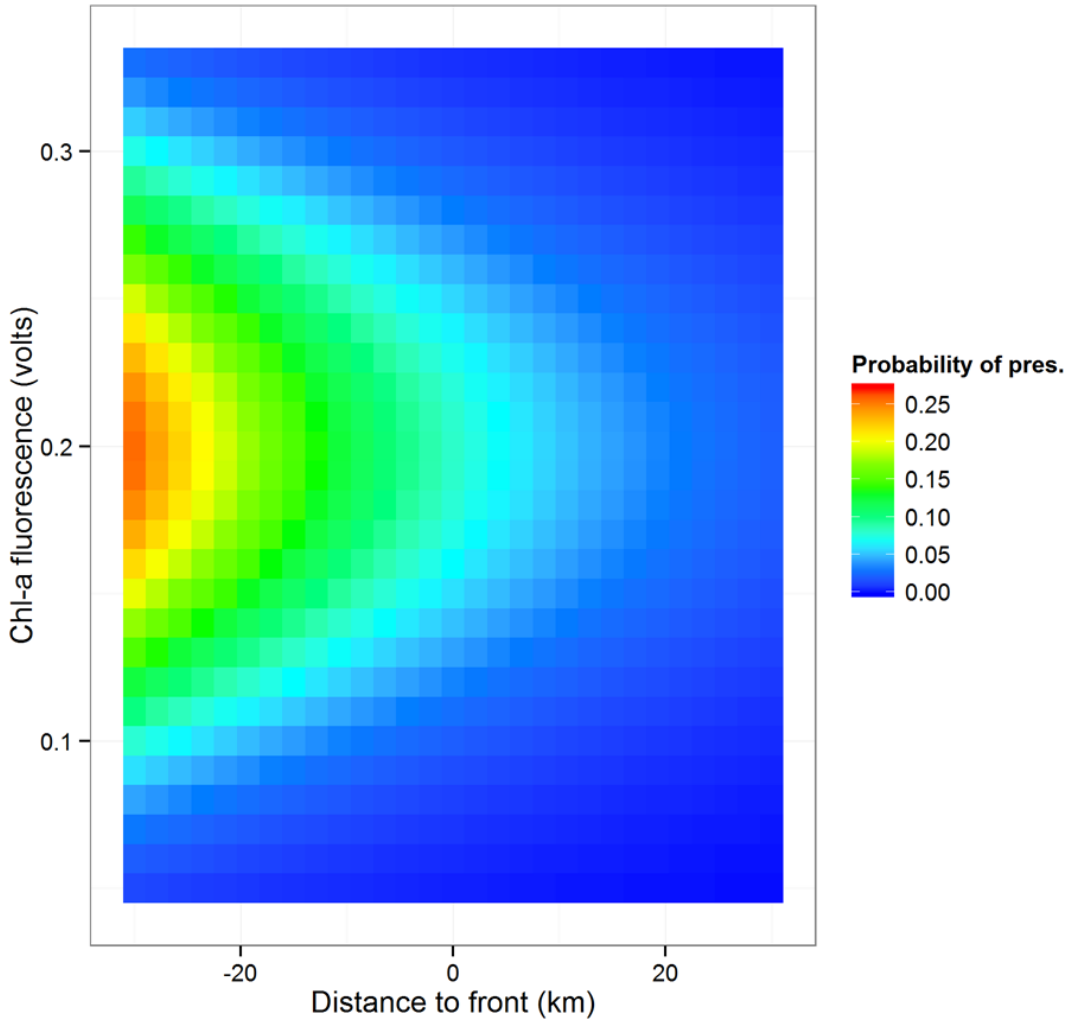

Figure 4.11. Distribution of different gelatinous zooplankton in relation to the 23.3, 23.8, and 25.0 isopycnals A) *Clytia* spp. B) *Persa* spp. C) Lobate ctenophores (*Bolinopsis* spp.) D) Miscellaneous ctenophores (mostly *Beroe* spp.) E) Siphonophores

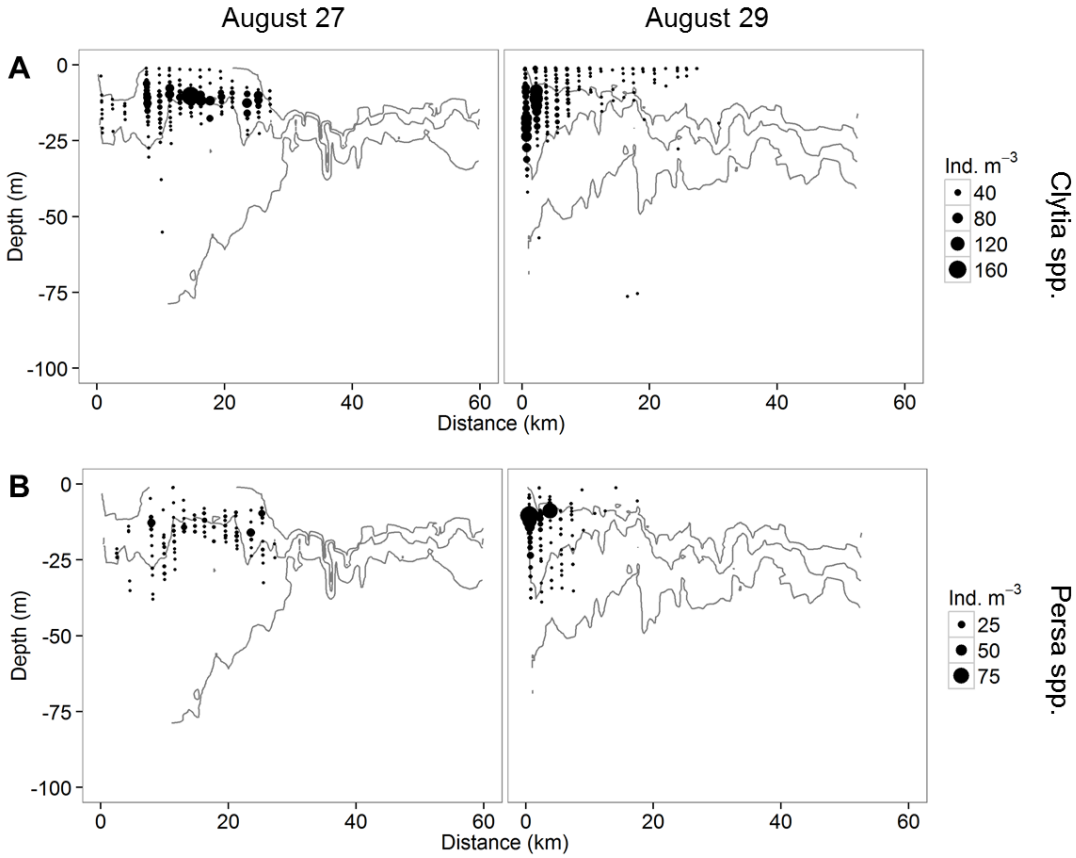

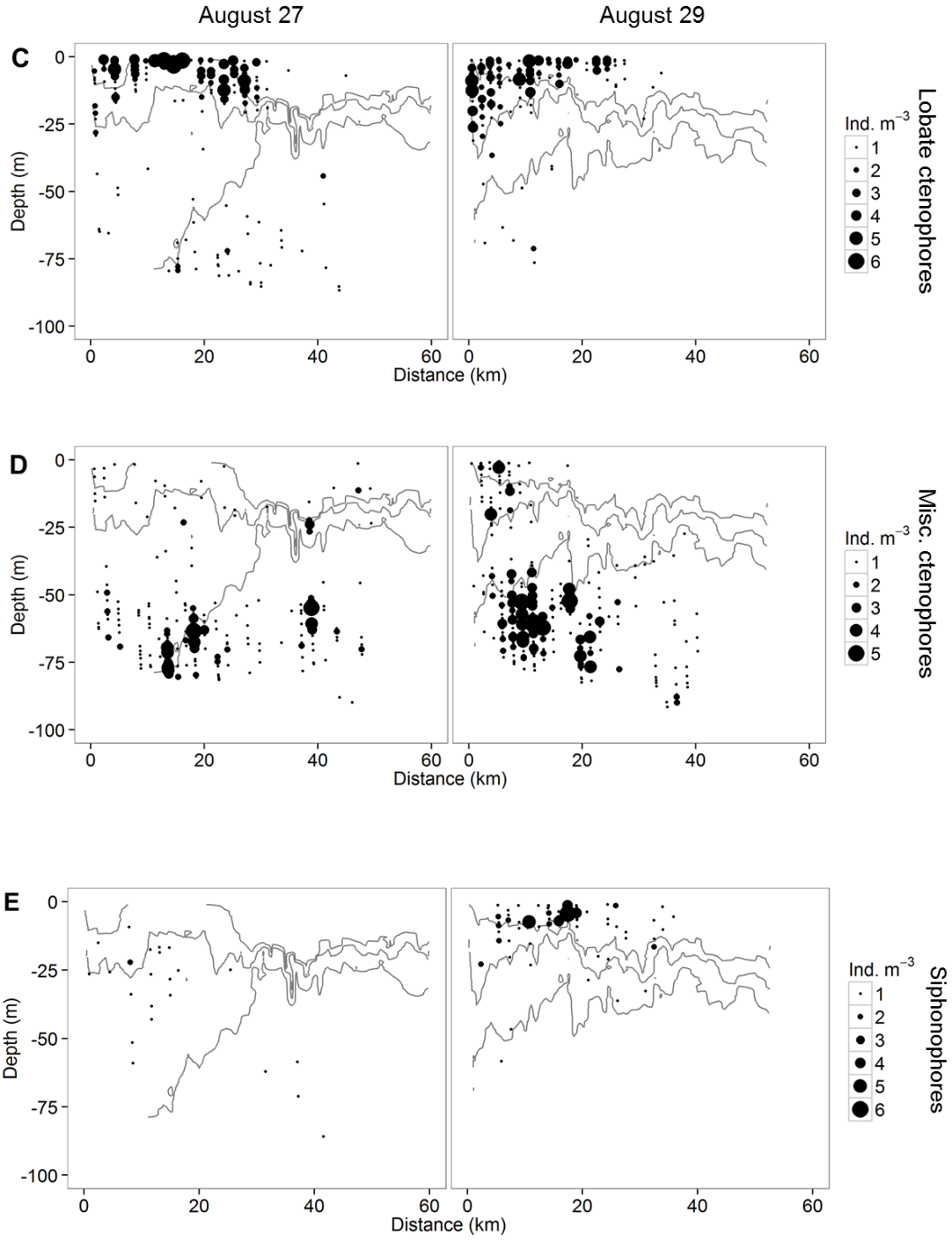
August 27
August 29
C
D
E
Depth (m)
0
-25
-50
-75
-100
0
20
40
60
Distance (km)
Ind. m^{-3}
1
2
3
4
5
6
Lobate ctenophores
Misc. ctenophores
Siphonophores

CHAPTER 5: GENERAL CONCLUSIONS

The description of fine-scale distributions of plankton provides indirect evidence of biophysical processes and important initial conditions needed to model a system through time. Prior to these studies, most research focusing on plankton interactions around physical features, such as fronts, sampled on a scale that was too coarse to understand potential predator-prey interactions or used methods, such as acoustics, with severe biases in organism detectability. Many fragile gelatinous organisms are severely under-sampled with traditional net techniques (Remsen et al. 2004) and not well resolved with acoustics (Brierley et al. 2004). As a consequence, gelatinous zooplankton are neglected links in the food web that likely play a strong role in processes influencing the fish population variability (Bailey and Houde 1989). This dissertation was an attempt to resolve the distributions of plankton near well-studied physical features and better understand the biophysical drivers of the distributions of diverse planktonic taxa.

The fundamental question addressed by this work is almost as old as the field itself: what factors drive plankton distributions in the ocean? This question will perhaps never be fully answered and depends on the dominant physical regimes on multiple spatial scales. However, new sampling technology allows oceanographers a fresh look at old problems, with the potential for new discoveries and a deeper understanding of these processes. The scientific movement towards higher-resolution sampling has happened in other fields (e.g., microscopes and DNA technology in biology), opening whole new avenues of research. In biological oceanography, this movement is exemplified by the numerous optical systems designed for fine-scale sampling (e.g., Video Plankton

Recorder, Underwater Video Profiler, etc.). The *In Situ* Ichthyoplankton Imaging System (ISIIS) fills a much needed niche in these systems by sampling plankton from a wide range of sizes (500 μm - 13 cm) with adequate tow speed and sampling volume to capture rarer, fast moving plankton (i.e., larval fishes, shrimps) within the context of their predator-prey field (Cowen and Guigand 2008). While we could not typically determine the exact mechanisms producing the patterns we described, the ability to sample multiple trophic levels at once gave new insights into predator-prey interactions at the ubiquitous coastal features including thin layers, internal waves, and fronts.

In Monterey Bay (Chapter 2), we studied the formation and dissipation of thin layers of phytoplankton over a two week period and the distributions of the primary and secondary consumer populations. This field research represented the first thin layer study incorporating gelatinous zooplankton, as well as likely some of the most accurate abundance estimates and short time scale variability of these organisms in the northern Monterey Bay waters. We capitalized on unique orientation information obtained in the image data to explain the aggregation of *Bolinopsis* spp. within density discontinuities, which corresponded to the location of diatom-dominated thin layers. We also documented what appeared to be avoidance of diatoms by copepods, potentially due to predator avoidance or the toxic effects of the dominant phytoplankton species, *Psuedo-nitzschia* spp., on grazing behavior. Based on these fine-scale data and previous thin layer research, we hypothesized that the large diatom flocs created a microhabitat within and below the chlorophyll-*a* maximum (sometimes aggregated in a thin layer) where gelatinous organisms could rely on contact predation.

Near Stellwagen Bank (Chapter 3), we examined how thin layers and distributions of planktonic taxa can be altered by the passage of tidally driven internal wave packets. Vertical distributions of copepods and gelatinous zooplankton were somewhat similar to those seen in Monterey Bay, with jellies aggregating at depth and copepods near the surface, strongly overlapping with the distribution of larval fishes. Application of the Distance to Next Encounter (DNE) metric to horizontal transects showed that patches of both larval fishes and gelatinous zooplankton were smaller during internal wave propagation. As would be expected by the input of vertical mixing, the distinct vertical partitioning of the water column was homogenized after the passage of the internal wave packet, and larvae showed decreased correlation with zooplankton prey and increased correlation with predators during internal wave propagation.

Chapter 4 examined two transects through a shelf-slope front located southeast of Georges Bank. Utilizing particle solidity, we could make strong predictions about the composition of particles in different portions of the water column. This showed copepods and appendicularians aggregating in surface waters just above the convergence of isopycnals, which defined the front. Chlorophyll-*a* fluorescence peaks followed isopycnals and were associated with low particle solidity, indicative of loose aggregates, and high concentrations of particles across a range of sizes. The location of the chlorophyll-*a* fluorescence peaks and particles suggested the formation of these aggregates was primarily due to growth in surface waters followed by physical coagulation. Larval fishes were restricted, along with most gelatinous zooplankton, to the shelf side of the front, with taxon-specific depth patterns that were often related to the position of isopycnals.

Though this body of work covered several regions with different oceanographic regimes, a few common themes emerged. High levels of chlorophyll-*a* fluorescence were typically dominated by diatom aggregates, lending support to the idea that physical coagulation could be an important driver of the formation of deep chlorophyll maxima near the base of the photic zone (Jackson 1990; Kiørboe et al. 1990). Thin, near surface layers of copepods occurred in all study regions, and did not overlap spatially with the peaks in chlorophyll-*a* fluorescence. This pronounced vertical separation suggests one of three potential bottom up drivers of their distributions: 1) copepods rely on diatoms before they coagulate at depth 2) they feed more on ciliates (Calbet and Saiz 2005) or dinoflagellates that are too small to be imaged by ISIIS (Gallager et al. 2004) and may form high density patches in surface waters characterized by high turbulence (Durham et al. 2013), or 3) they make short migrations into diatom populated zones of the water column. Alternatively, these copepod patches could be unrelated to feeding and exist primarily for the purpose of minimizing probability of predator encounter, avoiding contact predators at depth, or completely satiating a predator that finds these dense patches (Majaneva et al. 2013). Larval fishes were often found in surface waters, suggesting that they often experience much higher than average concentrations of prey items. Taxon and ontogenetic dependent differences in behavior could play a major role in larval fish vertical distributions, and thus their exposure to predators and prey.

Recommendations for future research

High-resolution sampling systems are gradually revealing more information about the dominant scales within the ocean. Our study lends support to the idea that many

plankton patches have vertical extent of approximately 5 m, indicating that this may be a dominant scale in the coastal ocean (Benoit-Bird et al. 2013). We documented distributions of many different taxa, including fish larvae, chaetognaths, hydromedusae and salps with vertical patch dimensions around 5-10 m. The finding of commonalities of distributions across diverse hydrographic regimes may indicate that organism behavior is a strong driver of plankton distributions. There are many avenues for future research that would build on the findings in this body of work.

The first and most obvious direction for research is increasing the spatial and temporal coverage of imaging system observation, which is limited by data quantity and costs of field oceanographic research. This work applied a variety of techniques to reveal unique information on plankton patch dynamics, which can serve as examples of how to analyze high-resolution data over larger temporal scales. The Stellwagen Bank area has great potential for future studies using optical systems because of the extremely high abundances and patchiness of a variety of taxa. Studies similar to Chapter 3 should take place on a seasonal basis and in conjunction with measurements of larval condition inside and outside of copepod patches. We need to better understand the temporal and spatial extent of near-surface copepod thin layers and what kind of effect these layers could have on year-class success and the distributions of other animals (fish, cetaceans, etc.). This would require a costly field campaign, but if it revealed a link between fine-scale prey patchiness to recruitment, could lead to new monitoring techniques to incorporate into fishery and natural resource management.

While this dissertation focused primarily on the use of the imaging system with synoptic physical measurements, this type of study could benefit greatly from the

application of other field techniques. Moored profilers, such as the ones used in Chapter 2, should be a requirement for any ISIIS study to better understand the large-scale physical dynamics before, during, and after sampling. Sediment traps could have been utilized in Chapter 4 to give an understanding of the particle flux and content in different parts of the front. We could then see if particle size, shape, or other descriptor has any impact on vertical flux, potentially allowing the use of image data to predict flux. ISIIS should continue to be used with net systems to aid in identification of larvae. Sophisticated databases need to be designed to allow for regional comparisons incorporating a suite of physical and biological measurements. Combining imaging technology with database management groups will facilitate the dissemination of data, fostering collaboration across diverse scientific and engineering fields, which is a necessity in modern science. I envision a day when plankton image samples are widely available, subject to a suite of analyses by many scientists with differing expertise, no longer lying dormant in laboratories after one analysis approach.

Mesocosm experiments from past researchers were used extensively to understand the behavior of different zooplankton and how they may react to the fine-scale gradients described in our study. Spatial co-distributions are typically not sufficient to understand the drivers of organism patchiness. Many of our results would complement further investigations using controlled experiments, which have the advantage of the ability to isolate various factors influencing patchiness. For example, are the surface layers of copepods formed through predation avoidance, prey seeking, or physical processes? The diversity of environments in which plankton patches form suggests a combination of factors at work, but only through controlled experiments can we gain an

understanding of how much each factor contributes to the overall distribution. This type of experiment would be particularly interesting and widely applicable due to the common characteristic of near surface copepod layers in the diverse hydrographic regimes studied.

Building on our understanding of the all-important initial conditions and drivers of plankton distributions will lead to improved models of biophysical interactions. Increased ability to represent biological processes in mathematical terms allows for the use of fine-scale observations to make predictions of larger scale processes, which are more relevant to management decisions and population connectivity (Cowen and Sponaugle 2009). Recent lab work has demonstrated thin layer formation can occur through a combination of cell motility and shear, causing motile phytoplankton to effective get "stuck" in a layer beyond a critical shear value (Durham et al. 2009). This kind of mechanistic understanding has been extended to copepods (Woodson et al. 2005) and should include higher trophic levels to allow for prediction of trophic impacts of small scale patches. With an improved mechanistic understanding of these processes, collection of fine-scale physical and biological variables could allow scientists to make predictions how plankton patches may evolve over time, allowing effective "scaling up" of observations. Research into plankton life history traits and trophic interactions must be a priority for ensuring the utility and correct parameterization of these models.

All of these potential applications of imaging systems to various aspects of biological oceanography hinges on reliable image analysis software. While we used some automated techniques to reveal aspects of the zooplankton distributions by taking advantage of relatively monospecific assemblages (e.g., diatom flocs in Chapter 2, copepods in Chapter 3), the most pressing need for advancement in this field is robust

taxon-specific image recognition software (Benfield et al. 2007). Many advances are being made in this area by using neural networks and Support Vector Machines (Hu and Davis 2006), but ISIIS images present a particularly difficult challenge due to the wide range of particle sizes and orientations that can be found within one image. The particles within an image must first be properly segmented as Regions of Interest (ROIs), but many transparent taxa have several compartments (i.e., siphonophores and salp chains), leading to over-segmentation (one organism treated as many ROIs). Without segmentation of the entire object, accurate recognition is impossible. Better post-processing techniques may be required to unite segments that all occur in the similar coordinates of a frame: a typical characteristic of over-segmentation. The recognition phase of image processing runs into problems because a 3D object with many possible orientations is being projected onto a 2D plane. Euphausiids, for example, can have dramatically different appearances depending on their orientation to the camera and *in situ* behavior (rolled up escape response or straight). Our group is making efforts to improve recognition by creating classes of the different orientations, but in reality, the number of shapes for a particular taxon is infinite. In an ideal situation, we would be able to create 3D descriptions of each taxon in space, project them onto a 2D plane, and use this as a training library, instead of current techniques of building libraries using human identified images in various common orientations. I am confident that future iterations of this segmentation and recognition software will lead to useful, fully automated analysis, greatly improving the cost-effectiveness of imaging system use in oceanography.

LITERATURE CITED

Aikman III F, Ou HW, Houghton RW (1988) Current variability across the new england continental shelf-break and slope. Cont Shelf Res 8:625-651

Akima, H., Gebhardt, A., Petzoldt, T., Maechler, M. (2013) Akima: Interpolation of irregularly spaced data. R package version 0.5-10

Albaina A and Irigoien X (2004) Relationships between frontal structures and zooplankton communities along a cross-shelf transect in the Bay of Biscay (1995 to 2003). Mar Ecol Prog Ser 284:65-75

Alldredge AL and Gotschalk CC (1989) Direct observations of the mass flocculation of diatom blooms: Characteristics, settling velocities and formation of diatom aggregates. Deep Sea Research Part A, Oceanographic Research Papers 36:159-171

Alldredge AL and Madin LP (1982) Pelagic tunicates: Unique herbivores in the marine plankton. Bioscience 32:655-663

Alldredge AL, Cowles TJ, MacIntyre S, Rines JEB, Donaghay PL, Greenlaw CF, Holliday DV, Dekshenieks MM, Sullivan JM, Zaneveld JRV (2002) Occurrence and mechanisms of formation of a dramatic thin layer of marine snow in a shallow pacific fjord. Mar Ecol Prog Ser 233:1-12

Anraku M (1956) Some experiments on the variability of horizontal plankton hauls and on the horizontal distribution of plankton in a limited area. Bulletin of the Faculty of Fisheries Hokkaido University 7:1-16

Arai MN (1976) Behavior of planktonic coelenterates in temperature and salinity discontinuity layers. In: Mackie GO (ed) *Coelenterate Ecology and Behavior*. Plenum Press, New York, p. 211-217

Ashjian CJ, Davis CS, Gallager SM, Alatalo P (2001) Distribution of plankton, particles, and hydrographic features across Georges Bank described using the Video Plankton Recorder. Deep-Sea Research Part II: Topical Studies in Oceanography 48:245-282

Atkinson L, Paffenhöfer G, Dunstan W (1978) Chemical and biological effect of a Gulf-stream intrusion off St. Augustine, Florida. Bull Mar Sci 28:667-679

Bailey KM and Houde ED (1989) Predation on eggs and larvae of marine fishes and the recruitment problem. Advances in Marine Biology 25:1-83

Bailey KM and Batty RS (1984) Laboratory study of predation by *Aurelia aurita* on larvae of cod, flounder, plaice and herring: Development and vulnerability to capture. Mar Biol 83:287-291

Baker LD and Reeve MR (1974) Laboratory culture of the lobate ctenophore *Mnemiopsis mccradyi* with notes on feeding and fecundity. Mar Biol 26:57-62

Bakun A (2006) Fronts and eddies as key structures in the habitat of marine fish larvae: Opportunity, adaptive response and competitive advantage. Scientia Marina 70:105-122

Bargu S, Lefebvre K, Silver MW (2006) Effect of dissolved domoic acid on the grazing rate of krill *Euphausia pacifica*. Mar Ecol Prog Ser 312:169-175

Barnes H and Marshall SM (1951) On the variability of replicate plankton samples and some application of 'contagious' series to the statistical distribution of catches over restricted periods. Journal of the Marine Biological Association of the United Kingdom 30:233-263

Barth JA, Hebert D, Dale AC, Ullman DS (2004) Direct observations of along-isopycnal upwelling and diapycnal velocity at a shelfbreak front. J Phys Oceanogr 34:543-565

Bates D, Maechler M, Bolker B (2012) Lme4: Linear mixed-effects models using S4 classes. R Packages Version 0.999999-0. http://CRAN.R-Project.org/package=lme4

Bathmann UV (1988) Mass occurrence of *Salpa fusiformis* in the spring of 1984 off Ireland: Implications for sedimentation processes. Mar Biol 97:127-135

Batty RS (1994) The effect of temperature on the vertical distribution of larval herring (*Clupea harengus* L.). J Exp Mar Biol Ecol 177:269-276

Baumgartner MF (2003) Comparisons of *Calanus finmarchicus* fifth copepodite abundance estimates from nets and an optical plankton counter. J Plankton Res 25:855-868

Benfield M, Schwehm C, Fredericks R, Squyres G, Keenan S, Trevorrow M (2003) ZOOVIS: A high-resolution digital still camera system for measurement of fine-scale zooplankton distributions. In: Seuront L and Strutton PG (eds) *Scales in Aquatic Ecology: Measurement, Analysis and Simulation*. CRC Press, Boca Raton, FL, p. 17-30

Benfield MC, Davis CS, Gallager SM (2000) Estimating the in-situ orientation of *Calanus finmarchicus* on Georges Bank using the Video Plankton Recorder. Plankton Biol Ecol 47:69-72

Benfield MC, Davis CS, Wiebe PH, Gallager SM, Gregory Loughj R, Copley NJ (1996) Video Plankton Recorder estimates of copepod, pteropod and larvacean distributions from a stratified region of Georges Bank with comparative measurements from a MOCNESS sampler. Deep-Sea Research Part II: Topical Studies in Oceanography 43:1925-1945

Benfield MC, Grosjean P, Culverhouse P, Irigoien X, Sieracki ME, Lopez-Urrutia A, Dam HG, Hu Q, Davis CS, Hansen A, and others (2007) Research on automated plankton identification. Oceanography 20:12-26

Benoit-Bird KJ, Shroyer EL, McManus MA (2013) A critical scale in plankton aggregations across coastal ecosystems. Geophys Res Lett 40:1-7

Benoit-Bird KJ, Cowles TJ, Wingard CE (2009) Edge gradients provide evidence of ecological interactions in planktonic thin layers. Limnol Oceanogr 54:1382-1392

Benoit-Bird KJ, Moline MA, Waluk CM, Robbins IC (2010) Integrated measurements of acoustical and optical thin layers I: Vertical scales of association. Cont Shelf Res 30:17-28

Berner L (1967) Distributional atlas of *Thaliacea* in the California current region. CalCOFI Atlas 8

Bez N (2000) On the use of Lloyd's index of patchiness. Fish Oceanogr 9:372-376

Bjornsen PK and Nielsen TG (1991) Decimeter scale heterogeneity in the plankton during a pycnocline bloom of gyrodinium aureolum. Mar Ecol Prog Ser 73:263-267

Blumberg AF, Signell RP, Jenter HL (1993) Modeling transport processes in the coastal ocean. Journal of Marine Environmental Engineering 1:1689-1705

Bochdansky AB and Bollens SM (2004) Relevant scales in zooplankton ecology: Distribution, feeding, and reproduction of the copepod *Acartia hudsonica* in response to thin layers of the diatom *Skeletonema costatum*. Limnol Oceanogr 49:625-636

Bollens SM, Frost BW, Thoreson DS, Watts SJ (1992) Diel vertical migration in zooplankton: Field evidence in support of the predator avoidance hypothesis. Hydrobiologia 234:33-39

Bonnet D, Harris RP, Yebra L, Guilhaumon F, Conway DVP, Hirst AG (2009) Temperature effects on *Calanus helgolandicus* (copepoda: Calanoida) development time and egg production. J Plankton Res 31:31-44

Breaker LC and Broenkow WW (1994) The circulation of Monterey Bay and related processes. Oceanography and Marine Biology: An Annual Review 32:1-64

Brickman D and Loder JW (1993) Energetics of the internal tide on northern Georges Bank. J Phys Oceanogr 23:409-424

Buckley L, Caldarone E, Ong T- (1999) RNA-DNA ratio and other nucleic acid-based indicators for growth and condition of marine fishes. Hydrobiologia 401:265-277

Buckley LJ and Lough RG (1987) Recent growth, biochemical composition, and prey field of larval haddock (*Melanogrammus aeglefinus*) and Atlantic cod (*Gadus morhua*) on Georges Bank. Can J Fish Aquat Sci 44:14-25

Burd BJ and Thomson RE (1993) Flow volume calculations based on three-dimensional current and net orientation data. Deep-Sea Research Part I 40:1141-1153

Butman B, Alexander PS, Scotti A, Beardsley RC, Anderson SP (2006) Large internal waves in Massachusetts Bay transport sediments offshore. Cont Shelf Res 26:2029-2049

Calbet A and Saiz E (2005) The ciliate-copepod link in marine ecosystems. Aquat Microb Ecol 38:157-167

Carr EF and Pitt KA (2008) Behavioural responses of zooplankton to the presence of predatory jellyfish. J Exp Mar Biol Ecol 354:101-110

Cass-Calay SL (2003) The feeding ecology of larval pacific hake (*Merluccius productus*) in the California current region: An updated approach using a combined OPC/MOCNESS to estimate prey biovolume. Fish Oceanogr 12:34-48

Catalán IA, Vollset KW, Morales-Nin B, Folkvord A (2011) The effect of temperature gradients and stomach fullness on the vertical distribution of larval herring in experimental columns. J Exp Mar Biol Ecol 404:26-32

Chapman DC and Lentz SJ (1994) Trapping of a coastal density front by the bottom boundary layer. J Phys Oceanogr 24:1464-1479

Cheriton OM, McManus MA, Stacey MT, Steinbuck JV (2009) Physical and biological controls on the maintenance and dissipation of a thin phytoplankton layer. Mar Ecol Prog Ser 378:55-69

Cheriton OM, McManus MA, Holliday DV, Greenlaw CF, Donaghay PL, Cowles TJ (2007) Effects of mesoscale physical processes on thin zooplankton layers at four sites along the west coast of the U.S. Estuaries and Coasts 30:575-590

Condon RH, Steinberg DK, Del Giorgio PA, Bouvier TC, Bronk DA, Graham WM, Ducklow HW (2011) Jellyfish blooms result in a major microbial respiratory sink of carbon in marine systems. Proc Natl Acad Sci USA 108:10225-10230

Costello JH, Sullivan BK, Gifford DJ, Van Keuren D, Sullivan LJ (2006) Seasonal refugia, shoreward thermal amplification, and metapopulation dynamics of the ctenophore *Mnemiopsis leidyi* in Narragansett Bay, Rhode Island. Limnol Oceanogr 51:1819-1831

Cowan JH and Houde ED (1993) Relative predation potentials of scyphomedusae, ctenophores and planktivorous fish on ichthyoplankton in Chesapeake Bay. Mar Ecol Prog Ser 95:55-65

Cowen RK (2006) Larval dispersal and retention and consequences for population connectivity. In: Sale PF (ed) *Coral Reef Fishes: Dynamics and Diversity in a Complex Ecosystem*. Academic Press, Burlington, Massachusetts, USA, p. 149-170

Cowen RK and Sponaugle S (2009) Larval dispersal and marine population connectivity. Annual Review of Marine Science 1:443-466

Cowen RK and Guigand CM (2008) *In Situ* Ichthyoplankton Imaging System (ISIIS): System design and preliminary results. Limnology and Oceanography: Methods 6:126-132

Cowen RK and Castro LR (1994) Relation of coral reef fish larval distributions to island scale circulation around Barbados, West Indies. Bull Mar Sci 54:228-244

Cowen RK, Greer AT, Guigand CM, Hare JA, Richardson DE, Walsh HJ (2013) Evaluation of the *In Situ* Ichthyoplankton Imaging System (ISIIS): Comparison with the traditional (bongo net) sampler. Fish Bull 111:1-12

Cowles TJ and Desiderio RA (1993) Resolution of biological microstructure through *in situ* fluorescence emission spectra. Oceanography 6:105-111

Cowles TJ, Desiderio RA, Carr ME (1998) Small-scale planktonic structure: Persistence and trophic consequences. Oceanography 11:4-9

Currie WJS, Claereboudt MR, Roff JC (1998) Gaps and patches in the ocean: A one-dimensional analysis of planktonic distributions. Mar Ecol Prog Ser 171:15-21

Cushing DH (1975) Marine ecology and fisheries. Cambridge University Press, London

Davies IE and Barham EG (1969) The Tucker opening-closing micronekton net and its performance in a study of the deep scattering layer. Mar Biol 2:127-131

Davis CS, Gallager SM, Solow AR (1992) Microaggregations of oceanic plankton observed by towed video microscopy. Science 257:230-232

Davis CS, Thwaites FT, Gallager SM, Hu Q (2005) A three-axis fast-tow digital Video Plankton Recorder for rapid surveys of plankton taxa and hydrography. Limnology and Oceanography: Methods 3:59-74

Davis CS, Flierl GR, Wiebe PH, Franks PJS (1991) Micropatchiness, turbulence and recruitment in plankton. J Mar Res 49:109-151

Dawidowicz P, Pijanowska J, Ciechomski K (1990) Vertical migration of chaoborus larvae is induced by the presence of fish. Limnology & Oceanography 35:1631-1637

De Robertis A (2002) Small-scale spatial distribution of the euphausiid *Euphausia pacifica* and overlap with planktivorous fishes. J Plankton Res 24:1207-1220

Deibel D and Paffenhöfer GA (2009) Predictability of patches of neritic salps and doliolids (tunicata, thaliacea). J Plankton Res 31:1571-1579

Dekshenieks MM, Donaghay PL, Sullivan JM, Rines JEB, Osborn TR, Twardowski MS (2001) Temporal and spatial occurrence of thin phytoplankton layers in relation to physical processes. Mar Ecol Prog Ser 223:61-71

Dennett MR, Caron DA, Michaels AF, Gallager SM, Davis CS (2002) Video Plankton Recorder reveals high abundances of colonial radiolaria in surface waters of the central north pacific. J Plankton Res 24:797-805

Donaghay PL, Rines HM, Sieburth JM (1992) Simultaneous sampling of fine scale biological, chemical, and physical structure in stratified waters. Arch. Hydrobiol. 36:97-108

Dower JF, Pepin P, Leggett WC (1998) Enhanced gut fullness and an apparent shift in size selectivity by radiated shanny (*Ulvaria subbifurcata*) larvae in response to increased turbulence. Canadian Journal of Fisheries and Aquatic Sciences 55:128-142

Durham WM, Kessler JO, Stocker R (2009) Disruption of vertical motility by shear triggers formation of thin phytoplankton layers. Science 323:1067-1070

Durham WM, Climent E, Barry M, De Lillo F, Boffetta G, Cencini M, Stocker R (2013) Turbulence drives microscale patches of motile phytoplankton. Nature Communications 4:2148

Fernández E, Cabal J, Acuña JL, Bode A, Botas A, García-soto C (1993) Plankton distribution across a slope current-induced front in the southern Bay of Biscay. J Plankton Res 15:619-641

Flood PR, Deibel D, Morris CC (1992) Filtration of colloidal melanin from sea water by planktonic tunicates. Nature 355:630-632

Folt C and Burns C (1999) Biological drivers of zooplankton patchiness. Trends in Ecology and Evolution 14:300-305

Folt C, Schulze PC, Baumgartner K (1993) Characterizing a zooplankton neighbourhood: Small-scale patterns of association and abundance. Freshwat Biol 30:289-300

Fournier RO, Marra J, Bohrer R, Vandet M (1977) Plankton dynamics and nutrient enrichment of Scotian-shelf. Journal of the Fisheries Research Board of Canada 34:1004-1018

Fraser JH (1962) Role of ctenophores and salps in zooplankton production and standing crop. Reports and Proceedings of the International Council of the Exploration of the Sea 153:121-123

Frost BW and McCrone LE (1974) Vertical distribution of zooplankton and myctophid fish at Canadian weather station P, with description of a new multiple net trawl. In: *Proceedings of the International Conference on Engineering in the Ocean Environment*, Halifax

Frost JR, Jacoby CA, Youngbluth MJ (2010) Behavior of *Nemopsis bachei* L. agassiz, 1849 medusae in the presence of physical gradients and biological thin layers. Hydrobiologia 645:97-111

Gallager SM, Yamazaki H, Davis CS (2004) Contribution of fine-scale vertical structure and swimming behavior to formation of plankton layers on Georges Bank. Mar Ecol Prog Ser 267:27-43

Gawarkiewicz G and Chapman DC (1992) The role of stratification in the formation and maintenance of shelf-break fronts. J Phys Oceanogr 22:753-772

Gawarkiewicz G, Ferdelman TG, Church TM, Luther III GW (1996) Shelfbreak frontal structure on the continental shelf north of Cape Hatteras. Cont Shelf Res 16:1751-1773

Genin A (2004) Bio-physical coupling in the formation of zooplankton and fish aggregations over abrupt topographies. J Mar Syst 50:3-20

Gordon A and Aikman F (1981) Salinity maximum in the pycnocline of the Middle Atlantic Bight. Limnology and Oceanography 26:123-130

Gorsky G, Picheral M, Stemmann L (2000) Use of the Underwater Video Profiler for the study of aggregate dynamics in the North Mediterranean. Estuar Coast Shelf Sci 50:121-128

Gotelli NJ and Ellison AM (2004) A primer of ecological statistics. Sinauer Associates, Inc., Sunderland, MA, USA

Govoni JJ and Grimes CB (1992) The surface accumulation of larval fishes by hydrodynamic convergence within the Mississippi River plume front. Cont Shelf Res 12:1265-1276

Graham WM (1993) Spatio-temporal scale assessment of an 'upwelling shadow' in northern Monterey Bay, California. Estuaries 16:83-91

Graham WM and Largier JL (1997) Upwelling shadows as nearshore retention sites: The example of northern Monterey Bay. Cont Shelf Res 17:509-532

Graham WM, Pagès F, Hamner WM (2001) A physical context for gelatinous zooplankton aggregations: A review. Hydrobiologia 451:199-212

Greene CH, Wiebe PH, Pershing AJ, Gal G, Popp JM, Copley NJ, Austin TC, Bradley AM, Goldsborough RG, Dawson J, and others (1998) Assessing the distribution and abundance of zooplankton: A comparison of acoustic and net sampling methods with D-BAD MOCNESS. Deep-Sea Research Part II: Topical Studies in Oceanography 45:1219-1237

Greene CH, Landry MR, Monger BC (1986) Foraging behavior and prey selection by the ambush entangling predator *Pleurobrachia bachei*. Ecology 67:1493-1501

Greer AT, Cowen RK, Guigand CM, McManus MA, Sevadjian JC, Timmerman AHV (2013) Relationships between phytoplankton thin layers and the fine-scale vertical distributions of two trophic levels of zooplankton. J Plankton Res 35:939-956

Greig-Smith P (1979) Pattern in vegetation. Journal of Ecology 67:755-779

Greve W (1970) Cultivation experiments on North Sea ctenophores. Helgoldnder Wiss. Meeresunters 20:304-317

Guigand CM, Cowen RK, Llopiz JK, Richardson DE (2005) A coupled asymmetrical multiple opening closing net with environmental sampling system. Mar Technol Soc J 39:22-24

Haeckel, E (1890) Planktostudien. Jenaische Zeitschrift XXV. Translated by GW Field as appendix 6 to *report of the commissioner for 1889 to 1891* (pp. 565-641). United States Commission of Fish and Fisheries, Washington.

Halpern D (1971) Observations on short-period internal waves in Massachusetts Bay. J Mar Res 29:116-132

Harrell, F.E., Dupont, C. and many others (2012) Hmisc: Harrell Miscellaneous. R package version 3.10-1. http://CRAN.R-project.org/package=Hmisc

Haury LR, Briscoe MG, Orr MH (1979) Tidally generated internal wave packets in Massachusetts Bay. Nature 278:312-317

Haury LR, McGowan JA, Wiebe PH (1978) Patterns and processes in the time-space scales of plankton distributions. In: Steele JH (ed) Spatial Pattern in Plankton Communities. Plenum, New York, p. 277-327

Haury LR, Wiebe PH, Orr MH, Briscoe MG (1983) Tidally generated high-frequency internal wave packets and their effects on plankton in Massachusetts Bay. J Mar Res 41:65-112

Hays GC, Kennedy H, Frost BW (2001) Individual variability in diel vertical migration of a marine copepod: Why some individuals remain at depth when others migrate. Limnol Oceanogr 46:pp. 2050-2054

Hensen V (1895) Methodik der untersuchungen. In: Ergebnisse der Plankton-Expedition der Humbolt-Stiftung. Lipsius and Tischer, Kiel

Herman AW (1992) Design and calibration of a new optical plankton counter capable of sizing small zooplankton. Deep Sea Research Part A, Oceanographic Research Papers 39:395-415

Herman AW (1988) Simultaneous measurement of zooplankton and light attenuance with a new optical plankton counter. Cont Shelf Res 8:205-221

Herman AW (1983) Vertical distribution patterns of copepods, chlorophyll, and production in northeastern Baffin Bay. Limnology & Oceanography 28:709-719

Hernandez FJ, Hare JA, Fey DP (2009) Evaluating diel, ontogenetic and environmental effects on larval fish vertical distribution using generalized additive models for location, scale and shape. Fish Oceanogr 18:224-236

Heron AC (1972) Population ecology of a colonizing species: The pelagic tunicate *Thalia democratica* I. individual growth rate and generation time. Oecologia 10:269-293

Hjort J (1914) Fluctuations in the great fisheries of northern Europe viewed in the light of biological research. Rapp P-v Reun Cons Int Explor Mer 20:1-228

Holliday DV, Greenlaw CF, Donaghay PL (2010) Acoustic scattering in the coastal ocean at Monterey Bay, CA, USA: Fine-scale vertical structures. Cont Shelf Res 30:81-103

Holliday DV, Pieper RE, Kleppel GS (1989) Determination of zooplankton size and distribution with multifrequency acoustic technology. Journal Du Conseil - Conseil International Pour l'Exploration De La Mer 46:52-61

Holliday DV, Pieper RE, Greenlaw CF, Dawson JK (1998) Acoustical sensing of small scale vertical structure in zooplankton assemblages. Oceanography 11:18-23

Holliday DV, Donaghay PL, Greenlaw CF, McGehee DE, McManus MM, Sullivan JM, Miksis JL (2003) Advances in defining fine- and micro-scale pattern in marine plankton. Aquat Living Resour 16:131-136

Holloway G and Denman K (1989) Influence of internal waves on primary production. J Plankton Res 11:409-413

Houde ED (2002) Mortality. In: Fuiman LA and Werner RG (eds) *Fishery Science: The unique contributions of the early life stages*. Blackwell Science Ltd, p. 64-87

Houde ED (1989) Comparative growth, mortality, and energetics of marine fish larvae: Temperature and implied latitudinal effects. Fish Bull 87:471-495

Houde ED (1987) Fish early life dynamics and recruitment variability. American Fisheries Society Symposium 2:17-29

Houde ED and Alpern Lovdal JD (1985) Patterns of variability in ichthyoplankton occurrence and abundance in Biscayne Bay, Florida. Estuar Coast Shelf Sci 20:79-103

Houghton RW (1997) Lagrangian flow at the foot of a shelfbreak front using a dye tracer injected into the bottom boundary layer. Geophys Res Lett 24:2035-2038

Houghton RW and Visbeck M (1998) Upwelling and convergence in the Middle Atlantic Bight shelfbreak front. Geophys Res Lett 25:2765-2768

Houghton RW, Aikman III F, Ou HW (1988) Shelf-slope frontal structure and cross-shelf exchange at the New England shelf-break. Cont Shelf Res 8:687-710

Houghton RW, Olson DB, Celone PJ (1986) Observation of an anticyclonic eddy near the continental shelf break south of New England. J Phys Oceanogr 16:60-71

Hu Q and Davis C (2006) Accurate automatic quantification of taxa-specific plankton abundance using dual classification with correction. Mar Ecol Prog Ser 306:51-61

Jackson GA (1990) A model of the formation of marine algal flocs by physical coagulation processes. Deep Sea Research Part A, Oceanographic Research Papers 37:1197-1211

Jackson JBC, Kirby MX, Berger WH, Bjorndal KA, Botsford LW, Bourque BJ, Bradbury RH, Cooke R, Erlandson J, Estes JA, and others (2001) Historical overfishing and the recent collapse of coastal ecosystems. Science 293:629-637

Jacobsen HP and Norrbin MF (2009) Fine-scale layer of hydromedusae is revealed by Video Plankton Recorder (VPR) in a semi-enclosed bay in northern Norway. Mar Ecol Prog Ser 380:129-135

Jaffe JS, Franks PJS, Leising AW (1998) Simultaneous imaging of phytoplankton and zooplankton distributions. Oceanography 11:24-29

Jaspers C, Titelman J, Hansson LJ, Haraldsson M, Ditlefsen CR (2011) The invasive ctenophore *Mnemiopsis leidyi* poses no direct threat to Baltic cod eggs and larvae. Limnol Oceanogr 56:431-439

Javidpour J, Molinero JC, Lehmann A, Hansen T, Sommer U (2009) Annual assessment of the predation of *Mnemiopsis leidyi* in a new invaded environment, the Kiel Fjord (western Baltic Sea): A matter of concern? J Plankton Res 31:729-738

Kingsford MJ and Suthers IM (1994) Dynamic estuarine plumes and fronts: Importance to small fish and plankton in coastal waters of NSW, australia. Cont Shelf Res 14:655-672

Kiørboe T and MacKenzie B (1995) Turbulence-enhanced prey encounter rates in larval fish: Effects of spatial scale, larval behaviour and size. J Plankton Res 17:2319-2331

Kiørboe T (2008) A mechanistic approach to plankton ecology. Princeton University Press, Princeton, New Jersey

Kiørboe T, Andersen KP, Dam HG (1990) Coagulation efficiency and aggregate formation in marine phytoplankton. Marine Biology 107:235-245

Klymak JM, Pinkel R, Liu C, Liu AK, David L (2006) Prototypical solitons in the South China Sea. Geophys Res Lett 33:- L11607

Kranck K and Milligan TG (1991) Grain size in oceanography. In: Syvitski JPM (ed) Principles, methods, and application of particle size analysis. Cambridge University Press, Cambridge, p. 332-345

Kushnir VM, Tokarev YN, Williams R, Piontkovski SA, Evstigneev PV (1997) Spatial heterogeneity of the bioluminescence field of the tropical Atlantic Ocean and its relationship with internal waves. Mar Ecol Prog Ser 160:1-11

Labat JP, Mayzaud P, Dallot S, Errhif A, Razouls S, Sabini S (2002) Mesoscale distribution of zooplankton in the sub-Antarctic frontal system in the Indian part of the Southern Ocean: A comparison between Optical Plankton Counter and net sampling. Deep-Sea Research Part I: Oceanographic Research Papers 49:735-749

Lai Z, Chen C, Beardsley RC, Rothschild B, Tian R (2010) Impact of high-frequency nonlinear internal waves on plankton dynamics in Massachusetts Bay. J Mar Res 68:259-281

Lamb KG (1997) Particle transport by nonbreaking, solitary internal waves. Journal of Geophysical Research 102:18641-18660

Lasker R (1975) Field criteria for survival of anchovy larvae - relation between inshore chlorophyll maximum layers and successful 1st feeding. Fish Bull 73:453-462

Leis JM (1991) Vertical distribution of fish larvae in the Great Barrier Reef lagoon, Australia. Mar Biol 109:157-166

Leising AW, Pierson JJ, Halsband-Lenk C, Horner R, Postel J (2005) Copepod grazing during spring blooms: Does *Calanus pacificus* avoid harmful diatoms? Prog Oceanogr 67:384-405

Lennert-Cody CE and Franks PJS (2002) Fluorescence patches in high-frequency internal waves. Mar Ecol Prog Ser 235:29-42

Lincoln JA, Turner JT, Bates SS, Léger C, Gauthier DA (2001) Feeding, egg production, and egg hatching success of the copepods *Acartia tonsa* and *Temora longicornis* on diets of the toxic diatom *Pseudo-nitzschia* multiseries and the non-toxic diatom *Pseudo-nitzschia pungens*. Hydrobiologia 453-454:107-120

Link JS and Ford MD (2006) Widespread and persistent increase of Ctenophora in the continental shelf ecosystem off NE USA. Mar Ecol Prog Ser 320:153-159

Llopiz JK and Cowen RK (2008) Precocious, selective and successful feeding of larval billfishes in the oceanic Straits of Florida. Marine Ecology Progress Series 358:231-244

Lloyd M (1967) Mean crowding. J Anim Ecol 36:1-30

Lougee LA, Bollens SM, Avent SR (2002) The effects of haloclines on the vertical distribution and migration of zooplankton. J Exp Mar Biol Ecol 278:111-134

Lough RG and Broughton EA (2007) Development of micro-scale frequency distributions of plankton for inclusion in foraging models of larval fish, results from a Video Plankton Recorder. J Plankton Res 29:7-17

MacIntyre S, Alldredge AL, Gotschalk CC (1995) Accumulation of marine snow at density discontinuities in the water column. Limnol Oceanogr 40:449-468

Mackas DL, Denman KL, Abbott MR (1985) Plankton patchiness: Biology in the physical vernacular. Bull Mar Sci 37:653-674

Mackas DL, Kieser R, Saunders M, Yelland DR, Brown RM, Moore DF (1997) Aggregation of euphausiids and Pacific hake (*Merluccius productus*) along the outer continental shelf off Vancouver Island. Can J Fish Aquat Sci 54:2080-2096

Madin L, Horgan E, Gallager S, Eaton J, Girard A (2006) LAPIS: A new imaging tool for macro-zooplankton. In: Proceedings, IEEE/MTS Oceans '06 Meeting.

Majaneva S, Berge J, Renaud PE, Vader A, Stübner E, Rao AM, Sparre Ø, Lehtiniemi M (2013) Aggregations of predators and prey affect predation impact of the Arctic ctenophore *Mertensia ovum*. Mar Ecol Prog Ser 476:87-100

Malkiel E, Abras JN, Widder EA, Katz J (2006) On the spatial distribution and nearest neighbor distance between particles in the water column determined from in situ holographic measurements. J Plankton Res 28:149-170

Malone TC (1977) Plankton systematics and distribution. MESA New York Bight Atlas Monographs 13:0-45

Mann KH and Lazier JRN (2006) Dynamics of marine ecosystems: Biological-physical interactions in the oceans, 3rd ed. Blackwell, Malden, Massachusetts, USA

Marra J, Houghton RW, Garside C (1990) Phytoplankton growth at the shelf-break front in the Middle Atlantic Bight. J Mar Res 48:851-868

Marra J, Houghton RW, Boardman DC, Neale PJ (1982) Variability in surface chlorophyll a at a shelf-break front (New York Bight). J Mar Res 40:575-591

Matsuura Y and Hewitt R (1995) Changes in the spatial patchiness of Pacific mackerel, *Scomber japonicus*, larvae with increasing age and size. Fish Bull 93:172-178

McClatchie S, Cowen R, Nieto K, Greer A, Luo JY, Guigand C, Demer D, Griffith D, Rudnick D (2012) Resolution of fine biological structure including small narcomedusae across a front in the southern california bight. Journal of Geophysical Research C: Oceans 117

McClatchie S, Rogers PJ, McLeay L (2007) Importance of scale to the relationship between abundance of sardine larvae, stability, and food. Limnol Oceanogr 52:1570-1579

McGurk MD (1986) Natural mortality of marine pelagic fish eggs and larvae: Role of spatial patchiness. Marine Ecology Progress Series 34:227-242

McManus MA, Kudela RM, Silver MW, Steward GF, Donaghay PL, Sullivan JM (2008) Cryptic blooms: Are thin layers the missing connection? Estuaries and Coasts 31:396-401

McManus MA, Cheriton OM, Drake PJ, Holliday DV, Storlazzi CD, Donaghay PL, Greenlaw CF (2005) Effects of physical processes on structure and transport of thin zooplankton layers in the coastal ocean. Marine Ecology Progress Series 301:199-215

McManus MA, Alldredge AL, Barnard AH, Boss E, Case JF, Cowles TJ, Donaghay PL, Eisner LB, Gifford DJ, Greenlaw CF, and others (2003) Characteristics, distribution and persistence of thin layers over a 48 hour period. Marine Ecology Progress Series 261:1-19

Miller RJ (1974) Distribution and biomass of an estuarine ctenophore population, *Mnemiopis leidyi* (A. agassiz). Chesapeake Science 15:1-8

Miller TJ (2002) Assemblages, communities, and species interactions. In: Fuiman LA and Werner RG (eds) *Fishery Science: The unique contributions of the early life stages*. Blackwell Science Ltd, p. 183-205

Miller TJ, Crowder LB, Rice JA, Marschall EA (1988) Larval size and recruitment mechanisms in fishes - toward a conceptual-framework. Can J Fish Aquat Sci 45:1657-1670

Mills CE (1984) Density is altered in hydromedusae and ctenophores in response to changes in salinity. Biological Bulletin 166:206-215

Miralto A, Barone G, Romano G, Poulet SA, Ianora A, Russo GL, Buttino I, Mazzarella G, Laablr M, Cabrini M, and others (1999) The insidious effect of diatoms on copepod reproduction. Nature 402:173-176

Morote E, Olivar MP, Bozzano A, Villate F, Uriarte I (2011) Feeding selectivity in larvae of the European hake (*Merluccius merluccius*) in relation to ontogeny and visual capabilities. Mar Biol 158:1349-1361

Munk P, Hansen BW, Nielsen TG, Thomsen HA (2003) Changes in plankton and fish larvae communities across hydrographic fronts off West Greenland. J Plankton Res 25:815-830

Neill WE (1990) Induced vertical migration in copepods as a defence against invertebrate predation. Nature 345:524-526

Nielsen TG and Munk P (1998) Zooplankton diversity and the predatory impact by larval and small juvenile fish at the fisher banks in the North Sea. J Plankton Res 20:2313-2332

Nielsen TG, Kiørboe T, Bjornsen PK (1990) Effects of a *Chrysochromulina polylepis* subsurface bloom on the planktonic community. Marine Ecology Progress Series 62:21-35

Norrbin MF, Vis CSDA, Gallager SM (1996) Differences in fine-scale structure and composition of zooplankton between mixed and stratified regions of Georges Bank. Deep-Sea Research Part II: Topical Studies in Oceanography 43:1905-1924

Ortner PB, Cummings SR, Aftring RP (1979) Silhouette photography of oceanic zooplankton. Nature 277:50-51

Oviatt CA and Kremer PM (1977) Predation on the ctenophore, *Mnemiopsis leidyi*, by butterfish, peprilus triacanthus, in Narragansett Bay, Rhode Island. Chesapeake Science 18:236-240

Paffenhöfer G and Lee TN (1987) Development and persistence of patches of Thaliacea. South African Journal of Marine Science 5:305-318

Paffenhöfer GA, Atkinson LP, Lee TN, Verity PG, Bulluck LRII (1995) Distribution and abundance of thaliaceans and copepods off the southeastern USA during winter. Cont Shelf Res 15:255-280

Pebesma, E.J. (2004) Multivariate geostatistics in S: the gstat packages. Computers & Geosciences 30:683-691

Pennington TJ and Chavez FP (2000) Seasonal fluctuations of temperature, salinity, nitrate, chlorophyll and primary production at station H3/M1 over 1989-1996 in Monterey Bay, California. Deep-Sea Research Part II: Topical Studies in Oceanography 47:947-973

Pepin P (2002) Population analysis. In: Fuiman LA and Werner RG (eds) *Fishery Science: The unique contributions of the early life stages*. Blackwell Science Ltd, p. 112-142

Pepin P (1991) Effect of temperature and size on development, mortality, and survival rates of the pelagic early life history stages of marine fish. Can J Fish Aquat Sci 48:503-518

Pielou EC (1977) Mathematical ecology. J. Wiley and Sons, New York

Pierson JJ, Leising AW, Halsband-Lenk C, Ferm N (2005) Vertical distribution and abundance of *Calanus pacificus* and *Pseudocalanus newmani* in relation to chlorophyll a concentrations in Dabob Bay, Washington. Prog Oceanogr 67:349-365

Pilskaln CH, Paduan JB, Chavez FP, Anderson RY, Berelson WM (1996) Carbon export and regeneration in the coastal upwelling system of Monterey Bay, central California. J Mar Res 54:1149-1178

Pineda J (1999) Circulation and larval distribution in internal tidal bore warm fronts. Limnol Oceanogr 44:1400-1414

Pinel-Alloul P (1995) Spatial heterogeneity as a multiscale characteristic of zooplankton community. Hydrobiologia 300-301:17-42

Pitchford WJ and Brindley J (2001) Prey patchiness, predator survival and fish recruitment. Bull Math Biol 63:527-546

Purcell JE (1991) A review of cnidarians and ctenophores feeding on competitors in the plankton. Hydrobiologia 216-217:335-342

R Core Team (2012) R: A language and environment for statistical computing. http://www.R-project.org

Ramp SR, Paduan JF, Shulman I, Kindle J, Bahr FL, Chavez F (2005) Observations of upwelling and relaxation events in the northern Monterey Bay during August 2000. Journal of Geophysical Research C: Oceans 110:1-21

Rasband WS (1997-2012) ImageJ, U.S. National Institutions of Health, Bethesda, Marlyand, USA.

Raskoff KA (2002) Foraging, prey capture, and gut contents of the mesopelagic narcomedusa *Solmissus* spp. (cnidaria: Hydrozoa). Mar Biol 141:1099-1107

Rees JT (1978) Laboratory and field studies on *Eutonina indicans* (coelenterata: Hydrozoa), a common leptomedusa of Bodega Bay, California. The Wasmann Journal of Biology 36:201-209

Reeve MR (1980) Population dynamics of ctenophores in large scale enclosures over several years. In: D.C. Smith YT (ed) Nutrition of the lower Metazoa. Pergamon, p. 73-86

Reeve MR, Walter MA, Ikeda T (1978) Laboratory studies of ingestion and food utilization in lobate and tentaculate ctenophores. Limnol Oceanogr 23:740-751

Remsen A, Hopkins TL, Samson S (2004) What you see is not what you catch: A comparison of concurrently collected net, Optical Plankton Counter, and Shadowed Image Particle Profiling Evaluation Recorder data from the northeast Gulf of Mexico. Deep Sea Research Part I: Oceanographic Research Papers 51:129-151

Richardson AJ, Bakun A, Hays GC, Gibbons MJ (2009) The jellyfish joyride: Causes, consequences and management responses to a more gelatinous future. Trends in Ecology and Evolution 24:312-322

Rines JEB, McFarland MN, Donaghay PL, Sullivan JM (2010) Thin layers and species-specific characterization of the phytoplankton community in Monterey Bay, California, USA. Cont Shelf Res 30:66-80

Rines JEB, Donaghay PL, Dekshenieks MM, Sullivan JM, Twardowski MS (2002) Thin layers and camouflage: Hidden *Pseudo-nitzschia* spp. (bacillariophyceae) populations in a fjord in the San Juan Islands, Washington, USA. Mar Ecol Prog Ser 225:123-137

Rosenfeld LK, Schwing FB, Garfield N, Tracy DE (1994) Bifurcated flow from an upwelling center: A cold water source for Monterey Bay. Cont Shelf Res 14:931-964

Rothschild BJ (1986) *Dynamics of marine fish populations*. Harvard University Press, Cambridge, Massachusetts, USA

Rothschild BJ and Osborn TR (1988) Small-scale turbulence and plankton contact rates. J Plankton Res 10:465-474

Ryan JP, McManus MA, Paduan JD, Chavez FP (2008) Phytoplankton thin layers caused by shear in frontal zones of a coastal upwelling system. Mar Ecol Prog Ser 354:21-34

Ryan JP, Fischer AM, Kudela RM, Gower JFR, King SA, Marin III R, Chavez FP (2009) Influences of upwelling and downwelling winds on red tide bloom dynamics in Monterey Bay, California. Cont Shelf Res 29:785-795

Samson S, Hopkins T, Remsen A, Langebrake L, Sutton T, Patten J (2001) A system for high-resolution zooplankton imaging. IEEE J Ocean Eng 26:671-676

Sangrá P, Basterretxea G, Pelegrí JL, Arístegui J (2001) Chlorophyll increase due to internal waves on the shelf break of Gran Canaria (Canary Islands). Scientia Marina 65:89-97

Scotti A and Pineda J (2004) Observation of very large and steep internal waves of elevation near the Massachusetts coast. Geophys Res Lett 31:1-5

Sevadjian JC, McManus MA, Benoit-Bird KJ, Selph KE (2012) Shoreward advection of phytoplankton and vertical re-distribution of zooplankton by episodic near-bottom water pulses on an insular shelf: Oahu, Hawaii. Cont Shelf Res 50-51:1-15

Shanks AL (1995) Orientated swimming by megalopae of several eastern north pacific crab species and its potential role in their onshore migration. J Exp Mar Biol Ecol 186:1-16

Shanks AL (1983) Surface slicks associated with tidally forced internal waves may transport pelagic larvae of benthic invertebrates and fishes shoreward. Mar Ecol Prog Ser 13:311-315

Sheldon RW, Prakash A, Sutcliffe WH (1972) The size distribution of particles in the ocean. Limnol Oceanogr 17:327-340

Shroyer EL, Moum JN, Nash JD (2011) Nonlinear internal waves over New Jersey's continental shelf. Journal of Geophysical Research C: Oceans 116

Sørnes TA and Aksnes DL (2004) Predation efficiency in visual and tactile zooplanktivores. Limnol Oceanogr 49:69-75

Stacey MT, McManus MA, Steinbuck JV (2007) Convergences and divergences and thin layer formation and maintenance. Limnol Oceanogr 52:1523-1532

Stanlaw KA, Reeve MR, Walter MA (1981) Growth, food, and vulnerability to damage of the ctenophore *Mnemiopsis mccradyi* in its early life-history stages. Limnol Oceanogr 26:224-234

Stanton TK, Wiebe PH, Chu Dezhanbg, Benfield MC, Scanlon L, Martin L, Eastwood RL (1994) On acoustic estimates of zooplankton biomass. ICES J Mar Sci 51:505-512

Steele JH (ed) (1978) Spatial pattern in plankton communities. Plenum Press, New York

Steele JH (1976) Patchiness. In: Cushing DH and Walsh JJ (eds) *The Ecology of the Seas*. W.B. Saunders and Co., Philadelphia, p. 98-115

Stemmann L and Boss E (2012) Plankton and particle size and packaging: From determining optical properties to driving the biological pump. Annual Review of Marine Science 4:263-290

Sullivan JM, Donaghay PL, Rines JEB (2010) Coastal thin layer dynamics: Consequences to biology and optics. Cont Shelf Res 30:50-65

Sumida BY and Moser HG (1980) Food and feeding of Pacific hake larvae, *Merluccius productus*, off southern California and northern Baja California. California Cooperative Oceanic Fisheries, Investigations Reports 21:161-166

Sutor MM and Dagg MJ (2008) The effects of vertical sampling resolution on estimates of plankton biomass and rate calculations in stratified water columns. Estuar Coast Shelf Sci 78:107-121

Taft BA (1960) A statistical study of the estimation of abundance of sardine (*Sardinops caerulea*) eggs. Limnology and Oceanography 5:245-264

Tiselius P (1992) Behavior of *Acartia tonsa* in patchy food environments. Limnology & Oceanography 37:1640-1651

Titelman J and Hansson LJ (2006) Feeding rates of the jellyfish *Aurelia aurita* on fish larvae. Mar Biol 149:297-306

Titelman J, Hansson LJ, Nilsen T, Colin SP, Costello JH (2012) Predator-induced vertical behavior of a ctenophore. Hydrobiologia 690:181-187

Tosti E, Romano G, Buttino I, Cuomo A, Ianora A, Miralto A (2003) Bioactive aldehydes from diatoms block the fertilization current in ascidian oocytes. Mol Reprod Dev 66:72-80

Toyokawa M, Toda T, Kikuchi T, Miyake H, Hashimoto J (2003) Direct observations of a dense occurrence of *Bolinopsis infundibulum* (ctenophora) near the seafloor under the Oyashio and notes on their feeding behavior. Deep-Sea Research Part I: Oceanographic Research Papers 50:809-813

Trevorrow MV, Mackas DL, Benfield MC (2005) Comparison of multifrequency acoustic and in situ measurements of zooplankton abundances in Knight Inlet, British Columbia. J Acoust Soc Am 117:3574-3588

Tucker GH (1951) Relation of fishes and other organisms to the scattering of underwater sound. Journal of Marine Research 10:215-238

Vlymen WJ (1977) A mathematical model of the relationship between larval anchovy (*Engraulis mordax*) growth, prey microdistribution, and larval behavior. Environ Biol Fishes 2:211-233

Wallace BC and Wilkinson DL (1988) Run-up of internal waves on a gentle slope in a two-layered system. Journal of Fluid Mechanics 191:419-442

Wang Z and Goodman L (2009) Evolution of the spatial structure of a thin phytoplankton layer into a turbulent field. Mar Ecol Prog Ser 374:57-74

Watson J, Alexander S, Chavidan V, Craig G, Diard A, Foresti GL, Gentili S, Hendry DC, Hobson PR, Lampitt RS, and others (2003) A holographic system for subsea recording and analysis of plankton and other marine particles (HOLOMAR). Ocean Conference Record (IEEE) 2:830-837

Weeks PJD and Gaston KJ (1997) Image analysis, neural networks, and the taxonomic impediment to biodiversity studies. Biodivers Conserv 6:263-274

Werner RG (2002) Habitat requirements. In: Fuiman LA and Werner RG (eds) *Fishery Science: The unique contributions of the early life stages*. Blackwell Science Ltd, p. 161-182

Wickham, H. (2009) Ggplot2: elegant graphics for data analysis. Springer, New York.

Wickham, H. (2011) The split-apply-combine strategy for data analysis. Journal of Statistical Software 40:1-29

Wiebe PH and Benfield MC (2003) From the Hensen net toward four-dimensional biological oceanography. Progress in Oceanography 56:7-136

Wiebe PH, Burt KH, Boyd SH, Morton AW (1976) A multiple opening/closing net and environmental sensing system for sampling zooplankton. J Mar Res 43:313-325

Wiebe PH, Morton AW, Bradley AM, Backus RH, Craddock JE, Barber V, Cowles TJ, Flierl GR (1985) New development in the MOCNESS, an apparatus for sampling zooplankton and micronekton. Mar Biol 87:313-323

Wiebe PH and Beardsley RC (1996) Physical-biological interactions on Georges Bank and its environs. Deep Sea Research Part II: Topical Studies in Oceanography 43:1437-1438

Woodd-Walker RS, Gallienne CP, Robins DB (2000) A test model for Optical Plankton Counter (OPC) coincidence and a comparison of OPC-derived and conventional measures of plankton abundance. J Plankton Res 22:473-483

Woodson CB, Webster DR, Weissburg MJ, Yen J (2007) Cue hierarchy and foraging in calanoid copepods: Ecological implications of oceanographic structure. Mar Ecol Prog Ser 330:163-177

Woodson CB, Webster DR, Weissburg MJ, Yen J (2005) Response of copepods to physical gradients associated with structure in the ocean. Limnol Oceanogr 50:1552-1564

Woodson CB, Washburn L, Barth JA, Hoover DJ, Kirincich AR, McManus MA, Ryan JP, Tyburczy J (2009) Northern Monterey Bay upwelling shadow front: Observations of a coastally and surface-trapped buoyant plume. Journal of Geophysical Research C: Oceans 114

Woodward G, Ebenman B, Emmerson M, Montoya JM, Olesen JM, Valido A, Warren PH (2005) Body size in ecological networks. Trends in Ecology and Evolution 20:402-409

Wrobel D and Mills CE (1998) *Pacific coast pelagic invertebrates: A guide to the common gelatinous animals*. Sea Challengers and Monterey Bay Aquarium, Monterey, CA

Zaret TM and Suffern JS (1976) Vertical migration in zooplankton as a predator avoidance mechanism. Limnol Oceanogr 21:804-813

Zuur AF, Ieno EN, Walker NJ, Saveliev AA, Smith GM (2009) Mixed effect models and extensions in ecology with R. Springer, New York

Appendix A: Size/frequency histograms of various planktonic taxa used to create size classes for particle counting in Chapter 4

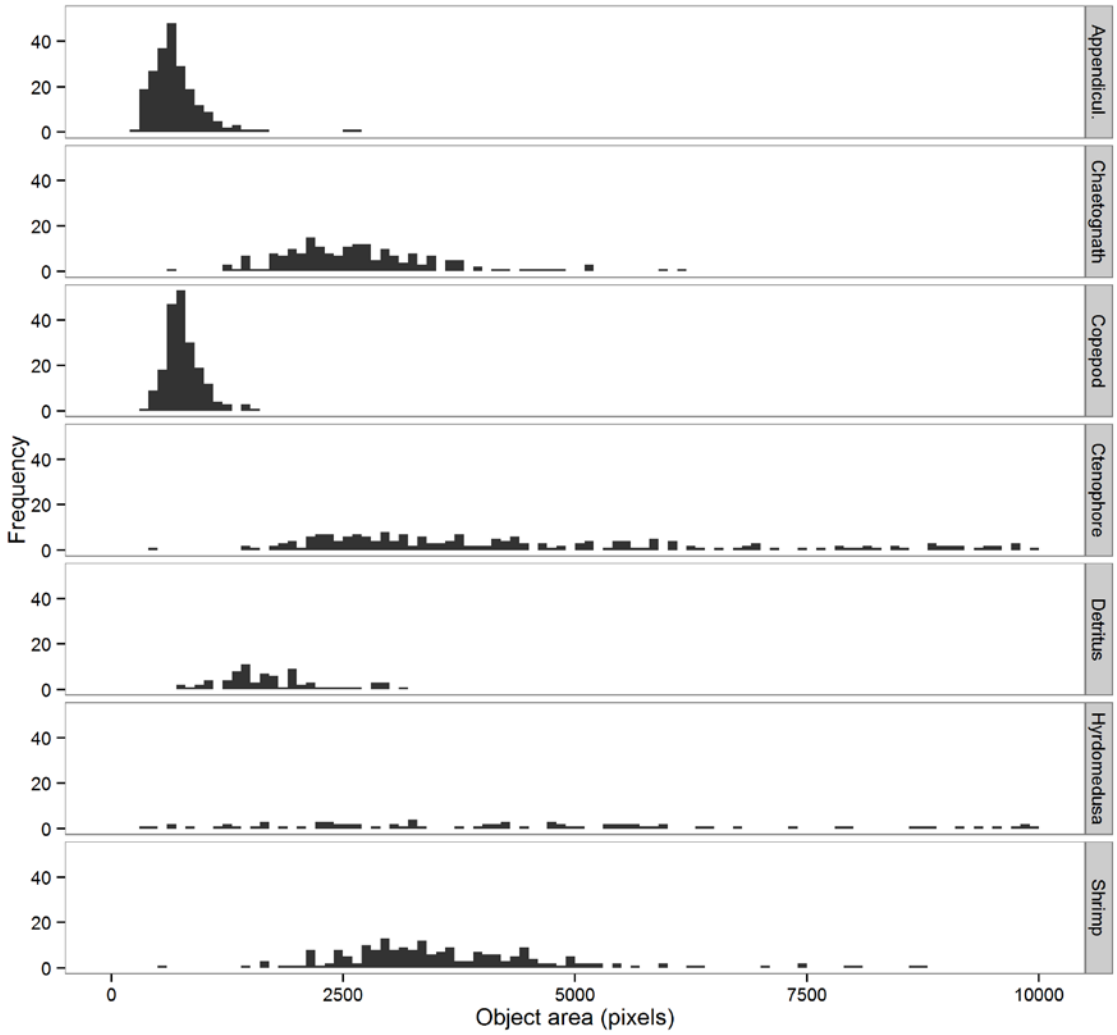

Appendix B: ImageJ macro program for flat-fielding a directory full of ISIIS tiff stacks. This program requires two plugins freely available at http://rsbweb.nih.gov/ij/plugins/: Image Calculator Plus and Stack Average.

```
//This macro requires the plugin StackAverage_.java and Image Calculator Plus
//Need to have at least 4000 MB of memory available to ImageJ
//This macro produces a flat-fielded stack of ISIIS images in the directory of your
//choosing.
//by Adam T. Greer
//University of Miami 2013

dir = getDirectory("Choose a Directory");//directory of images to be processed
filelist = getFileList(dir);
max = lengthOf(filelist);

//loop over all files in the directory
for (i=0; i<max; i++)  {
open(dir+filelist[i]);

//Get average of the stack as a reference image
run("StackAverage ");
stackname = getTitle();
x=nSlices;
run("Make Substack...", "delete slices="+x);
selectWindow("Substack ("+x+")");
rename("ff");

//run the flat fielding
selectWindow(stackname);
run("Calculator Plus", "i1=stackname i2=ff operation=[Divide: i2 = (i1/i2) x k1 + k2]
k1=235 k2=0 create");

//save
saveAs("Tiff", "D:/FlatFieldedImages/"+filelist[i]); //specify the output directory here
close();
close();
close();
}
```

Appendix C: ImageJ macro program for automatically counting copepods or particles from tiff stacks with summarized output and image histogram statistics used for filtering out potentially erroneous counts.

```
//This macro runs on a directory of previously flat fielded images.
//It obtains the image histogram statistics then
//automatically counts and sizes
//copepods in ISIIS images >30 pixels and <600 pixels in size after applying a threshold
//by Adam Greer, University of Miami, January 2013

dir = getDirectory("Choose a Directory");
filelist = getFileList(dir);
max = lengthOf(filelist);

for (i=0; i<max; i++)  {
open(dir+filelist[i]);
run("8-bit");
if (nSlices>1) run("Clear Results");
     n = getSliceNumber();
     for (j=1; j<=nSlices; j++) {
        setSlice(j);
        getRawStatistics(count, mean, min, max, std);
        row = nResults;
        if (nSlices==1)
          setResult("Pixels", row, count);
        setResult("Mean ", row, mean);
        setResult("Std ", row, std);
     }
     setSlice(n);
     updateResults();
selectWindow("Results");
saveAs("txt", "D:/HistogramStats/"+filelist[i]+".txt");
selectWindow("Results");
run("Close");

setAutoThreshold("Default");
//run("Threshold...");
setThreshold(0, 110, "Black & White");

run("Set Measurements...", "area perimeter bounding display redirect=None decimal=3");
run("Analyze Particles...", "size=30-600 circularity=0.10-1.0 show=Nothing clear
summarize stack");
selectWindow("Summary of "+filelist[i]);
saveAs("txt", "D:/CopepodCounts/"+filelist[i]+".txt");
close();
}
```